Title
HA Concentration-Dependent Invasion of Patient-Derived Gliomaspheres in 3D Hydrogels

Author
Safarians, Gevick

Publication Date
2022

Peer reviewed|Thesis/dissertation

UNIVERSITY OF CALIFORNIA

Los Angeles

HA Concentration-Dependent Invasion of Patient-Derived Gliomaspheres in 3D Hydrogels

A thesis submitted in partial satisfaction

of the requirements for the degree Master of Science

in Bioengineering

by

Gevick Safarians

2022

ABSTRACT OF THE THESIS

HA Concentration-Dependent Invasion of Patient-Derived Gliomaspheres in 3D Hydrogels

by

Gevick Safarians

Master of Science in Bioengineering

University of California, Los Angeles, 2022

Professor, Stephanie K. Seidlits, Co-Chair

Professor, Wentai Liu, Co-Chair

Glioblastoma (GBM) is the most common and lethal primary central nervous system (CNS) tumor with a median survival of 12 – 15 months post-diagnosis. GBM aggression is, in part, due to high invasion of tumor cells into the CNS parenchyma which leads to therapeutic evasion as well as tumor recurrence. Mechanochemical cues within the GBM tumor microenvironment create environments conducive for cell survival and migration. Bioengineered in vitro systems which mimic features of the peritumoral niche can recapitulate *in vivo* GBM tumor cell behavior *ex vivo*. Thus, we developed three-dimensional (3D), hyaluronan (HA)-based hydrogels of varied HA concentrations and similar poroelastic properties corresponding to the peritumoral environment. Patient-derived spheroids encapsulated in our 3D hydrogels each displayed unique degrees and morphologies of invasion independent of conventional GBM molecular classification. We discovered strengths of cytoskeletal engagement, mediated by ezrin-radixin-moesin (ERM) complex, determined the propensity for cellular invasion, while cluster of differentiation 44 (CD44) expression densities determined the amounts of invasion. Furthermore, blocking the HA binding domain of receptor for hyaluronan-mediated motility (RHAMM)

resulted in increased invasion, suggesting further studies on the roles of extracellular RHAMM are critical for further understanding how HA within the TME affects GBM cell invasion.

The thesis of Gevick Safarians is approved.

Harley I. Kornblum

Song Li

Stephanie K. Seidlits, Co-Chair

Wentai Liu, Co-Chair

University of California, Los Angeles

2022

ACKNOWLEDGEMENTS

Dr. Seidlits for your mentorship and allowing me to grow as a young scientist. Your guidance and care have made my Master program everything I could imagine and more in regard to personal and professional growth, development of critical thinking, and better understanding academia as a field altogether. Thank you for strengthening my commitment to a lifelong career in science and medicine.

Dr. Sohrabi for your leadership, dedication to my betterment as a scientist, and mentorship. You have always been one text message away from answering seemingly bewildering problems to me that arise in lab. Your guidance helped me develop as a problem solver and thinker through situations. Thank you for your incredible patience through the years and friendship.

Dr. Xiao for your virtual assistance with any and all questions I have had throughout the years. Your optimism for my projects and inclinations to provide knowledge or data are highly appreciated.

Dr. Liang for firmly challenging me to grow as a critical thinker. Our conversations were essential for me becoming comfortable with thinking through data and organizing future experiments.

Itay Solomon for laying the groundwork for any of this to even be possible. You and Alireza performed many preliminary studies which I used to develop future experiments.

Drs. Soniya Bastola, Jessica Chen, and Bill Wang for your valuable friendships and discussions with me throughout my masters regarding my future as a scientist. During my time in the Seidlits lab, I have watched you each with great admiration and thank you as role models.

Nicholas Bayley and Nathanson Lab for our discussions regarding RNA sequencing analysis as well as providing code for cluster typing.

DEDICATION

This thesis is dedicated to: my family Rubina, Edick, Hrand, Jasmine, Aram, Ninush, and Janet for immigrating as refugees to the United States so that I may receive a well-rounded education and instilling kindness and patience in my heart; my younger sister Naieri to achieve all that she dreams and desires; my childhood friends Mihir, Levon, Karpis, and Andranik for the memories, support, and happiness they have given me throughout my life; and my dearest Taline for being my backbone and constant motivation to be better each day. I also dedicate this to all my relatives who passed from cancer.

Most importantly, I dedicate this thesis to any and all patients, caregivers, and communities affected by glioblastoma. While physicians and patients may feel powerless now in the face of this lethal cancer, I remain hopeful that the work presented in this thesis contributes to and fosters the development of future therapeutics or diagnostic technologies. Through the knowledge gained, may we come ever closer to ridding humanity of this ailment.

TABLE OF CONTENTS

CHAPTER 1: INTRODUCTION

Current State of Glioblastoma Treatment and Care

Disease Epidemiology

Glioblastoma (GBM), previously known as Glioblastoma Multiforme, is the most common, lethal, and aggressive form of all primary central nervous system (CNS) cancers with a reported prevalence of 9.23 cases per 100,000 population in the United States and a median age of diagnosis of approximately 65 years.[1,2] Without medical treatment and only palliative care, individuals may only survive 4 – 6 months post-diagnosis.[1,3–5] With aggressive treatment, survival is still exceedingly uncommon with median survival among treated cases being 12 – 15 months and only 5.8% of patients surviving beyond 5 years post-diagnosis.[6,7]

No well-established risk factors for GBM have been identified beyond exposure to ionizing radiation and genetic predisposition.[1,8] The lack of appropriate biomarkers indicating vulnerability or resistance to therapies contributes to an incidence of 3.2 cases per 100,000 population in the United States and an increasing incidence in the geriatrics aged 75 – 84 at 15.24 cases per 100,000 population.[9,10] Differentials in diagnosis and outcome based on sex, race/ethnicity, and region are apparent. Specifically, males are more likely to be diagnosed with GBM than females, non-Hispanic whites have generally the highest incidence rates among all other racial/ethnic groups, and North America, Australia, and Northern/Western Europe possess the highest incidence rates globally.[1,11,12]

GBM is a terminal illness detrimental to both patient and caregiver quality of life. Rare, long-term survivors, similar to their terminally affected counterparts, are often burdened with prolonged neurological and social deficits in addition to general physiological or psychological

difficulties.[13] The work provided in this thesis aligns with ongoing efforts to develop mechanochemically tunable, biomimetic *in vitro* models to characterize GBM phenotypes and response to therapeutics in a patient-specific manner.

Diagnostics and Classification

Clinically, GBM patients initially present with a single or combination of general neurological disturbances that may be gradual (e.g. headaches, intracranial pressure) or sudden (e.g. epilepsy, motor deficits) in onset.[14] Given the non-specificity of clinical indications, computed tomography (CT) is initially deployed to consider the presence of a solid, intracranial tumor mass to rule out non-tumoral differential diagnoses (e.g. epilepsy, encephalitis). Upon discovery, contrast-enhanced magnetic resonance imaging (MRI) further reveals potentially malignant features of the identified tumor mass.[15] For GBM masses specifically, T2-fluid-attenuated inversion recovery (FLAIR) MRI often presents intra-tumoral hypo-enhancement indicative of pseudopalisading necrosis, peri-tumoral hyperintensity indicative of edema, and non-uniform development and compression on neighboring, non-neoplastic tissues.[15] However, formal diagnosis of GBM does not occur until exclusion of further differential diagnoses of lower-grade CNS tumors (e.g. anaplastic astrocytoma, oligodendroglioma, ependymoma) by histopathological characterization of the resected tumor mass.[16,17]

Early efforts in differentiating GBM from other CNS cancers used DNA microarray technologies for transcriptomic profiling. Sallinen *et al*. (2000) identified more than 200 gene expression alterations in GBM.[18] In a comparative analysis, Rickman *et al*. (2001) identified 360 genes differentially expressed in GBM compared to lower grade astrocytomas.[19] Utilizing differentially expressed genes across GBM patient samples, Phillips *et al.* (2006) designated classifications of GBM as being proneural, proliferative, or mesenchymal.[20] Proneural subtypes

had the best prognosis and had neuronal gene signatures, such as NCAM, while mesenchymal subtypes had upregulated markers associated with angiogenesis and invasion. Beyond differential gene expression, a key hallmark of GBM is genetic alterations including copy number changes, chromosomal deletions, and somatic gene amplifications or mutations. Most commonly, TP53, TERT promoter, or IDH1 gene mutations, PDGFRA or EGFR gene amplifications, and PTEN gene deletions can result in distinct GBM tumor phenotypes. Moreover, certain patients may genotypically present with gains in chromosomes 19 and 20 or 1p/19q chromosomal co-deletions, further adding to intertumoral heterogeneity prevalent in GBM cases.[21]

In 2008, the Cancer Genome Atlas (TCGA) was initially introduced as a database for GBM, lung squamous carcinoma, and ovarian serous adenocarcinoma cancers.[22] This joint effort to store and make genomic data freely available on a per-patient basis has motivated further efforts in GBM molecular characterization and more recent establishment of online databases for GBM-specific data, such as the Chinese Glioma Genome Atlas (CGGA) and Ivy Glioblastoma Atlas Project. Building upon previous work by Phillips *et al.* (2006), Verhaak *et al.* (2010) performed consensus clustering on TCGA patient genotype data and identified four GBM subtypes: proneural, mesenchymal, neural, and classical.[23] In recent years, efforts in transcriptomic and RNA profiling of GBM has led to a diversity of cell type categorizations for GBM cells. For example, Bhaduri *et al.* (2020) performed clustering of GBM cells according to signatures of mature or stem/progenitor CNS cell states, while Garofano *et al.* (2021) classified certain GBM cells according to metabolic activity (i.e. glycolysis or oxidative phosphorylation).[24,25]

In 2021, the World Health Organization (WHO) defined GBM as a grade IV astrocytoma, the highest grade of glioma.[26] Even with the addition of novel GBM subclassifications, the WHO has not changed its clinical guidelines on GBM classification since 2016.[27] Specifically, the WHO

classifies GBM according to isocitrate dehydrogenase 1 (IDH) mutation status as IDH mutant, IDH wildtype, or not otherwise specified. IDH mutant tumors typically contain R132H point mutations and comprise approximately 10% of all primary GBM cases and 80% of all recurrent GBM cases. IDH wildtype tumors are considered more lethal and have a later age of onset compared to mutant tumors. Both primary and recurrent IDH mutant tumors have higher instances of TP53 and ATRX gene mutations.[27] Interestingly, proneural GBM heavily consists of IDH and TP53 mutations and is, correspondingly, the least aggressive subtype of GBM identified by Verhaak *et al.* (2010). Yet, many IDH mutant cell lines used in culture have been classified as not only proneural, but also mesenchymal and classical. Thus, classifications by WHO and independent investigators are not absolutely correlative.

Therapeutic Developments

In 2005, Stupp *et al.* published a clinical trial building upon the previously established standard of care for GBM, which included maximal resection followed by courses of radiotherapy. Results demonstrated that groups having undergone resection and radiotherapy with concomitant administration of the temozolomide (TMZ) exhibited a median survival of 14.6 months compared to just 12.1 months survival by those not having received the chemotherapeutic.[6] TMZ is a lipophilic agent that alkylates DNA nucleotides to induce cellular apoptosis. Carmustine (intravenous or in implanted Gliadel™ wafers) and lomustine (oral) belong to a similar class of clinically approved alkylating agents that could be included in adjunction to the Stupp protocol especially in cases of advanced progression or recurrence.[28] Generally, such small molecule therapeutics are disadvantageous compared to their more modern, peptide- and immune-based counterparts for a variety of reasons including the lack of GBM cell specificity, poor penetrability or drug efflux at the blood-brain barrier (BBB), and the onset of antagonizing processes by cells

to the drug's mechanisms of action, such as O(6)-methylguanine-DNA methyltransferase expression reversing DNA methylation by TMZ.[29] Yet, resistance is not limited to small molecule inhibitors. For example, FDA-approved Bevacizumab is a monoclonal antibody therapy which binds free vascular endothelial growth factor (VEGF) to reduce peritumoral angiogenesis. However, GBM cell networks can surmount such treatment efforts by transdifferentiating into endothelial-like cells which fuse with peritumoral vasculature to continue circulation within the tumor mass.[30–32] Anti-angiogenic therapies may even potentiate GBM transdifferentiation to endothelial-like phenotypes.[33]

Immunotherapeutics may offer GBM-targeted therapies with limited interaction with healthy tissue. Chimeric antigen receptor (CAR) T cells have emerged as a means of re-educating autologous CD4+ and CD8+ T cells to initiate immune response upon binding specific cell-surface proteins.[34] While no CAR T cells have successfully passed Phase III clinical trials, those developed against EGFRvIII, HER2, and IL13Ra2 have generally exhibited promising amounts of tumor regression in several pre- or early-phase clinical studies.[35–37] GBM is characterized as a "cold" tumor, meaning tumors contain lower immune cell infiltration and activity at the tumor site relative to other neoplasms, which may explain the failure of monoclonal antibody administration against CTLA-4 and PD-1 in GBM compared to melanoma or non-small cell lung cancer.[38,39] Yet, vaccines to boost immune system recognition, infiltration, and clearance of GBM cells, which may, in turn, augment the effects of CAR T cells and/or antibodies.[39] Still, approximately 40-50% of GBM tumor mass consists of tumor associated macrophages (TAMs), which display high heterogeneity and play a critical role in GBM aggression.[40–42] Further characterization of TAMs could lead to the development of improved immunotherapeutics.[40]

Peptide drugs combine the advantages of small molecule drugs and immunotherapeutics, given their ability to interact with both intracellular and extracellular targets with high biological specificity.[43,44] Yet, inherent disadvantages of peptidic therapies include high rates of hydrolysis or proteolytic degradation when administered systemically as well as poor membrane permeability if not properly modified through, for example, poly-ethylene glycol (PEG) functionalization.[43,44] Peptide drugs developed against GBM primarily serve to inhibit protein function or protein-substrate interaction as part of a larger signaling cascade. For example, Chlorotoxin is a peptide derived from scorpion venom that both reduces chloride channel activation and matrix metalloproteinase-2 (MMP-2) activity – both critical elements for GBM invasion.[45] Although peptides and immunotherapeutics are generally GBM-specific, the challenges of poor BBB penetrability combined with immunosuppressive signaling and antigen-loss by GBM cells impede clinical translation of existing therapeutic candidates.

Tumor treating fields (TTFs) are the latest development to be added to the list of effective, FDA-approved therapeutics for GBM, which include TMZ, carmustine, lomustine, bevacizumab. In a phase III clinical trial published in 2017, Stupp *et al.* demonstrated an increased median survival time in patients treated with temozolomide and TTFs in combination (20.9 months) versus temozolomide alone (16.0 months).[46] The clinical repertoire of treatments against GBM is evidently limited compared to the disease heterogeneity elaborated upon in the previous section titled "Diagnostics and Classification". Developments of novel *in vitro* drug screening and cancer classification paradigms may accelerate the quantity of clinically approved therapeutics.

Interdependency of GBM Invasion and the Peri-Tumoral Microenvironment

Histopathological Profiling of GBM Invasion in Brain

GBM malignancy can in part be attributed to aggressive cell invasion, or migration, from the tumor periphery into surrounding parenchyma. Migrating cells exhibit a high likelihood of evading systemically or intratumorally administered therapeutics and initiating tumorigenesis at novel regions within the brain or, less commonly, spinal cord.[47,48] In GBM, extraneural metastases are more rare, occurring in less than two percent of GBM cases.[49] Rather, cells preferentially migrate along defined structures within the CNS, denoted as the secondary structures of Scherer.[50] Tumorigenesis conventionally occurs within white matter regions of the CNS, characterized as "highways" for GBM migration. Cells may spread to subpial surfaces and cortical tissues, where further differentiation may ensue.[47,50] Recurrent tumors and adjacent lesions typically occur within a 2 – 3 cm locus of the primary tumor edges, a region that usually presents as a hyperintensity on T2-FLAIR MRI.[15] This surrounding region is associated with high levels of edema and cellular infiltration attributed, in part, to ongoing angiogenesis and the presence of local vasculature which drive the degree and directionality of cellular invasion.[15,47]

Microenvironment-Driven Invasion

GBM invasion is a function of integrated chemical, mechanical, and electrical cues present within the peritumoral parenchyma. The local microenvironment around cells near the tumor periphery are nonuniform given their exposure to varying regions of CNS tissues along the tumor circumference.[47] Beyond the expression of glioblastoma stem cell (GSC) marker CD133, GBM edge cells from single patient samples display molecular properties matching both mesenchymal and proneural classifications, likely as an outcome of native microenvironmental cues.[51] Molecular profiling and lineage tracing of patient lines suggest GBM cell networks have highly dynamic transcriptional states that follow both hierarchical (directional) and plastic (stochastic) patterns of organization through time.[52,53] Exponential models and reaction-diffusion models typically used

to model bulk GBM spreading fail to account for the multitude of ECM-cell, cell-cell, and ECM-ECM interactions which effect GBM cell transcriptional states during not only migration, but also proliferation, senescence, and quiescence.[54,55] Mapping the effects of specific microenvironmental cues on GBM patient line phenotypes will lead to the development of more informed computational models to not only elucidate invasive phenotypes, but also perform drug screening, GBM characterization, and transitional forecasting of future cell states in the event of recurrent tumors.

Soluble factors secreted by both GBM and non-GBM cells along with direct cell-cell contacts act in tandem to promote cellular invasion.[47] GBM-mediated immunosuppression is essential to its infiltration of local tissue.[56] Suppression of local T cells, monocytes, and macrophages occurs via GBM cell secretion of prostaglandin E_2, TGF-b, and PD-L1-expressing extracellular vesicles among other factors.[56] TGF-b expression by tumor-associated macrophages (TAMs) further facilitates MMP-9-mediated invasion by GBM cells, which is likely augmented by further TGF-b and MMP-9 expression by local reactive microglia.[57,58] The presence of TGF-beta GBM-secreted TNF-alpha may induce a pro-inflammatory phenotype by local TAMs and astrocytes.[59] Angiogenesis adds an additional layer of complexity to the positive-feedback network between GBM, immune, and glial cells. VEGF secretion by GBM cells promotes local angiogenesis. The innate leakiness of the angiogenic and vasculogenic processes combined with the presence of VEGF, IL-6, and IL-1β facilitates the recruitment of TAMs as well as their pro-inflammatory transition.[57] Chemokines are another type of soluble factor actively secreted by GBM and non-GBM cells. CXCL12 is produced by endothelial cells, microglia, and TAMs and induces GBM cell chemotaxis.[60,61] CXCR4 is abundantly expressed by GBM cells along the tumor periphery. CXCL12 binding of CXCR4 elicits activation of the pro-migratory PI3K/AKT,

JAK/STAT, and ERK signaling networks within the peripheral cells.[62] Homocellular interactions between heterogeneous GBM cell types are also critical to invasive behaviors. Orthotopic xenografts of both core and peripheral tumor cells in mice yielded greater tumorigenesis and invasion than xenografts of peripheral cells alone, indicating cell-cell contacts or signaling between core and edge cells intensifies GBM's invasive capacity.[51]

The CNS extracellular matrix (ECM), comprising approximately 20% of the total brain volume, is composed of various proteoglycans, glycoproteins, glycosaminoglycans of varying molecular weights, chemical configurations, and concentrations.[63,64] GBM cells synthesize ECM molecules found in healthy brain and perivascular parenchyma, and a balance of local matrix deposition and degradation facilitates motility. Proteoglycans and glycosaminoglycans of heparan sulfate (HS), dermatan sulfate (DS), and chondroitin sulfate (CS) are commonly upregulated in GBM tissues and interact with local growth factors to drive GBM migration.[65]

Compared to lower grade CNS cancers, GBM tissue exhibits elevated concentrations of certain glycoproteins, such as vitronectin and laminin.[66] The presence of the arginylglycylaspartic acid (RGD) motif in glycoproteins, such as tenascin-c (TNC), fibronectin (FN), laminin (LN), type IV collagen (CN), and vitronectin (VN), enables GBM cell adhesion to local matrix via RGD-recognizing integrin receptors composed of heterodimerized alpha and beta subunits.[67] Integrins $\alpha_2 - \alpha_6$, α_v, β_1, β_3, and β_5 subunits are typically overexpressed in GBM versus normal tissues.[68,69] $\alpha_v\beta_5$ integrin binding FN or VN are the most well-studied integrin-ECM interactions responsible for GBM invasion. $\alpha_3\beta_1$ association with type IV CN is particularly critical to GBM cell perivascular migration.[69] Integrin receptors exhibit preferential binding to ECM proteins based on specific amino acids motifs present. For example, a_vb_5 binds both VN and FN while a_vb_3 binds only VN.[69] Moreover, protein-integrin interactions dictate GBM cell spreading morphologies. In

the case of TNC, culture of U251-MG glioma cells on TNC resulted in shorter processes and poorer spreading than cell seeded on FN.[70] Moreover, TNC-integrin interactions have been implicated in driving more mesenchymal-like GBM cell states.[71] Specifically in mesenchymal GBM cells, integrin signaling in GBM is associated with increased production of matrix metalloproteinase (MMP) and a disintegrin and metalloproteinase (ADAM).[47] Furthermore, integrin association with receptor tyrosine kinases (RTKs) likely amplify pro-invasive intracellular programs.[72] Interestingly under hypoxic conditions, U87-MG GBM cells gain motility and FAK/SRC signaling upon VN binding to integrin β_3/EGFRvIII complexes.[73] The presence of soluble factors may also spur pro-invasive matrix production, as in the case of IL-33-induced TN-C secretion by GBM cells.[74]

The physical structure of matrix, which includes topography, porosity, and viscoelasticity, also determines GBM cell adhesion and motility. Topographical guidance cues improve the potential for glioma cell dispersion. Several *in vitro* studies have reported improved cell adhesion and motility on aligned nanofibrous scaffolds versus randomly structured scaffolds.[75,76] Durotaxis, the phenomenon by which cells demonstrate motile preference towards stiffer or softer environments, is observable across cells and is critical to tissue organization during development. Porosity and shear pressure are variables of matrix stiffness and are regarded as deterministic features driving cell motility.[77]

Individual GBM patient lines exhibit unique mechanical thresholds for invasion. For instance, Grundy *et al.* reported patient line-dependent invasion by gliomaspheres grown on polyacrylamide hydrogels of varying elasticity moduli (0.2, 1.0, 8.0, and 50 kPa). The cellular invasion rate for patient lines JK2 and PR1 significantly increased from 0.2 to 1.0 kPa, while no differences were apparent for WK1, SJH1, and RN1. Moreover, cells derived from different

patients each presented a unique profile of invasion and spreading across stiffness levels.[78] Additionally, Marhuenda *et al.* demonstrated peak invasion by gliomaspheres seeded atop 3D-ex-polyacrylonitrile nanofiber scaffolds at 166 kPa stiffness in the range of 3, 166, 542, and 1260 kPa scaffolds.[79] Together, the findings by Grundy *et al.* and Marhuenda *et al.* suggest an optimal microenvironment stiffness is required to elicit cellular invasion in a patient line-dependent manner.

Models and Mechanisms of GBM Cell Migration

Cellular migration can be regarded as a mechanistically complex optimization problem such that excessive or suboptimal ECM-receptor and/or receptor-cytoskeletal engagement could stall directional cellular movement. Specifically, the complexity is a result of the myriad of protein-protein interactions and associated signaling required for migration mechanotransduction. Early work by Goodman *et al.* (1989) described a biphasic, or parabolic, relationship between laminin concentration and skeletal myoblast motility.[80] Subsequently, DiMilla *et al.* (1991) mathematically defined the biphasic relationship as the viscoelastic-solid (VS) model for tissue cells, building upon the general VS model by Schmid-Schonbein *et al.* (1981).[81] Briefly, a cell is compartmentalized into segments of size L/6, where L is the length of a cell. Each cell body compartment consists of Hookean springs (elasticity) and dashpots (viscosity) in parallel with a contractile element which is displaced according to the net contractile forces generated by adhesions at the lamellipodal (leading) and uropodal (trailing) ends of the cell.[82] The motor-clutch model, proposed by Chan and Odde (2008), is the latest adaptation of the VS model and has iteratively been refined since its initial publication.[83] In this model, springs labeled molecular clutches represent intracellular anchoring events of transmembrane receptors, such as integrin, to filamentous actin (F-actin) by anchoring/adapter proteins, such as ankyrin or the ezrin-radixin-

moesin complex (ERM). Motility can then be modeled as a function of retrograde force (pulling towards the soma) transmitted by myosin "motors" and anterograde force (pulling towards ECM) transmitted by the engagement of molecular "clutches" with extracellular substrates. Echoing work by Marhuenda *et al.* (2021) and Grundy *et al.* (2017), Bangasser *et al.* (2017) found optimal UG251 cell migration to occur on polyacrylamide gels with a Young's modulus of 100 kPa over the range of 0.05 – 200 kPa. Reducing the engagement of motors and clutches following the administration of blebbistatin and cyclic RGD (CRGD), respectively, reduced the optimal stiffness for motility and cell spreading. The combined administration of inhibitors resulted in greater (lesser) cell motility in environments of low (high) stiffness indicating optimal mechanics for ECM-driven invasion in single GBM cells are tunable according to their engagement of myosin motors and integrin clutches.[84]

The motor-clutch model is applicable to simulating both single and collective cell migration, the latter of which requires cell-cell interactions in addition to cell-ECM adhesions.[84–86] Collectively migrating cells may present morphologically as sheets, tubes, clusters, or strands, each with unique elements of adherens junction signaling and shear stress sensation which ultimately determine migratory polarity and velocity.[87] Moreover, cells within clusters are often distinguishable as leaders (migration front) or followers (migration rear), each with their own distinct molecular signaling profiles and specialized roles in organized migration.[87] While collective migration is an attribute of numerous cancers, its occurrence in GBM remains controversial and may be a phenomenon exclusively to *in vitro* spheroid cultures.[88–90]

Proteomic profiling of GBM cells has revealed the PI3K/AKT, MAPK/ERK, RhoA/ROCK, and/or JAK/STAT3 signaling axes primarily regulate both invasion and proliferation.[47,91–93] However, the "Go or Grow" hypothesis suggests GBM cell programs for

proliferation and migration cannot occur simultaneously in single cells – of note, this has not been described for collectively migrating cells.[94] Multivariate modeling approaches have been deployed to elucidate which ECM features, in conjunction with key proteomic initiators and regulators, independently drive migration or proliferation. Agent-based and continuum *in silico* models are commonly deployed to simulate single and collective cell invasion, respectively.[95] Building on the cell-ECM adhesions present in the motor-clutch model of cell invasion, novel *in silico* models include variables such as local oxygen saturation, angiogenesis, cellular metabolic activity, and cell-cell adhesions.[55,96] Frieboes *et al.* (2006) modeled morphological and spatial distributions of collectively migrating GBM cells using reaction-diffusion equations quantifying angiogenesis, matrix degradation, and tumor cell density.[97] Martinez-Gonzalez *et al.* (2012) mathematically modeled the migration patterns of hypoxic and normoxic glioma cells present within pseudopalisading regions of GBM.[98] One model even identified the dichotomy of proliferation and migration was not apparent in environments with high concentrations of growth factors.[96] Complementary *in vitro* studies validate the phenomenologically realistic outcomes of *in silico* models. "Chain-like" and "disc-like" invasion patterns observed in ECM gel-encapsulated U87-MG tumorspheres were mathematically modeled according to concentrations of nutrients and cell-secreted chemotactic signals in the culture media.[99] As such, combined *in silico* and *in vitro* methods offer new modes of characterizing GBM invasion.

Infiltrating cells are conventionally classified as mesenchymal or ameboid based on apparent morphological and molecular profiles.[100] Mesenchymal GBM cells have an elongated morphology coupled with high levels of cell-ECM interactions which typically entail balanced action of matrix degradation proteins, such as MMPs and ADAMs, and matrix deposition.[101,102] In an ameboid state, GBM cells exhibit a rounded morphology and predominantly RhoA-ROCK axis

signaling.[93,101] Moreover, their reduced cell-ECM interactions are substituted with mechanisms to regulate cell volume via hydrostatic pressure changes. In fact, migrating GBM cells reduce their volume by 30%. The hydrodynamic model of GBM ameboid invasion explains ionic efflux and influx by Na-K-Cl co-transporter channels (NKCCs) contributes to cell volume regulation by creating hypo- and hypertonic intracellular environments, respectively.[101,103] This, in turn, allows GBM cells to maneuver local matrix as well as initiate EGFR-mediated invasion signaling.[101] A further complication to the development of therapeutic directed towards either ameboid or mesenchymal GBM cells is that migrating cells may transition between mesenchymal and ameboid states as a result of exogenous, pharmacological intervention or endogenous, environment-induced transdifferentiation.[104] Administration of Rac1 inhibitor, NSC23766, to U87-MG cells encapsulated in 3D hydrogels resulted in an ameboid-to-mesenchymal transition (AMT) of migration.[105] Conversely, administration of pan-MMP inhibitor, Ilomistat, resulted in mesenchymal-to-ameboid transition (MAT) by U251 and T98G cells.[106] Moreover, MAT could, in part, explain the low efficacy of Cilengitide given when GBM cells transitioned to ameboid-like invasion have lesser reliance on ECM engagements through integrins. With sufficient disruption of cell-cell adhesions, collectively migrating cells may also switch into an ameboid, single cell migratory phenotype. While such collective-to-ameboid transition (CAT) has been described in breast and head and neck squamous cell cancers, it has not been described in GBM.[107]

Epithelial-to-mesenchymal transition (EMT) is the acquisition of migratory capacity by originally stationary cancer cells. EMT and its converse, mesenchymal-to-epithelial transition (MET), are cell differentiation paradigms apparent in various epithelial cancers including prostatic, hepatic, and pancreatic.[108] Whether similar transitions arise in GBM, a non-epithelial cancer, remains unclear.[109–112] Rather, a proneural-to-mesenchymal transition (PMT) may explain gained

motility by GBM cells along the peritumoral edge. While the core mechanisms of PMT are undetermined, transitioned cells present upregulated expression of vimentin, N-cadherin, YKL-40, hepatocyte growth factor receptor, and cluster of differentiation receptor 44 (CD44).[112] Various reports have suggested that radio- and chemo-therapy may induce PMT, causing originally proneural tumors to assume a mesenchymal phenotype upon recurrence.[113,114] While many investigators have characterized the influence of specific matrix components on proneural and mesenchymal GBM cell motility in isolation, there is virtually no work investigating ECM-induced PMT. However, work by Renner *et al.* (2016) suggests a similar EMT-like shift may occur in GSCs via the FN-$\alpha_5\beta_1$ integrin binding axis.[115] Specifically, this transition was termed a glial-to-mesenchymal, echoing the aforementioned characterization of radial glial-like GSCs cells by Bhaudri *et al.* (2020).[24,115]

Hyaluronic Acid-Mediated GBM Invasion

Role of Hyaluronic Acid in GBM Invasion

Hyaluronic acid (HA), or hyaluronan, is a negatively charged glycosaminoglycan of repeating D-glucuronic acid and N-acetyl-D-glucosamine disaccharide subunits and presents from oligomeric to high-molecular-weight (HMW) forms in the CNS.[116–118] Typically, HA is integral to key physiological processes including neural stem/progenitor cell growth and differentiation, leukocyte trafficking, wound healing, and tissue organization.[116,119,120] Within the CNS, HMW HA creates an immobilized, 3D network with which soluble proteins, membranous proteoglycans, and linker proteins may interact to drive cellular behavior.[116,117] Low-molecular weight and oligomeric forms are also present as soluble components in the ECM; however, how HA chain size contributes to GBM progression remains unknown. In the 1970s, two seminal papers introduced HA's

potentially malignant in GBM. In 1970, Dorfman and Ho successfully identified and isolated mucopolysaccharides, including HA, chondroitin sulfate, and heparan sulfate, in glioma cell cultures.[121] Subsequently, in 1978, Glimelius *et al*. reported greater HA production in cultures of glioma cells compared to healthy cells and provided the first discussion of its potential role in GBM malignancy.[122] Today, HA is recognized as a key regulator of GBM cell proliferation, invasion, survival, and therapeutic resistance through its interaction with receptors including CD44 and CD168 (also known as the Receptor for Hyaluronan Mediated Motility (RHAMM), LYVE-1, or HMMR1) and potentially other HA binding proteins.[116,118] Histopathological and transcriptomic characterizations of resected tumors have indicated HA along with its synthases and degradation enzymes positively correlate with glioma aggression and lethality in patients.[118,123–127] Consequently, HA synthesis inhibitors, such as 4-MU, and oligomeric competitive binding inhibitors have been proposed therapeutics to HA-driven malignancy.[128,129] Unfortunately, it is poorly understood how HA-CD44 and HA-RHAMM interactions affect migration, thus, diminishing the translational likelihood of *in vitro* developments.[116] No clinically approved therapeutics targeting the HA signaling exist for GBM. Although several nanoparticle systems are in development for targeting GBM tumors by binding HA.[130–132]

HA-CD44 Interactions

CD44 is a glycosylated transmembrane receptor with functional significance in neural and immune tissues with processes such as dendritic spine plasticity[133] or leukocyte trafficking.[134] In its standard conformation, the CD44 receptor is comprised of a ten exon sequence coding an extracellular ligand binding domain, transmembrane region, and cytoplasmic tail. Nine exons coding extracellular domains can be additionally inserted, forming variant subtypes of CD44. CD44 activity has been linked to cellular resistance phenotypes across cancers, including breast,

lung, and colon carcinoma. Similar to HA, CD44 expression in GBM patient tumor samples positively correlates with glioma grade.[135–139] Interestingly, Wei *et al.* (2010) reported that in the cohort with the highest grade glioma, additional CD44 expression beyond the median expression value resulted in diminished tumor aggression and greater patient survivability likelihood.[140,141] In light of this finding, Klank *et al.* (2017) investigated the effects CD44 status on tumor invasiveness in NrasG12V/SV40LgT glioma mouse models and identified a concave-up, biphasic relationship between CD44 expression and single cell motility in resected tumors. Specifically, cell motility was similar in CD44 knock-out mice (low CD44) and mice producing CD44 in excess (high CD44); however, migration in both cases was significantly reduced compared to wildtype mice (intermediate CD44). Survivability and CD44 expression collected from both mice and TCGA-derived human GBM datasets also following a biphasic trend.[141] Thus, the motor-clutch hypothesis explaining integrin-mediated GBM cell motility [may also be applicable to CD44-mediated migration.[84,85]

Inhibition or complete knock out of CD44 would not inform its applicability to the motor-clutch model given the heterotypic nature of its activity. Extracellularly, CD44 also binds ligands other than HA, such as osteopontin and chondroitin sulfate, and associates with peri-membranous proteases or other glycoproteins.[123,142] Specifically, CD44 may cluster with RTKs, integrins, or other local CD44 receptors for enhanced cell signaling and matrix adhesions, while MMPs and ADAMs can conversely cleave and solubilize the ectodomain of CD44, consequently disrupting matrix adhesions.[142] Moreover, the FAK or Src binding interactions with the intracellular domain (ICD) of CD44 may initiate Rho-, ERK1/2-, or AKT-associated signaling.[123] The ICD also forms cytoskeletal adhesions via anchoring proteins, such as the ezrin-radixin-moesin complex (ERM) or ankyrin.[143,144]

The ERM Domain

Given ERM is a molecular clutch mediating the engagement of CD44 and filamentous actin (F-actin), directly targeting ERM could reduce migration driven by HA-CD44 interactions.[144] Serially inhibiting ERM activity could inform how reductions in the clutch protein's activity, and thus cellular membrane-to-cytoskeletal adhesions, could modulate cellular migration. Bulut *et al.* (2012) introduced a small molecular inhibitor directly targeting ERM, NSC668394, which inhibited the invasion of both osteosarcoma cells *in vitro* and embryonic zebrafish cells *in vivo*.[145] Since then, many have studied ERM-associated mechanotransduction and signaling in osteosarcoma and non-cancerous cell types, such as endothelial cells.[146–151] While increased ERM expression has generally correlated with higher GBM malignancy,[152] only two studies have systematically evaluated the consequences of directly modulating ERM activity in GBM cells, both utilizing clonal lines. Qin *et al.* (2014) mitigated radixin expression using RNA interference and found reduced tumor growth in RNA silenced, orthotopically implanted GBM cells.[153] However, their study performed a global shutdown of radixin RNA translation, without considering the apparent dose-dependent effects when inhibiting molecular clutch proteins, such as integrins. Zhu *et al.* (2013) considered dose-dependent effects, finding inhibition of moesin-CD44 binding with CD44pep and radixin-CD44 binding with DX-52-1 resulted in stark reductions in gliomasphere sizes and GBM cell proliferation in culture.[154] Generally, greater inhibition resulted in lesser proliferation. However, it is important to note that neither Quin *et al*. (2014) nor Zhu *et al.* (2013) utilized 3D culture methods. The concave-up, biphasic relationship of CD44 activity and migration, as reported by Klank *et al.* (2017) who used 3D brain slice cultures, was not apparent by modulating CD44-moesin or CD44-radixin binding interactions.[141] To date, there are no studies regarding the relationship of the HA-CD44-ERM-Actin axis and GBM cellular

invasion using 3D culture methods and patient-derived cell lines, which could provide more translational findings, as elaborated on in future sections.

HA-RHAMM Interactions

RHAMM expression is correlated with greater GBM malignancy and is a key factor in driving tumorigenesis and inflammatory diseases, like osteoarthritis or lung fibrosis.[123] Extracellularly, RHAMM binds HA with its BX7B amino acid motif. Lacking a transmembrane domain, it is typically anchored to the membrane via glycosyl-phosphatidylinositol moieties.[123] Moreover, RHAMM may indirectly participate in ERK- and SRC-associated signaling through interactions with local CD44 and RTKs.[116,123]

Unlike CD44, RHAMM mechanisms and functions pertaining to GBM invasion have not been well characterized; however, it is known RHAMM typically localizes in perimembranous and perinuclear domains of cells in general and is involved in mediating cellular migration and mitosis.[123,129] In the first study of HA-RHAMM interactions, Akiyama *et al.* (2001) reported RHAMM of 85 kDa and 58 kDa isotypes are ubiquitously expressed across glioma cell lines and soluble peptides inhibited migration on HA-coated surfaces.[155] Pibuel *et al.* (2021) most recently studied HA-RHAMM interactions in GBM by performing wound closure assays using GBM cells on 2D, HA-coated surfaces. Anti-CD44 and anti-RHAMM antibodies acted in similar fashion, reducing cellular migration and hence wound closure.[129]

Anti-RHAMM antibodies and peptides are both potential therapeutics options for GBM; however, both have associated risks given the poorly studied nature of HA-RHAMM interactions.[116] Importantly, we found no studies on HA-RHAMM interaction in GBM that used 3D culture or *in vivo* methods. RHAMM-mimetic peptides that bind HA, like P15-1, mimic the structural and chemical properties of RHAMM and have been used to interrogate the relationships

of HA-RHAMM binding and cell phenotypes.[123,156,157] However, RHAMM-mimetic peptides like P15-1 disrupt not only HA-RHAMM but also HA-CD44 cellular binding events, which may introduce confound outcomes when studying the nature of GBM phenotypes given the typically high expressions of both CD44 and RHAMM. Esguerra *et al.* (2015) developed high affinity, HA-mimetic peptides which uniquely bind RHAMM. Using a TRITC-collagen degradation assay, the investigators found peptide 14a with amino acid sequence 'FTEAESNMNDLV' reduced the invasion of PC3MLN4 prostate cancer cells by approximately 80%.[158] The peptide would serve as a valuable candidate to specifically study the role of extracellular RHAMM in GBM biology.

In Vitro Modeling of HA-Mediated GBM Invasion

While *in vivo* studies of GBM typically involving murine models are most representative of the nascent CNS microenvironment, they are expensive, lengthy, and laborious in nature; moreover, experimentally decoupling the effects of the various physical, chemical, and electrical cues present within the tumor niche becomes impractical *in vivo*.[159,160] Thus, *in vitro* systems with tunable, physiologically relevant physical and chemical features have been deployed to study GBM invasion in a biomimetic manner.[159] In general, bioengineered systems are more representative of *in vivo* cell behavior compared conventional cell culture methods using non-coated plastic or glass surfaces.[159–162] Such bioengineered systems may be two-dimensional (2D), cells are interfaced with surfaces, or three-dimensional (3D), cells are encapsulated in scaffolds, and have been applied to study the dynamics of single cell and gliomasphere invasion.[159] Studies utilizing HA-incorporated 2D and 3D models to specifically investigate or report GBM invasion are limited.

<u>2D Systems</u>

To study HA-driven motility using a 2D system approach, GBM cells may be seeded atop surfaces pre-laden with HA. As one of the earliest studies, Akiyama *et al.* (2001) seeded clonal GBM cell lines in wells coated with 1 mg/mL HA and allowed to spread over the course of 7-days. While the addition of anti-CD44 antibodies did not hinder cell migration, peptides directed towards RHAMM reduced cellular invasion across multiple clonal lines, thus, informing RHAMM as a critical target for reducing GBM invasion.[155] A more recent study by Erickson *et al.* (2019) deployed a composite of HA with chitosan-polycaprolactone (C-PCL) polyblend nanofibers to study the invasion of U87-MG cells. Cells seeded on 0.50% HA-C-PCL surfaces exhibited the greatest displacement and migratory rate compared to 0.10% HA-C-PCL and uncoated polystyrene plates. Given the inclusion of PCL, this model could be deployed in the future to study effects of conductance on GBM spread while incorporating HA and chitosan - potentially informing TTFs' mechanisms of action.

Besides coating plates, HA-modified Boyden chambers to perform transwell assays are utilized as an additional form of 2D study. Early studies identified incorporation of HA into a Matrigel coating on the bottom of a transwell facilitated invasion of GBM cells at a greater rate through micropores.[163,164] Fascinatingly, Rao *et al.* (1993) added concentrations of HA ranging from 0 to 1000 μg/mL and identified the greatest percentage of invading cells occurred at 200 μg/mL. This is the first-known identification of a potential biphasic relationship between HA concentration and GBM cell invasion.[163] Kim and Kumar 2014 later performed a transwell assay having coated wells with 2 mg/mL of HMW HA. HA functionalized with RGD-containing peptides yielded greater cell invasion compared to HA alone, indicating RGD-integrins interactions are synergistic to HA-CD44 or HA-RHAMM interactions in promoting migration.[165]

Overall, invasive phenotypes in GBM starkly vary when seeded on uncoated surfaces versus HA-coated surfaces. For example, while U87-MG invasion was greater than other clonal lines using a scratch wound assay, U343-MG had higher when cultured on HA-based hydrogels.[166] Moreover, U118-MG cells seeded on chitosan-HA hydrogels expressed elevated levels of TWIST, MMP-2, and MMP-9 mRNA, CD44 and Nestin protein, and overall invasion.[167] Thus, HA affects GBM cell invasive phenotypes and should be incorporated in bioengineered systems to study invasion.

3D Systems

Given tumor cells navigate a 3D environment within CNS tissues, engineering 3D systems can better recapitulate the chemical, fluidic, and physical features of the nascent tumor microenvironment (TME) compared to 2D systems.[159] Hermida *et al*. (2019) found U87-MG cells encapsulated in bioprinted matrices consisting of RGD-alginate, HA, and collagen I demonstrated greater resistance to chemotherapeutics compared to 2D monolayer culture.[168] Complementarily, Xiao *et al.* (2018) reported patient-derived GSs encapsulated in hydrogels with 0.50% (w/v) HA exhibited greater resistance to the RTK inhibitor erlotinib compared to gliomasphere (GS) culture in media alone.[169] Beyond drug resistant phenotypes, cell-matrix adhesion phenotypes vary between 2D and 3D systems. For example, focal adhesions presented by cells in 2D systems are not present when cells are encapsulated in 3D scaffolds.[170,171]

The initial 3D systems used to evaluate GBM invasion *in vitro* occurred between 1970-1980 included excised fragments of animal tissues, such as chick heart fragments or smooth muscle cells. Notable is the study of de Ridder *et al.* (1987) which documented the infiltration of human clonal line gliomaspheres into chick heart fragments.[172] Soon, such cultures would be replaced by Matrigel, a matrix scaffold derived from Engelbreth-Holm-Swarm mouse sarcoma cells. Matrigel

contains an abundance of glycoproteins (e.g. laminin, collagen) and glycosaminoglycans (e.g. chondroitin sulfate) present within most tumorigenic environments.[173,174] And while it has been used as a 3D system to study GBM cell migration, it has two major disadvantages. First, given it originates from sarcoma tissues, it lacks key components specific to the GBM TME like HMW HA. Second, the pre-existing matrix components of Matrigel cannot be readily removed or substituted, making mechanochemical modifications difficult.[174]

3D HA Hydrogels

Chemically defined hydrogels address Matrigel's shortcomings as they are an aqueous scaffold that may be mechanochemically tuned to resemble the native CNS and GBM pericellular environment. Hydrogels are networks of hydrophilic polymers (e.g. HA) covalently or non-covalently cross-linked.[175] HA-containing, or HA-based, hydrogels have most commonly been utilized to study GBM motility. Most HA-based hydrogels follow thioester bond formation chemistry by covalently crosslinking thiolated HA with other moieties functionalized with maleimide or acrylate.[66,169,176–178]

Ananthanarayanan *et al*. (2011) pioneered the use of HA-based hydrogels to study GBM mechanobiology. They encapsulated clonal GBM line spheroids in scaffolds of methacrylate functionalized HA and thiolated RGD motif-containing peptides (RGD) using a DL-dithiothreitol crosslinker. All cell lines displayed greater invasiveness in 3 weight percent (wt%) HA matrices of softer 150 Pa elasticity than 5 wt% HA matrices of stiffer 5 kPa elasticity. However, the morphologies and degrees of invasiveness varied between individual cell lines.[179] Rao *et al.* (2013) developed composite hydrogels consisting of collagen IV and HA. With increasing concentrations of HA in the range of 0 – 2 wt%, single cell migration velocity decreased.[178]

The aforementioned studies and the majority of studies investigating HA concentration-dependent GBM invasion in hydrogels utilize scaffolds of varying diffusivity or poroelasticity. Tuning the mechanical characteristics of hydrogels to be equal across varying concentrations of HA is critical to determine whether changes in chemical concentration, alone, drive changes in cell behavior, given that local tissue mechanics heavily influence cell phenotypes. For example, using HA-RGD hydrogels based on maleimide-thiol chemistry, Xiao *et al.* (2018) demonstrated patient-derived GBM cells acquired resistance to erlotinib treatment at slower rates when encapsulated in 0.50% (w/v) HA hydrogels of 2 kPa than 1 kPa compressive moduli.[169] Moreover, Wang *et al.* (2021) demonstrated greater storage moduli of HA-RGD hydrogels, based on thiol-ene photo-click chemistry, resulted in lesser GS invasion and greater resistance to TMZ. Notably, hydrogels utilizing thiol-ene photo click chemistry reactions are more favorable than thiol-maleimide and thiol-acrylate reactions given their faster reaction rates and more stable network conformations.[180]

CD44-mediated adhesions are critical for migration of GBM cells interfaced with HA-RGD scaffolds. Kim and Kumar (2014) detailed the nuances of HA-CD44 and RGD-Integrin interactions driving GBM single cell migration when seed on top of hydrogel surfaces. While migration speed steadily increased with increasing concentrations of RGD peptides (5 – 100 μM) in the hydrogels, this effect was abrogated following the RNAi knockdown of CD44. Moreover, lamellipodia densities were significantly less in HA-only hydrogels compared to HA-RGD hydrogels, indicating both HA and RGD interactions were necessary for the formation of stable adhesions and cellular migration.[165,181] In a 3D culture study by Wolf *et al.* (2020), single cells extended “microtentacles” and form adhesions via CD44 at a far slower rate than cells interfaced in 2D with the HA-RGD hydrogels. Moreover, the leading edge of microtubules were observed to

be enriched with actin and myosin cytoskeletons, indicative of active motor-clutch dynamics.[182] The IQGAP1/CLIP170 complex was targeted via CRISPR/Cas9-mediated knock out of IQGAP1 given the complex participated in anchoring CD44, actin, and microtubules. Knockout resulted in fewer cells with microtentacles of >10 μm length and greater blebbing along the edge of single cells. Spreading still occurred on hydrogel surfaces, but cells exhibited an ameboid-like, circular morphology during migration.[182] The nature of inhibiting IQGAP1/CLIP170 complex activity was not further explored in 3D invasion; however, the same HA and RGD interactions driving 2D migration are also critical for 3D invasion. Xiao *et al.* (2020) encapsulated patient-derived gliomaspheres (GSs) in 0.50% (w/v) HA hydrogels based on maleimide-thiol chemistry and similar poroelastic properties. Cell-ECM adhesions within the HA-RGD matrices were critical for CD44 and integrin αV colocalization throughout GSs. Moreover, lentiviral knockdowns of CD44 and integrin αV resulted in greater cell death and loss of invasive phenotypes by GSs typically expressed in wildtype conditions.[181]

CHAPTER 2: MOTIVATION

Hyaluronic acid (HA) hydrogels are mechano-chemically tunable, biomimetic, *in vitro* models with which glioblastoma (GBM) phenotypes and response to therapeutics can be characterized in a patient-specific manner. Studies of HA concentration-dependent GBM invasion generally evaluate migration phenotypes in the range of 1% - 5% (w/v) HA. Previous works by Pedron *et al.* have consistently demonstrated minute changes in HA concentration within the range of 0%–1% (w/v) HA has substantial effects on gene expression profiles of pro-migratory factors.[183–185] Yet, no studies have morphologically characterized potential variations in GBM migratory phenotypes within the minute, 0%–1% (w/v) HA range which is also more representative of physiological concentrations of HA found in mammalian brain.[186,187] Furthermore, to better mimic cell-cell interactions between GBM cells, we will encapsulate gliomaspheres (GS) of our patient-derived lines and defined cell densities within the hydrogels. Similar to past findings, we hypothesize increased HA concentration will spur greater GS invasion into matrix. However, we remain curious whether the certain lines may display biphasic relationship between HA concentration and motility given findings by Pedron *et al.* (2013) and Klank *et al.* (2017).[141,183]

Given a more thorough understanding of how HA receptors function to promote migration is needed to develop novel therapeutics against invasion, we will evaluate potential variations in cell interaction with surrounding matrix through cluster of differentiation 44 (CD44) and receptor for hyaluronan mediated motility (RHAMM). Specifically, we will investigate potential differences in HA receptor expression between patient lines and HA concentration conditions. We will further block HA-RHAMM binding using the peptide developed by Esguerra *et al.* (2015) to investigate effects on GBM migration in a 3D environment. We look to build upon 2D system studies of RHAMM biology in GBM, such as those by Akiyama *et al.* (2001) and Pibuel *et al.*

(2021), by blocking HA-RHAMM binding in cells encapsulated in our 3D hydrogels. To specifically block extracellular HA-RHAMM interactions, we will use the peptide developed by Esguerra *et al.* (2015). Moreover, our system will include 3D cell-cell and cell-matrix interactions, more representative of in vivo conditions. Thus, we hope our findings better inform the effects of extracellular RHAMM inhibition in vivo.

While CD44 biology has been more thoroughly interrogated compared to RHAMM, its multifaceted nature of driving cellular phenotypes requires a more nuanced understanding of its mechanisms of driving GBM motility, such as through cytoskeletal engagement, kinase signaling, or extracellular cleavage. By seeding GBM cells on HA-RGD hydrogels, Kim and Kumar (2014) found CD44 could be a mechanosensitive signaling receptor given changes in hydrogel stiffnesses. Klank *et al.* (2017) later demonstrated that excess CD44 expression in a single GBM cell line resulted in less aggressive tumors *in vivo* and lesser invasion in brain slice cultures compared to cells with wildtype (intermediate) levels of CD44 expression. These findings further implicate CD44 as a mechanotransduction receptor that is not only sensitive to local tissue mechanics, but also matrix interactions. To further explore CD44's potential as a mechanosensitive receptor in the context of varied HA concentration, we will target the ezrin-radixin-moesin complex (ERM), an anchoring protein bindings CD44 to filamentous actin, using the small molecule inhibitor developed by Bulut *et al.* (2012). By administering varying concentrations of inhibitor to GSs encapsulated in environments with varying concentrations of HA, we seek to better understand how varying the strengths of receptor-cytoskeleton bindings, or molecular clutches, can affect cell motility in the context of potentially varied HA-receptor interactions.

Previous investigators have not successfully controlled for mechanical properties across hydrogels of varied HA content, introducing confounding variables in the studies of HA

concentration effects on GBM invasion. Fabricating HA hydrogels using our thiol-ene photo-click chemistry-based formulation offers the ability to control for HA content and mechanics independently given the addition of 4-arm thiolated polyethylene-glycol macromolecules. Moreover, by encapsulating GSs within hydrogels, we can study GBM cell invasiveness in the presence of both 3D cell-ECM and cell-cell interactions.

We hope our findings provide greater motivation to study GBM biology using highly tunable, 3D biomimetic systems as described. Beyond studying GBM biology, our hydrogel technology has clinical applicability as a theranostic tool, as elaborated on by Liang *et al.* (in publication). In a broader context, the system presented in our studies can be expanded to both study or diagnose patient-derived GBM cell phenotypes over a range of peptide types or concentrations, HA molecular weights and concentrations, as well as storage moduli representative of corresponding GBM microenvironment features. Moreover, various therapeutics may be screened for efficacy against individual patient cells encapsulated in the diversity of mechanochemical contexts.

CHAPTER 3: METHODS

HA Thiolation and Hydrogel Fabrication

Approximately 4.5-6% of D-glucuronic acid carboxylic acid groups in the repeating hyaluronic acid (HA) disaccharide chain (M_W = 700kDa, LifeCore Biomedical) was thiolated via carbodiimide chemistry (*N*-hydroxysuccinimide (NHS); 1-ethyl-3-[3-dimethylaminpropyl] (EDC)), and reaction with cysteamine (Sigma-Aldrich) to yield HA-SH. Following reduction with Dithiothreitol (DTT) and subsequent dialysis for purification, proton nuclear magnetic resonance spectroscopy and an Ellman's Test were conducted to verify HA-SH thiolation percentage.

Prior to gelation, compounds were buffered in 4-(2-hydroxyethyl)-1-piperazineethanesulfonic acid (HEPES; Fischer BioReagents) with Hank's Buffer Salt Solution (HBSS; Sigma-Aldrich) to yield the following solution densities: 10 mg/mL HA-SH; 100 mg/mL thiol-terminated 4-arm polyethylene glycol (PEG-SH, M_W = 20kDa, Laysan Bio); 100 mg/mL 8-arm polyethylene glycol norbornene (PEG-Norb; M_W = 20kDa, Laysan Bio); 4mM thiolated RGD peptide (RGD-SH, 'GCGYGRGDSPG'; GenScript); 1-3 mg/mL Lithium phenyl-2,4,6-trimethylbenzoylphosphinate (LAP; Sigma-Aldrich). Prepared gel solutions contained 0.25% w/v LAP, 0.25 mM RGD-SH, and either 0.10, 0.25, 0.50, or 0.75 percent weight per volume (w/v) of HA-SH.

The crosslink factor was empirically determined to provide sufficient crosslinking and avoid the thiol-ene click chemistry termination reaction series to ensue. The remainder of the formulation consisted of HEPES:HBSS, which was added to achieve a desired volume. 30 mL of finalized gel solutions were added to 30 mm^3 cylindrical slots in silicone molds. These solutions were then exposed to 3.95 – 4.05 mW/cm^2magnitude of 365 nm UV radiation for 15 seconds to

initiate gelation. Gel products were removed from molds and maintained in phosphate buffered saline (PBS, Dulbecco's PBS) until characterization.

Hydrogel Characterization

Mechanical Property Testing

Hydrogel storage moduli (G') were measured using a discovery hybrid rheometer-2 (DHR-2, TA Instruments) at 37 °C. Frequency sweeps were performed under 1% constant strain in the range of 0.1 to 1.0 Hz. Storage modulus of each sample was calculated as the average value of the linear region of the storage curve from the frequency sweep plot. For statistical analysis, 3 separate measurements were taken in which 5 samples from each condition were measured.

Mass-Swelling Ratio

Fabricated hydrogels without cells were weighed using a scale ($Weight_{i,1}$) and subsequently incubated in 1X PBS at 37°C and 5% CO_2. After 24 hours, the weight of each hydrogel was again recorded ($Weight_{i,2}$). The formula below was used to calculate the mass swelling ratio per hydrogel.

$$Mass\ Swelling\ Ratio = \frac{Weight_{i,2}}{Weight_{i,1}}$$

Diffusion Modeling

For diffusion measurements, we used fluorescence recovery after photo-bleaching (FRAP). Hydrogels were incubated with fluorescein isothiocyanate-dextran (FITC-Dextran) solution (0.33 mg/ml in PBS) overnight. Five pre-bleach images were taken at 10% power of 488 laser under a SP5 laser scanning confocal microscope (Leica). In order to bleach, 30 μm region of hydrogels were exposed to a 488 laser (600 μm pinhole) for 20 seconds. 1000 frame of images were taken as post bleached images. t_d values (time for half recover) were calculated from fluorescence recovery graphs. Diffusion coefficients (D_e) were calculated using simplified Fick's law[188]:

$$\frac{M_t}{M_{inf}} = 2\left[\frac{D_e t}{\pi x^2}\right]^{1/2}$$

Patient-Derived GBM Cell Culture

GS54, HK177, HK217, and HK408 were the patient-derived GBM lines used in this study. Patient line GS54 (passages 14 – 18) and lines HK177 (passages 15 – 17), HK217 (passages 11 – 22), and HK408 (passages 15 – 24) were generously provided by Dr. David Nathanson (UCLA, GS54) and Dr. Harley Kornblum (UCLA, HK lines), respectively. While all patient lines were sphere-forming, HK217, HK177, and GS54 were in suspension while HK408 was adhesive. All GBM cells were cultured in T-75 flasks with complete media which consisted of DMEM/F12 with L-glutamine and 15mM HEPES in 1X Gem21, 0.2% Normocin, 20 ng/mL human fibroblast growth factor-basic (hFGF-2), 50 ng/mL human epidermal growth factor (hEGF), and 25 mg/mL heparin. Both 2D and 3D cultures were incubated in 5% CO_2 and 37°C throughout the course of all experiments.

For passaging, cells were centrifuged at 400g for 5 minutes and resuspended in 1X TrypLE (Life Technologies) for no longer than 5 minutes. Following the addition of 4 mL of complete media, cells were again centrifuged at 400g for 5 minutes. As final steps, cells were reconstituted in 1 mL media, filtered using a 40 mm cell strainer, and manually counted by use of a hemocytometer. A 100,000 cells/mL cell seeding density for culturing was maintained following each passage.

Gliomasphere (GS) Culture and 3D Encapsulation

Following passaging, single GBM cells were seeded (600,000 cells/well) into individual wells of a 24-well AggreWell™ plate pre-coated with 5% Pluronic in 1X PBS solution. Centrifugation (300 g for 3 minutes) and incubation (5% CO_2 and 37°C) followed. After 18 hours, GSs were prepared for suspension culture or 3D encapsulation within hydrogels.

For suspension culture, GSs were harvested using a p1000 pipette and resuspended them in 10 mL media over the course of experiments. For 3D encapsulation, GSs were similarly harvested and resuspended in prepared gel solutions (0.10% – 0.75% w/v) (see "HA Thiolation and Hydrogel Fabrication" in Methods). Gelation of mixed gel and GS solutions ensued as previously described in the methods and yielded the 3D hydrogels containing the patient-derived GBM spheroids.

Microscopy and Quantification of Invasion

Phase contrast images were obtained using the Zeiss Axio-Observer microscope and Zen software, and image analysis was performed using the ImageJ software. GS invasion was quantified by shape factor, a ratio of a GS's area to its squared perimeter, and migration length, the maximum protrusion radius from a GS's periphery. Perimeter and area values were obtained by manually tracing GSs, and shape factor was calculated using the following formula:

$$\text{Shape Factor} = \frac{4\pi A}{P^2}$$

Cryopreservation, Immunostaining, and Confocal Imaging

Hydrogels underwent fixation in 4% paraformaldehyde (PFA) in 1X PBS solution for 1 hour at room temperature. Then followed sequential incubations in solutions of 5% and 20% sucrose in 1X PBS for 1 hour time periods. After leaving the hydrogels in 20% sucrose solutions overnight at 4°C, hydrogels were embedded in 20% sucrose in preservation molds containing 1X Optimal Cutting Temperature (OCT) compound for 3 hours at 4°C and flash frozen in 2-methylbutane. Frozen hydrogels were cut into 12 mm sections using the Leica Cryostat.

Sections were fixed in 4% PFA in 1X PBS solution for 12 minutes before being subsequently washed using 0.10% tween-20 in 1X tris-buffered saline (TBS-T) and blocked with 4% bovine serum albumin (BSA) in 1X TBS-T for 1 hour in room temperature. Then, sections

were incubated at 4°C overnight with primary antibodies for CD44 (1:400, Cell Signaling Technology), RHAMM (1:400, Novus Biologicals), Ezrin (1:200 Cell Signaling Technology), Ki-67 (1:100, Invitrogen), and cleaved PARP (Cl-PARP, 1:400, Cell Signaling Technology) or biotinylated HA binding protein (HABP; EMD Millipore) diluted in blocking solution according to the provided manufacturer's recommendations (Table 1). The next day, samples were incubated in Hoechst 33342 and appropriate secondary antibody solutions with limited light exposure for 1 hour. Following a final wash, slides were mounted using coverslips with applied Fluoromount G (Southern Biotech, Birmingham, AL, USA).

Confocal laser scanning microscopy was performed at the Advanced Light Microscopy/Spectroscopy Laboratory and the Leica Microsystems Center of Excellence at the California NanoSystems Institute at UCLA with funding support from NIH Shared Instrumentation Grant S10D025017 and NSF Major Research Instrumentation grant CHE-0722519.

Table 3.1: Primary antibody and protein dilutions and reference.

Primary	Dilution	Catalog Number
CD44	1:400	37259T
RHAMM	1:400	NBP1-76538
Ezrin	1:200	3145S
Ki-67	1:100	PA5-16785
Cl-PARP	1:400	5625S
HABP	1:100	385911-50UG

Cell Extraction from Hydrogels and EdU Proliferation Assay

Cultured and encapsulated spheres were incubated in a 1:1000 dilution of EdU solution (Cayman Chemical Company 20518) for 4 hours. Following a wash in PBS, hydrogel samples were broken down using a 10 mL syringe with a 20G needle and passed through a 40 mm filter into collection tubes. Cultured samples were not broken down using a 20G needle to avoid mechanically induced stress and were rather incubated in TrypLE solution for 5 minutes, resuspended in media, and passed through a 40 mm filter. All samples were subsequently centrifuged (400g for 5 minutes), resuspended in 4% PFA in 1X PBS, and stored in 4°C overnight.

The following day, samples were centrifuged (400g for 5 minutes) and washed in 1% BSA in 1X PBS. Cells were permeabilized for 15 minutes in permeabilization buffer (0.1% Saponin and 1% BSA in 1X PBS). Staining solution was prepared (Table 3) and added to the cells undergoing the permeabilization reaction. After 30 minutes of incubation without light in room temperature, samples were washed twice and ultimately resuspended in permeabilization buffer. Flow cytometry data was collected using the Guava easyCyte™ Flow Cytometer and analyzed using FlowJo™ software.

Cell Viability Quantification

Encapsulated GSs were incubated at 37°C and 5% CO_2 for 15 minutes in LIVE/DEAD working reagent prepared by diluting 2 mM Ethidium homodimer-1 (1:500) and 4 mM Calcein AM solution (1:2000) stock solutions in 1X PBS. Spheres were imaged and three separate counters quantified the presence of live or dead cells in images provided.

Tissue Microarray (TMA) HA Staining and Scoring

TMAs were prepared by clinically isolated tissue biopsy samples from 39 GBM and 19 lower-grade CNS cancer (grade I-III astrocytoma, grade I-III oligodendroglioma, pituitary gland

cancer, and meningioma) patients, prepared and provided by Dr. William Yong and the UCLA Brain Tumor Tissue Resource. Paraffin-embedded slides of 5 mm thickness were de-paraffined using 100% xylene and a 5-step reduction in alcohol presentation from 100% ethanol to deionized water. Samples were washed (0.1% Tween in 1X TBS), blocked (5% normal goat serum and 1% BSA in washing solution), and incubated with biotinylated HA binding peptide (HABP) overnight at 4°C. The following day, samples were washed and incubated using Vectastain ABC kit reagents and 3,3'-diaminobenzidine (DAB) substrate. Samples were mounted onto slides using a toluene solution. Images were taken using the Zen Axio-Observer microscope and images were semi-quantitatively scored according to a previously described method.[189]

Statistics

All statistics were performed using GraphPad Prism software. Kolmogorov-Smirnov test was performed to assess normality of data. For parametric data, a Student's T-test and one- or two-way Analysis of Variance (ANOVA) was performed to assess significance between two and multiple data sets, respectively, followed by post-hoc Tukey's multiple comparisons test. In the case of non-parametric data, a Kruskal-Wallis ANOVA was used to assess significant differences between any data sets followed by post-hoc Dunn's multiple comparisons test. Modes of significance were reported as follows: ns, non-significant; *, $p < 0.05$; **, $p < 0.01$; ***, $p < 0.001$; ****, $p < 0.0001$.

CHAPTER 4: RESULTS

Greater HA Deposition in Higher Grade Gliomas

HA deposition is a key feature in GBM pathophysiology. To assess potential differences in HA deposition in clinical brain tumors, we performed tissue microarray (TMA) staining for HA in GBM (N = 34) and lower-grade CNS (N = 19) tumor samples. Representative images of tissue samples are shown, with darker brown coloration being indicative of greater HA abundance within samples (Figure 4.1A). On average, HA concentration was elevated in GBM tissues relative to lower grade CNS cancers ($p = 0.008$) (Figure 4.1.B). Notably, the spatial distribution of HA in the samples was nonuniform, containing regions with relatively high (darker brown) and low (lighter brown) HA concentrations (Figure 4.1.C). Even following orthotopic implantation in mice, HK408 cells demonstrated greater HA deposition especially along the tumor edge, where high rates of invasion occur (Figure 4.1.D). Matching the phenotype described in patient samples, HA concentration in xenografts also was heterogeneous along the tumor edge (Figure 4.1.E).

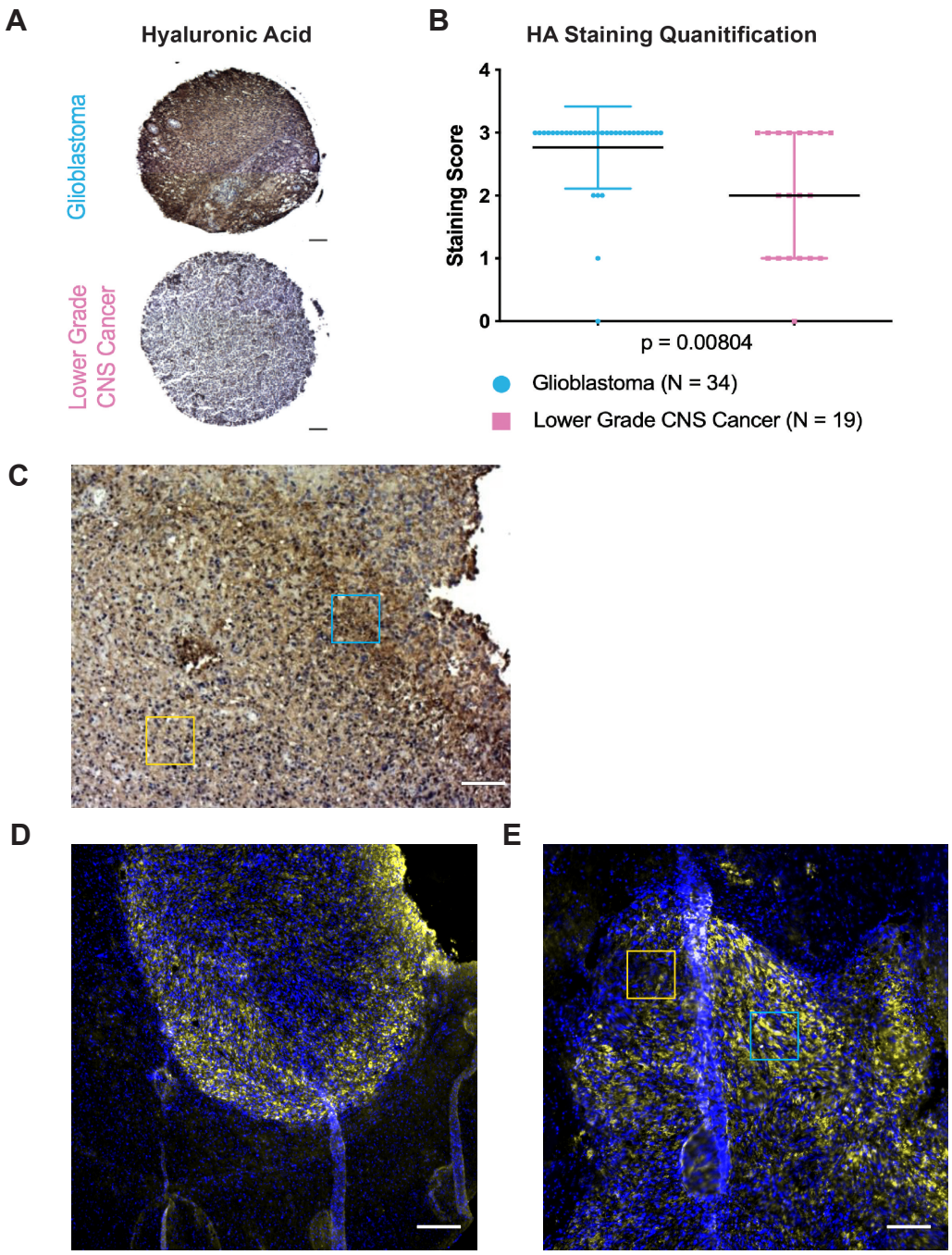

Figure 4.1: HA importance in GBM pathophysiology. A) Representative image of IHC staining of TMA slides. Brown, positive stain; dark blue, hematoxylin. Scale bar = 100 μm. B) 34 GBM and 19 lower-grade CNS cancer TMA stainings semi-quantitatively scored. Mann-Whitney U Test was used to assess significance. C) Staining of patient-resected tumor sample. Blue square = area of high HA concentration. Yellow square = area of low HA concentration. Scale bar = 100 μm. D) HA (yellow) staining images of HK408 xenograft. Scale bar = 200 μm E) HA (yellow) staining images of HK408 xenograft. Scale bar = 100 μm.

Fabrication of HA Concentration-Tunable, Biocompatible Hydrogels

To investigate the effects of varying HA concentration on GBM phenotypes, we encapsulated GSs in mechanochemically tunable, 3D hydrogels, as previously described in Liang *et al.* (in publication). Specifically, we fabricated HA hydrogels with 0.10%, 0.25%, 0.50%, and 0.75% weight per volume (w/v) HA. All hydrogels contained 0.025% (w/v) of RGD peptides, were exposed to equal intensities and durations of UV radiation during gelation and had similar mechanical properties. Swelling characterization was performed by incubating priorly weighed hydrogels in Dulbecco's phosphate buffered saline (D-PBS) for 24 hours. The ratio of the final to initial mass, or mass swelling ratio, gradually increased with increasing HA concentrations in the hydrogels (Figure 4.2.A). Given that the total polymer content was constant between hydrogels, this result demonstrates that hydrogel hygroscopy was associated with its HA content. Moreover, hydrogels had similar storage moduli of 115.1 ± 14.2 (G') Pa, 116.3 ± 19.0 (G') Pa, 116.3 ± 20.3 (G') Pa, 124.4 ± 16.3 (G') Pa for the 0.10% - 0.75% (w/v) HA conditions, respectively (Figure 4.2.B). Low storage moduli were used to mimic the mechanical integrity of healthy brain tissue interfaced with the GBM peritumoral environment. The associated porosity across hydrogels was also similar. Using fluorescence recovery after photobleaching (FRAP), we noted the effective diffusion rates of 20 kDa and 70 kDa FITC-Dextran polymers were equivalent to that of PBS and between 0.10% - 0.75% (w/v) hydrogels (Figure 4.2.C). As such, moieties up to 70 kDa in size, which includes the important media components (EGF and FGF) and the later-used small molecule inhibitor, can freely diffuse throughout the gel.

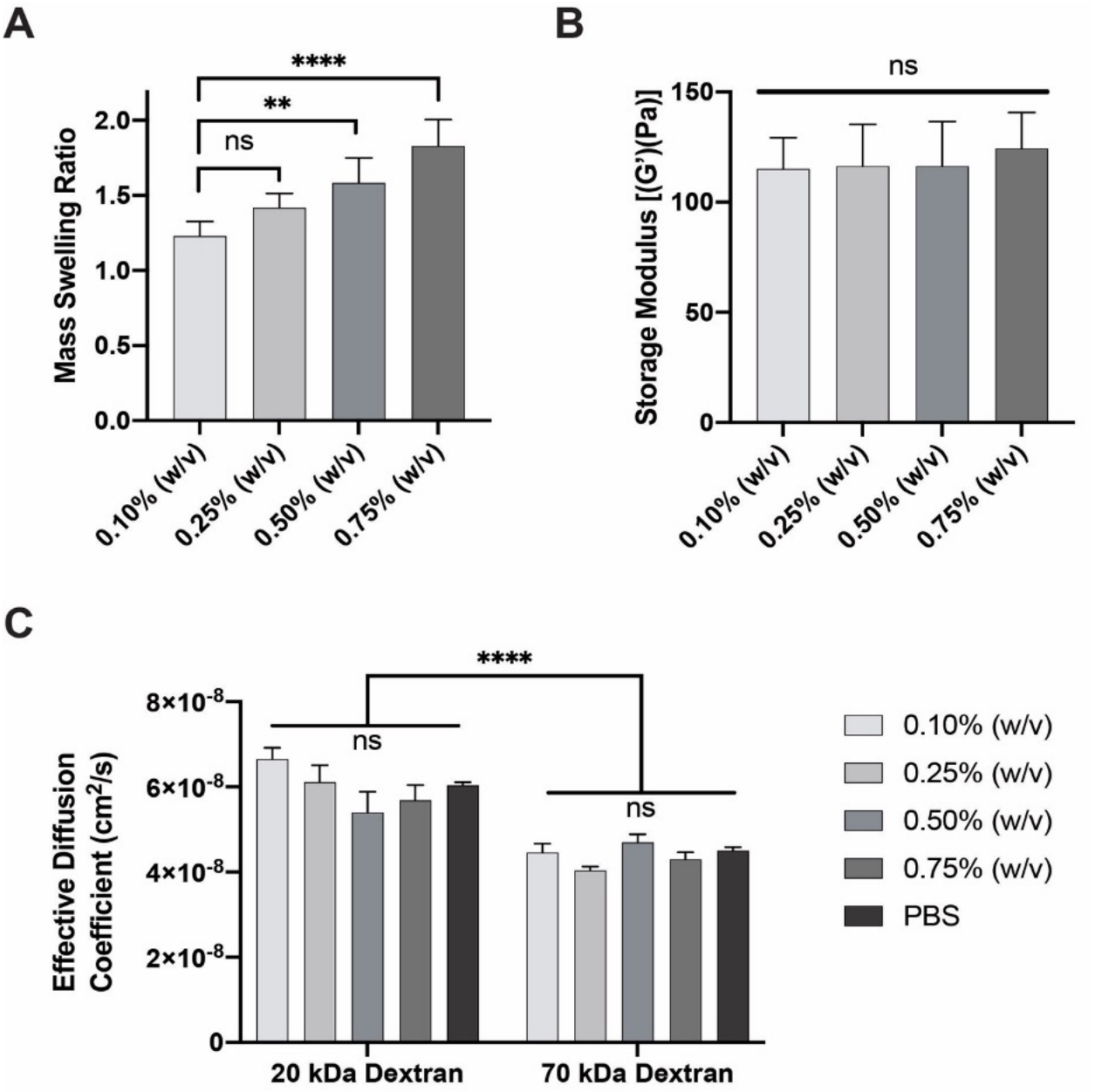

Figure 4.2: Hydrogel characterization. A) Mass swelling ratios of individual hydrogels following fabrication. B) Storage moduli of hydrogels of varied HA concentrations show no significant differences. C) Diffusion rates of 20 kDa and 70 kDa FITC-Dextran polymers are similar across hydrogel conditions and match that of PBS controls.

Given GSs better capture cell-cell adhesions and interactions normally present within nascent tumors compared to 2D monolayer culture, we formed GSs of controlled sphere size using AggreWell™ plates and encapsulated them in our hydrogels. The viability of GSs patient lines at experimental endpoints remained high over the course of our studies (Figure 4.3.A). To quantify the numbers of apoptotic cells within GSs, we performed immunostaining for cleaved PARP (Cl-PARP). GSs of both patient lines exhibited low apoptosis in hydrogels. Specifically, HK408 GSs in 0.10%, 0.25%, 0.5%, and 0.75% (w/v) HA hydrogels had 6 ± 2%, 3 ± 2%, 3 ± 1%, and 3 ± 1% apoptotic cells, respectively, while GS054 GSs had 2 ± 1%, 2 ± 1%, 2 ± 1%, and 2 ± 1% apoptotic cells, respectively (Figure 4.3.B). Additionally, we performed immunostaining for proliferation marker Ki-67, which we found was heavily expressed by most cells within GSs across hydrogels (Figure 4.3.C). Notably, HK408 GS in 0.10% (w/v) HA hydrogel had observably fewer proliferative cells than in suspension-cultured GSs in 0.25% - 0.75% (w/v) HA hydrogels. An EdU assay was next used to investigate potential differences S and G2 phase cell cycle activity in the HK408 line. Confirming our Ki-67 stainings, HK408 GSs in the low HA environment had significantly fewer cells in S & G2 phases of proliferation than GSs in higher HA environments ($p = 0.0001$ [0.25% (w/v)]; $p = 0.0062$ [0.50% (w/v)]; $p = 0.0011$ [0.75% (w/v)]). Interestingly, GSs in 0.25%-0.75% (w/v) HA hydrogels had similar percentages of cells in S and G2 phase (Figure 4.3.D).

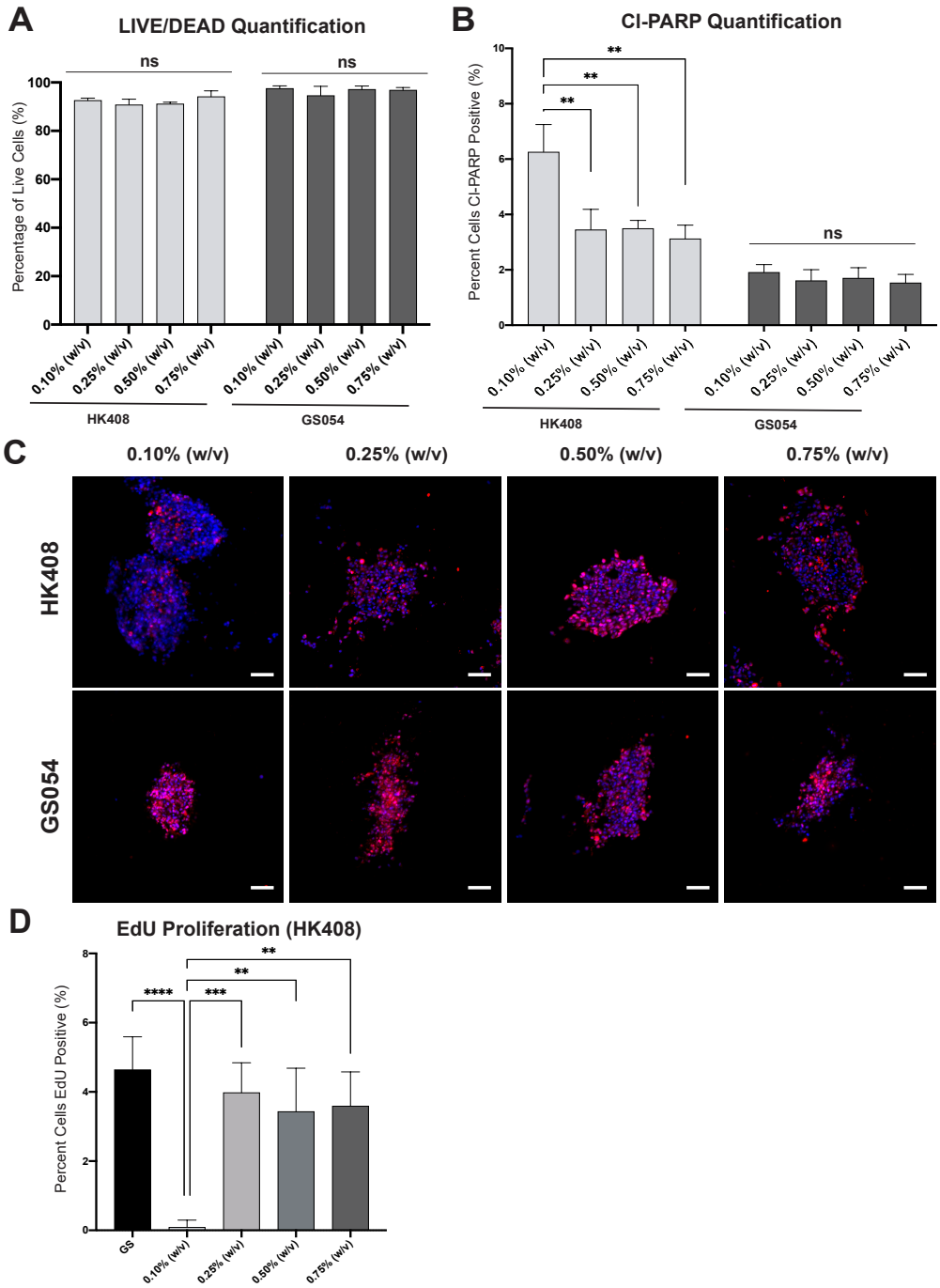

Figure 4.3: Characterization of GSs in 3D culture conditions. A) LIVE/DEAD staining and subsequent quantification was performed to assess cell viability following 6 days in culture for HK408 and GS054 gliomaspheres. B) Quantification of Cl-PARP positive cells in HK408 and GS054 GS sections following 6 days in culture. C) Representative images of Ki-67 staining of HK408 and GS054 GS sections following 6 days in culture. Red = Ki-67; Blue = Hoechst 33342. Scale bar = 50 μm. D) EdU proliferation assay performed at day 6 for HK408 GSs in hydrogel and media culture. **, $p < 0.01$; ***, $p < 0.001$; ****, $p < 0.0001$.

Determining Optimal HA Concentration for Invasion in Patient Lines

At the endpoint, GSs in 3D culture displayed diverse morphologies dependent on both the patient line as well as hydrogel HA concentration. Interestingly, the migration morphologies were independent of the patient's GBM classification as proneural (HK408, HK217) or mesenchymal (GS054, HK177). While HK217 and GS054 GSs displayed mainly thinner, single cell protrusions extending into matrix, the periphery of HK408 and HK177 GSs heavily displayed thicker, multicellular protrusions indicative of collective migration (Figure 4.4.A; Figure 4.5.A). Still, instances of single and collective cell migration were noted in all patient lines. Uniquely, GS054 spheroids encapsulated in 0.75% (w/v) HA hydrogels adopted polarized, crescent-like shapes, which did not resemble the invasive phenotypes observed in 0.10%–0.50% (w/v) HA hydrogel cultures or for other cell lines. In accordance with previous work by Xiao *et al.* (2020), both HA and RGD peptide interactions were necessary for elongated cell migration phenotypes depicted across conditions.[181]

Migratory activity of GSs across hydrogels was quantified over the course of six days for HK408, HK177, and GS054, and nine days for HK217. Migration length quantified the maximum Euclidian displacement by a single cell or multicellular protrusion from the sphere periphery into matrix, while shape factor quantified the circularity of spheroids as a scaled ratio of area to squared circumference and approximated the overall protrusion density per GS. In general, GSs across patient lines exhibited greater cell migration in 0.25%–0.75% (w/v) HA hydrogels compared to 0.10% (w/v) HA. Yet, any significant variations of GS invasiveness in hydrogels with 0.25% (w/v) HA were patient-line dependent. Interestingly, HA concentrations for peak, or optimal, invasiveness were apparent for the HK408 and HK177 patient lines in ≥0.25% (w/v) HA hydrogels. For HK408, differences in shape factor were nonsignificant in ≥0.25% (w/v) HA

hydrogels (Figure 4.4.B). However, the median migration length of GSs in 0.75% (w/v) HA hydrogels was significantly less than those in 0.50% (w/v) HA ($p = 0.0343$) and approximate to the median migration length in 0.25% (w/v) HA hydrogels ($p = 0.8633$) (Figure 4.4.C). The median shape factor for HK177 GSs was lower in hydrogels with 0.25% (w/v) % HA compared to 0.50% (w/v) ($p = 0.0013$) and 0.75% (w/v) ($p < 0.0001$) HA hydrogels, while differences migration lengths between these conditions were non-significant (Figure. 4.5.B; Figure. 4.5.C). Thus, even though the median protrusion density of spheres was relatively similar in conditions of ≥0.25% (w/v) HA, the concentration of 0.50% (w/v) HA was optimal for cellular displacement from the sphere periphery in HK408 GSs. In contrast, 0.25% (w/v) HA was optimal for HK177 GS protrusion density, while HA concentrations ≥0.25% (w/v) did not influence maximal cellular displacement. No HA concentration was identified within the 0.25%–0.75% (w/v) HA range as a maximum of migratory activity for GS054 and HK217. Specifically, both the median shape factor and migration lengths of GS054 GSs were the greatest in 0.75% (w/v) HA hydrogels, with no significant differences in 0.25% and 0.50% (w/v) HA conditions (Figure 4.4.D; Figure 4.4.E). No significant differences in HK217 GS motility were apparent across ≥0.25% (w/v) HA hydrogels (Figure 4.5.D; Figure 4.5.E).

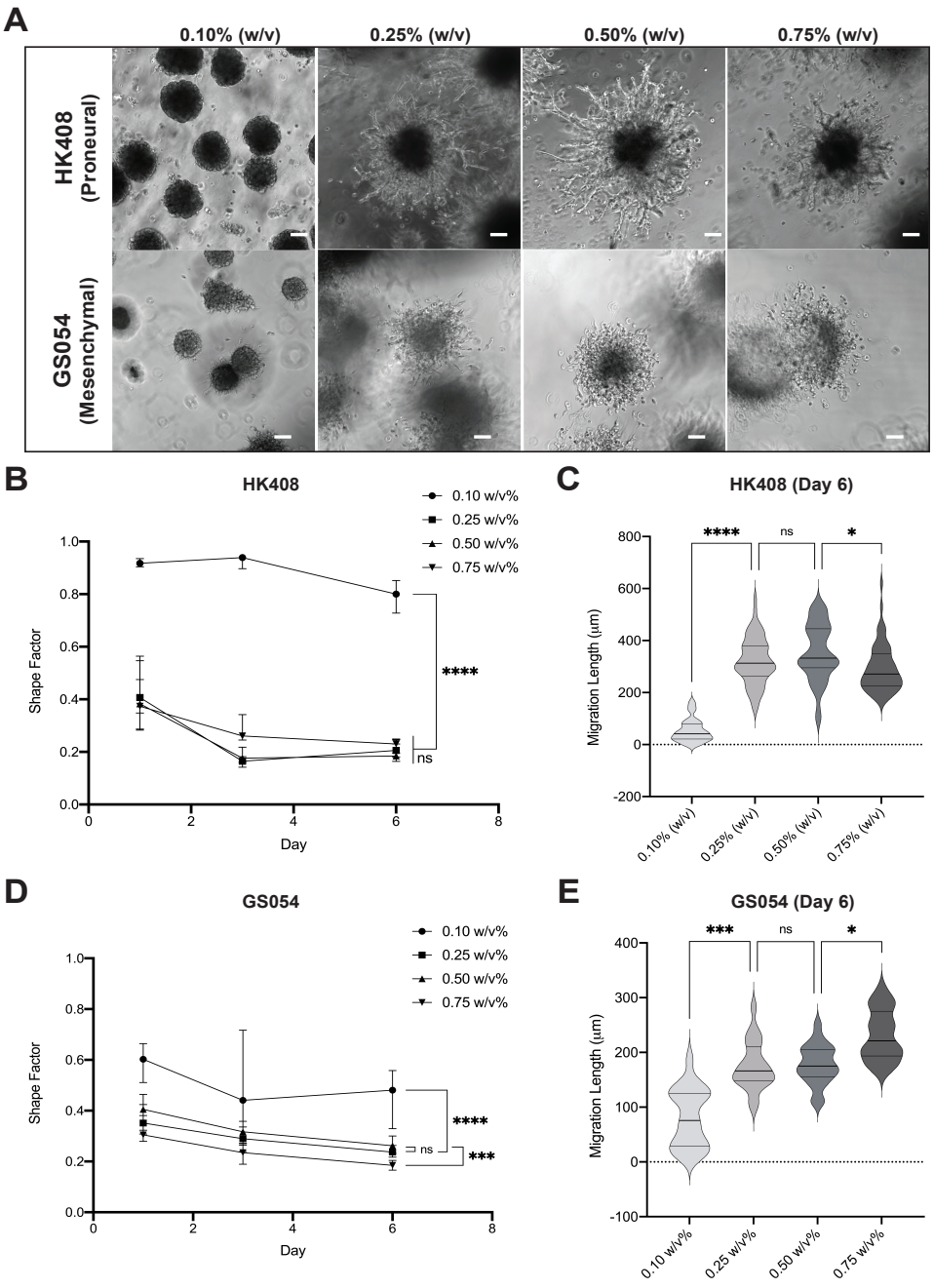

Figure 4.4: A) Representative images of HK408 and GS054 GSs following 6 days in culture. Scale bar = 100 µm. B) Shape factor quantification of HK408 GSs from days 1 – 6. C) Migration lengths of HK408 GSs at the end of sixth day in culture. D) Shape factor quantification of GS054 GSs from days 1 – 6. E) Migration lengths of GS054 GSs at the end of sixth day in culture. *, $p < 0.05$; ***, $p < 0.001$; ****, $p < 0.0001$.

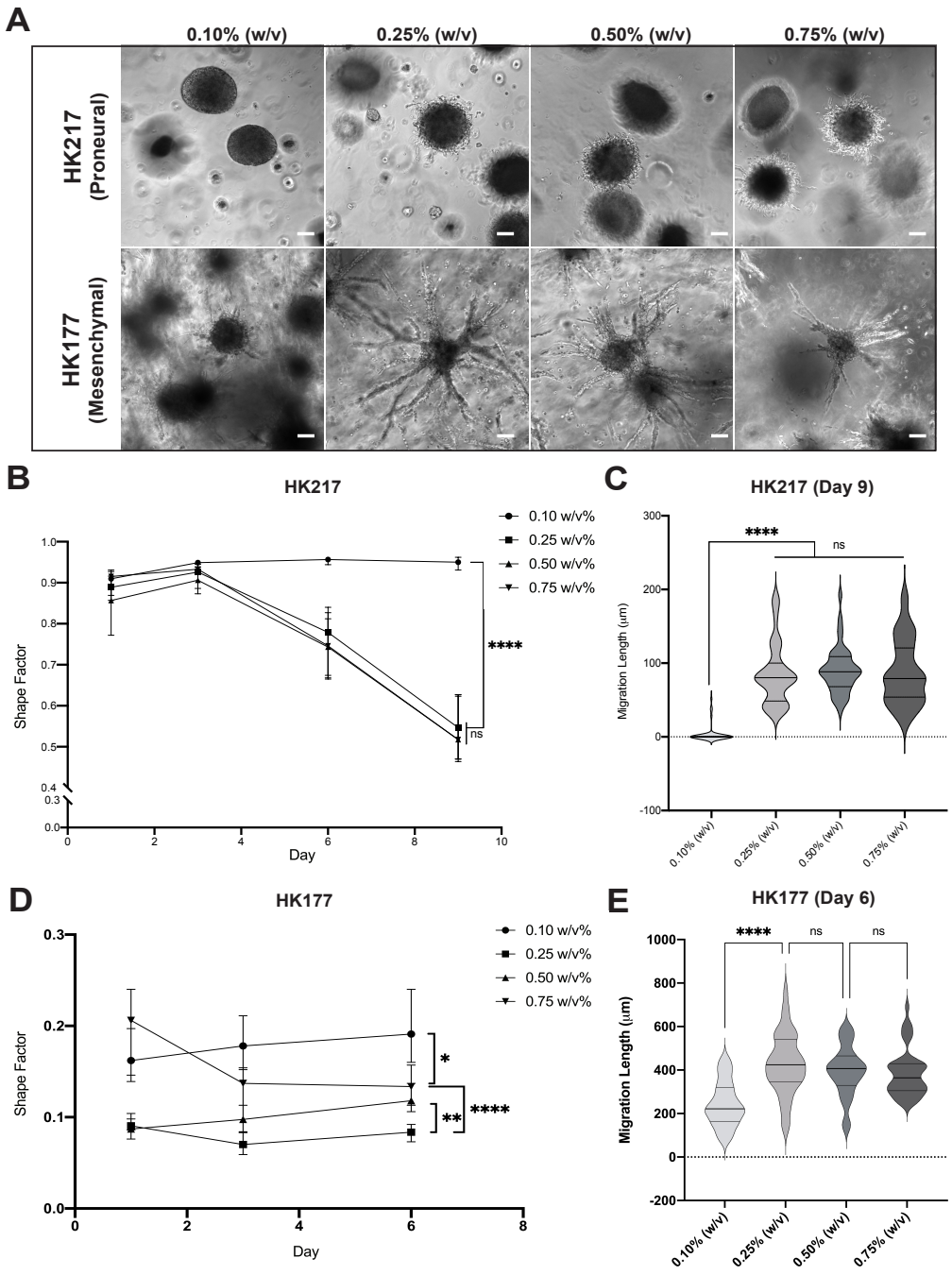

Figure 4.5: A) Representative images of HK217 and HK177 GSs following 6 days in culture. Scale bar = 100 μm. B) Shape factor quantification of HK217 GSs from days 1 – 6. C) Migration lengths of HK217 GSs at the end of sixth day in culture. D) Shape factor quantification of HK177 GSs from days 1 – 6. E) Migration lengths of HK177 GSs at the end of sixth day in culture. *, $p < 0.05$; **, $p < 0.01$; ****, $p < 0.0001$.

Greater Cellular CD44 Expression in More Invasive GSs

Next, we investigated the roles of the HA receptors CD44 and RHAMM in determining the invasive profiles of GSs across HA conditions. To avoid potential errors introduced while dissociating the CD44 and RHAMM from the HA matrix, we did not perform absolute protein quantification between conditions using methods such as Western Blot or Flow Cytometry. Instead, we completed immunofluorescent staining of GSs at experimental endpoints to evaluate potential differences in the spatial distribution of HA receptors CD44 and RHAMM. HK408 and GS054 GSs both exhibited similar patterns of CD44 and RHAMM protein expression such that CD44 was localized to membranous and pericellular regions while RHAMM was primarily localized within the cytoplasmic and nuclear domains of cells. However, HK408 GSs expressed greater densities of CD44 per cell compared to GS054 GSs which had intermittent CD44 expression at lower densities along cell membranes. Yet, for both lines, CD44 was presumed to be the main receptor mediating cell-ECM interactions given its location at the cell membrane. Interestingly, no variations in HA receptor expression were obvious between migratory and stationary regions of the GS peripheries within each HA condition (Figure 4.6; Figure 4.7). In addition, the spatial patterns of expression for CD44 and RHAMM in HK408 GSs within 3D hydrogels were very similar to those observed in HK408 xenografts (Figure 4.8.A). Insets provided of stained cells reveal the HK408 cells are extending microtentacles as reported by Wolf et al. (2020) and may be performing mechanosensation of local microenvironment via CD44 (Figure 4.8.B).[182]

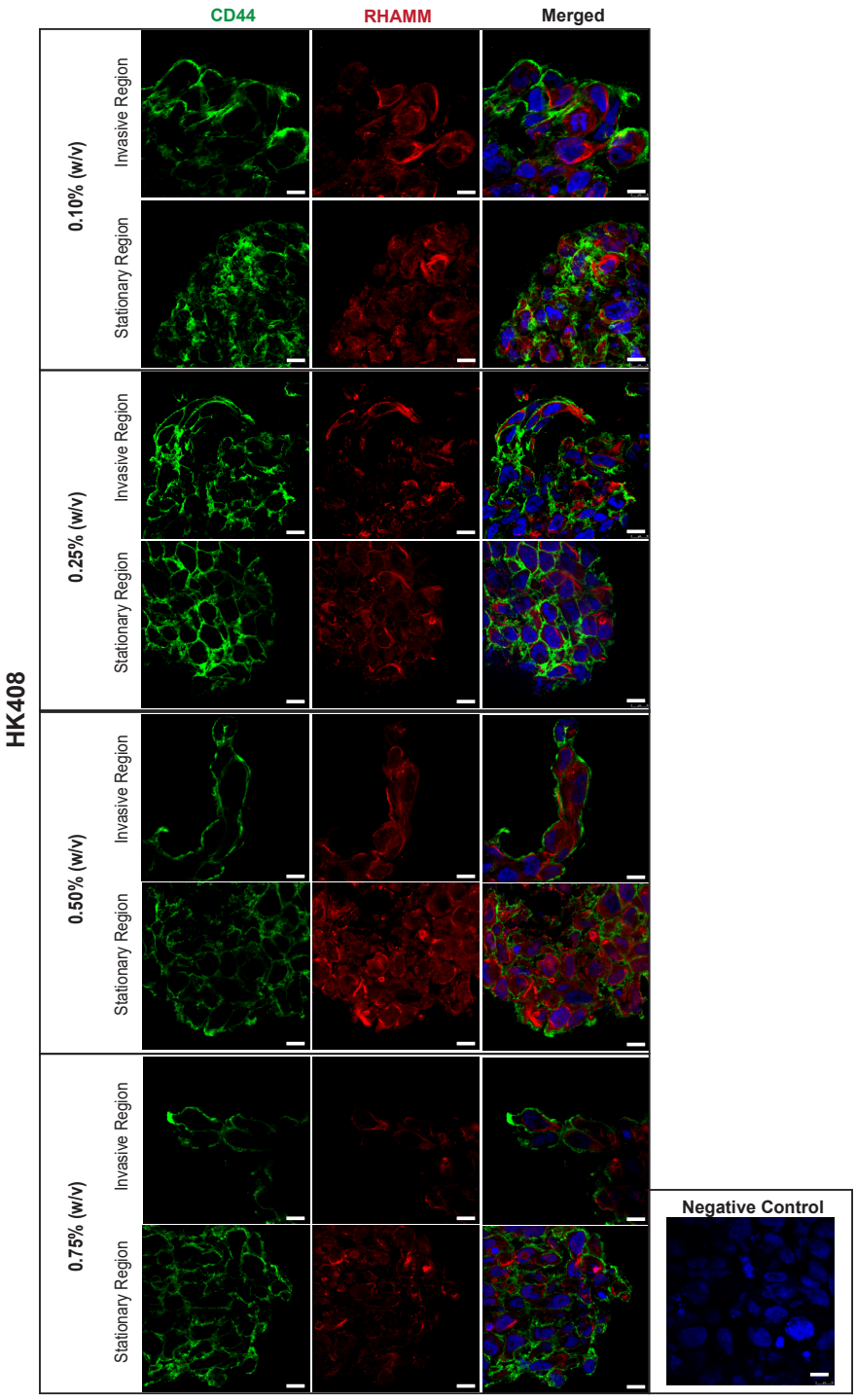

Figure 4.6: Representative images of HK408 GSs stained for CD44 and RHAMM following 6 days of culture. Scale bar = 10 μm.

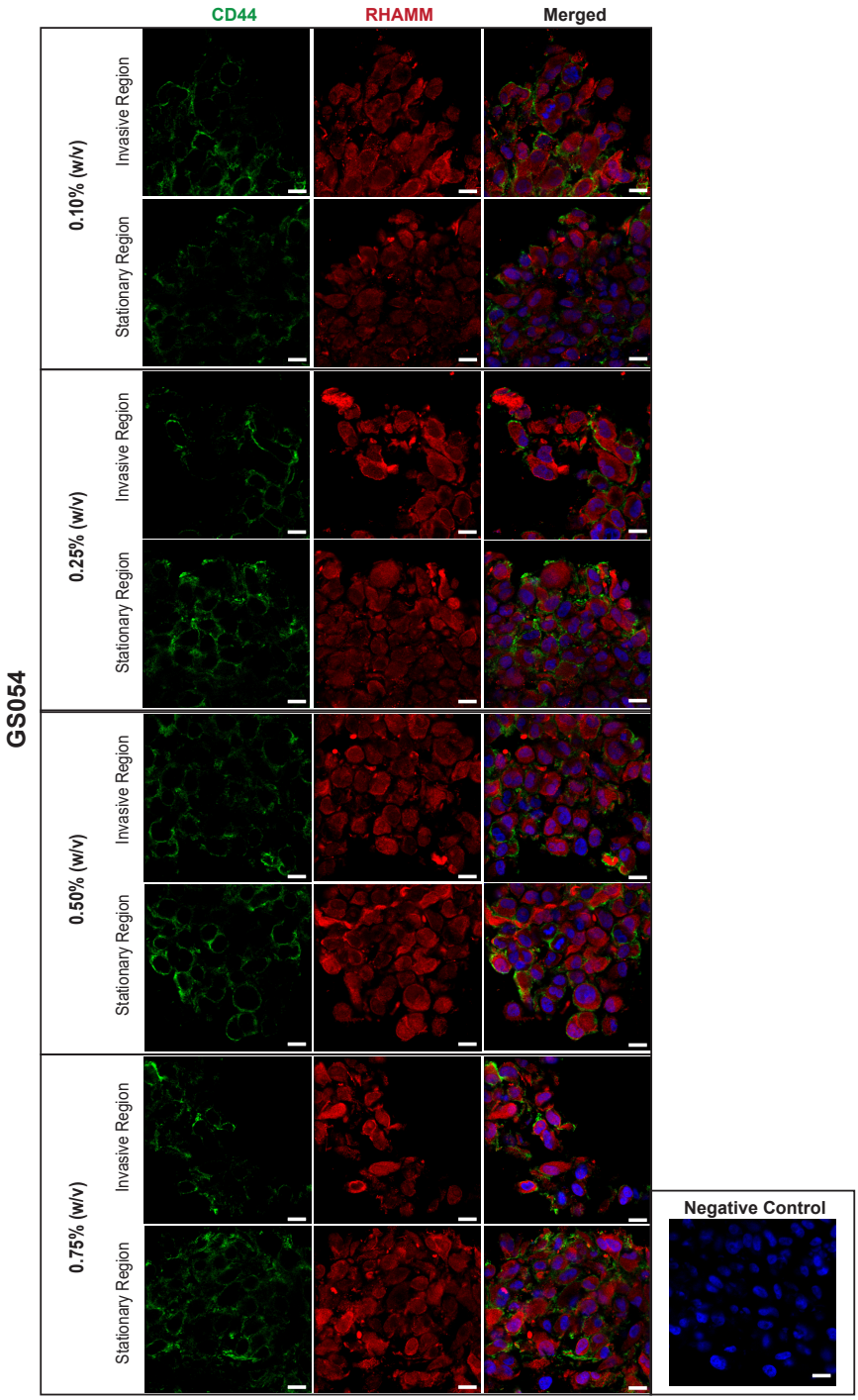

Figure 4.7: Representative images of GS054 GSs stained for CD44 and RHAMM following 6 days of culture. Scale bar = 10 μm.

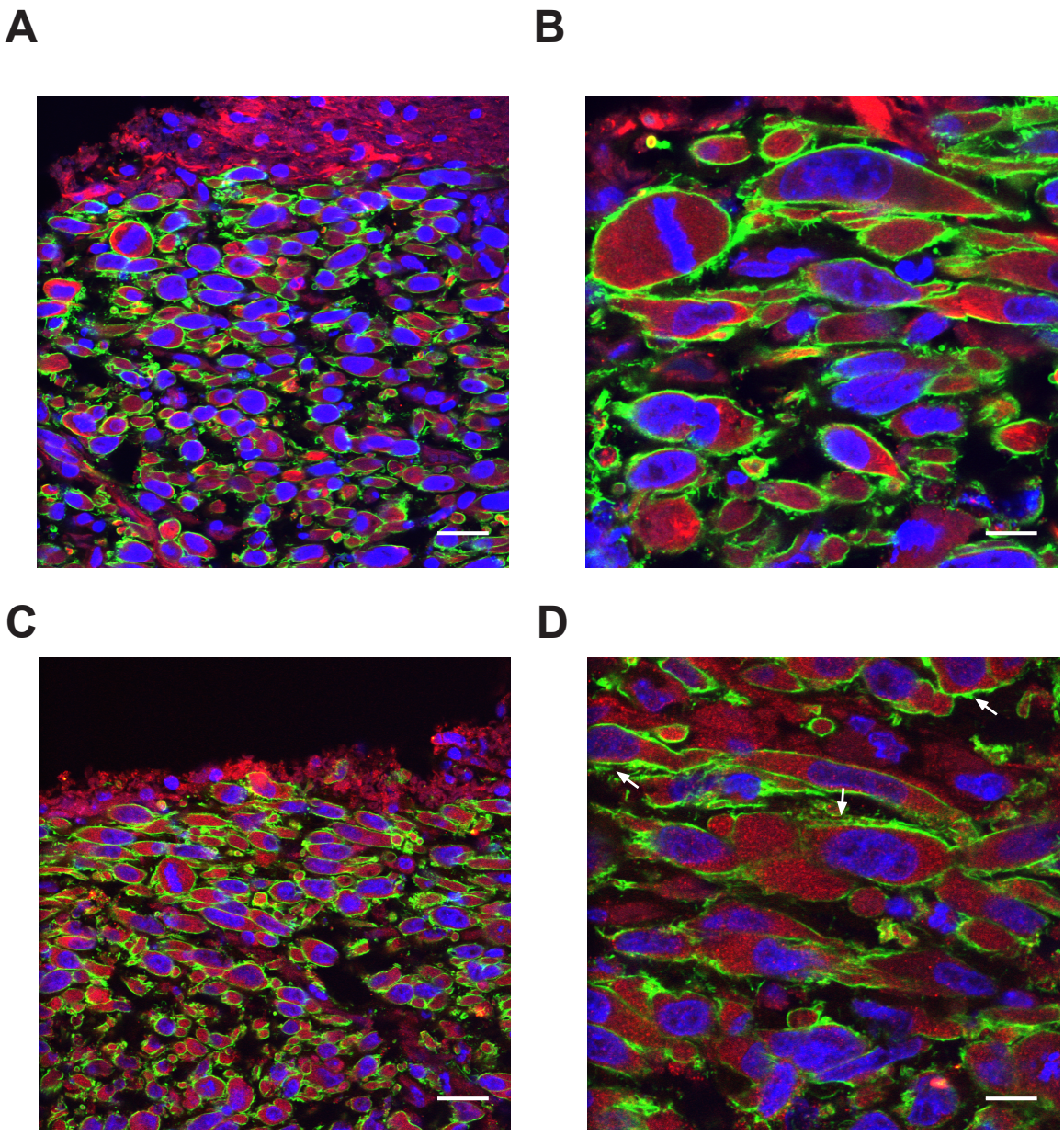

Figure 4.8: Representative images of HK408 xenografts stained for CD44, RHAMM, and Ezrin. A) Image of HK408 cells stained for CD44 (green) and RHAMM (red). Scale bar = 25 μm. B) Insets of HK408 cells stained for CD44 (green) and RHAMM (red). Scale bar = 10 μm. C) Image of HK408 cells stained for CD44 (green) and Ezrin (red). Scale bar = 25 μm. D) Insets of HK408 cells stained for CD44 (green) and Ezrin (red). Scale bar = 10 μm. Arrows designate regions of relatively higher overlap between CD44 and Ezrin in migrating and mechanosensing cells. High levels of collective migration also notable.

CD44-ERM-Actin Engagement Determines GS Propensity to Invade

Given no clear instances of CD44-mediated mechanosensation in the xenografts, we next investigated potential variations in receptor-cytoskeleton engagement. Specifically, we performed immunofluorescent staining for CD44 and the ezrin subunit of ERM. Within HK408 xenografts, instances of CD44 and ezrin colocalization seemed high especially towards the peripheral regions of the tumor mass, where we also identified higher concentrations of HA. Moreover, the cells along the tumor periphery are migratory given their phenotype, complementing our findings of higher HA concentrations causing higher migration in our hydrogels (Figure 4.8.C). At punctuate points along the cell membrane, high degrees of overlap between CD44 and ezrin occurred, suggesting CD44-mediated mechanosensation could be the result of ERM-mediated cytoskeletal anchoring (Figure 4.8.D). We next performed immunostaining of our hydrogel samples to investigate whether relatively minute differentials in HA concentrations could contribute to variations in CD44 and ezrin colocalization at the cell membrane. The Pearson correlation coefficient (r) metric was used to assess degrees of CD44 and ERM overlap, or colocalization, in 100X magnification confocal microscopy images. Remarkably, CD44-ERM colocalization of HK408 gliomaspheres in 0.10% (w/v) HA hydrogels was significantly lower than 0.25% (w/v) HA ($p < 0.0001$), 0.50% (w/v) HA ($p = 0.0158$), and 0.75% (w/v) HA ($p = 0.0009$) hydrogels, while no differences in colocalization were apparent for GS054 GSs across 0.10%–0.75% (w/v) HA hydrogels (Figure 4.9.A; Figure 4.9.B; Figure 4.10.B). Interestingly, CD44-ERM colocalization was not limited to cells in direct contact with the HA matrix at GS edges, but included cells located within the spheroid mass (Figure 4.9.A). Thus, the HA concentration in the surrounding matrix appeared to mediate levels CD44-ERM engagement in not only single cell, but throughout GSs, perhaps through cell-cell or cell-ECM-cell connections.

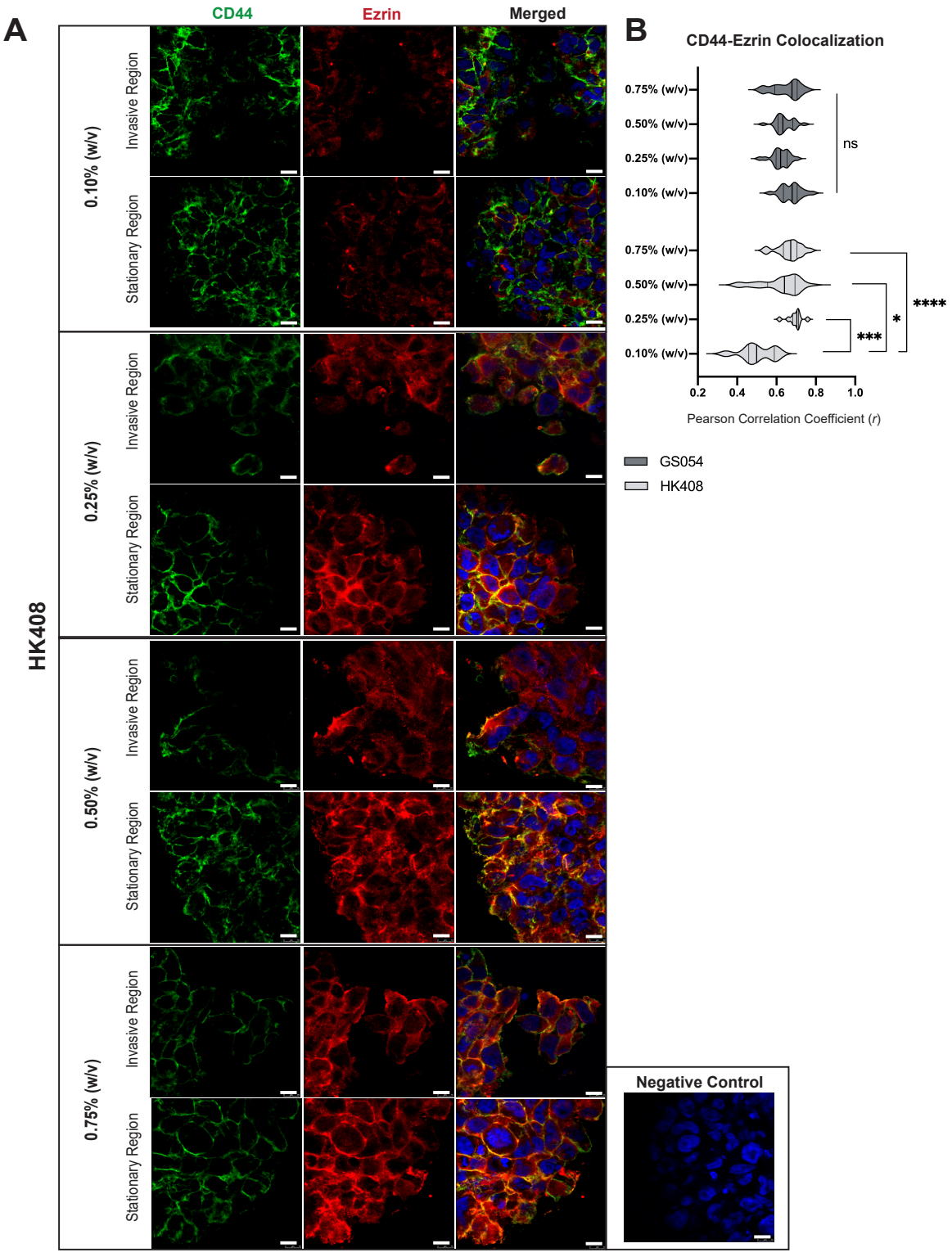

Figure 4.9: Representative images of HK408 GSs stained for CD44 and Ezrin following 6 days of culture. Scale bar = 10 μm. B) Pearson correlation coefficient distribution of overlapping green and red pixel per staining for HK408 and GS054 GSs. *, $p < 0.05$; ****, $p < 0.0001$.

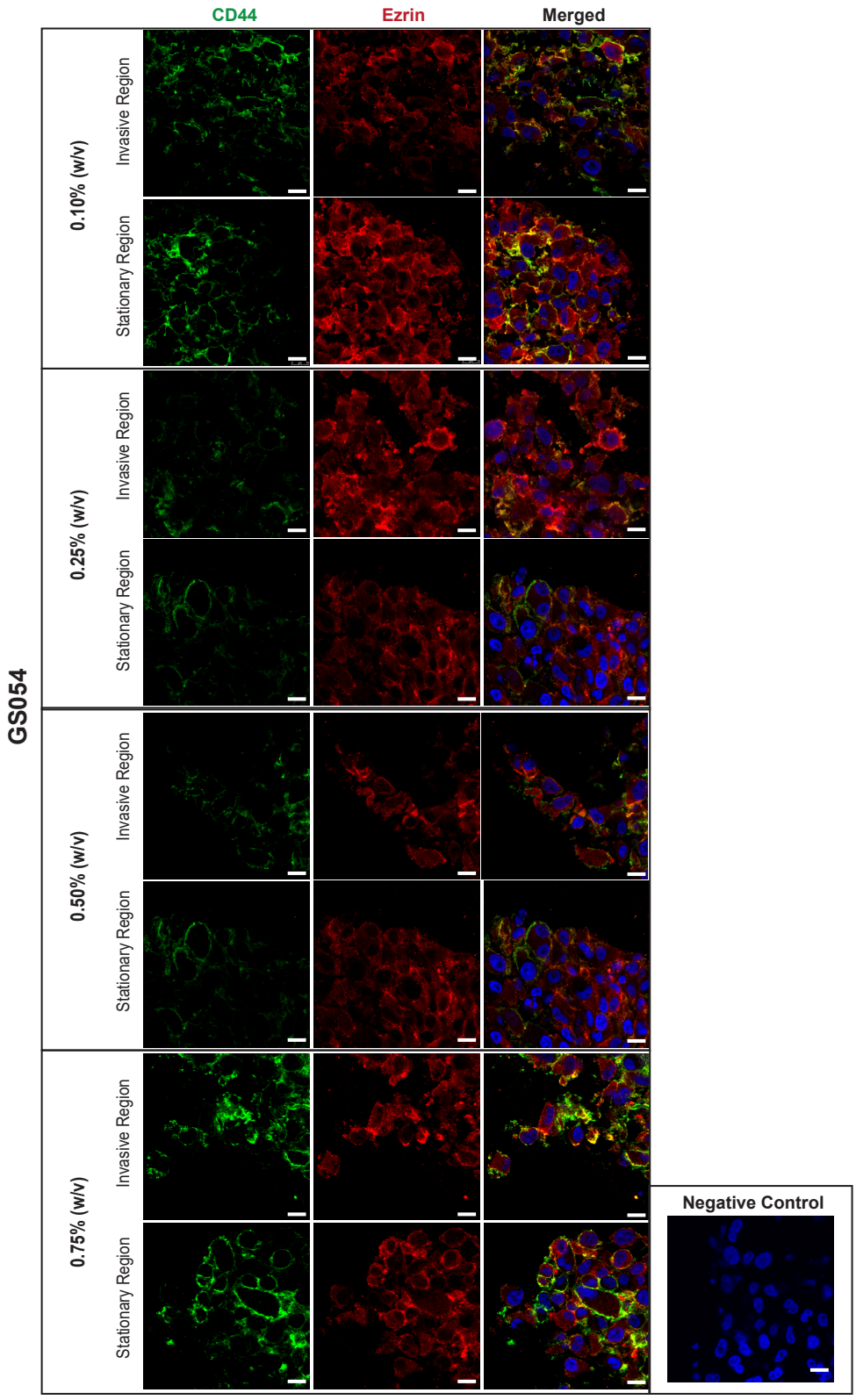

Figure 4.10: Representative images of GS054 GSs stained for CD44 and Ezrin following 6 days of culture. Scale bar = 10 µm.

CD44-ERM Axis Inhibition Modules GBM Invasion in Patient-Dependent Manner

To further assess ERM-mediated CD44 engagement of the actin cytoskeleton in individual patient lines, we performed pharmacological inhibition of ERM using the small molecule inhibitor NSC668394 (ERMi). 5 μM was selected as the initial working concentration in accordance with past studies.[145,190] To evaluate potential concentration-dependent effects by the inhibitor, 10 μM and 20 μM regimens were also completed. The inhibitor was administered 15 hours following encapsulation, when initial signs of invasion were observed across patient lines, and every 48 hours thereafter until the experimental endpoint.

Following administration of 5 μM ERMi to ≥0.25% (w/v) HA hydrogels, GS054 GSs underwent complete loss of invasiveness ($p < 0.0001$) (Figure 4.11.A; Figure 1.11.C). Furthermore, HK217 GSs in 0.25% and 0.50% (w/v) HA hydrogels had significantly higher shape factors compared to respective controls ($p < 0.0001$ [0.25% (w/v)]; $p = 0.0002$ [0.50% (w/v)]). No difference in HK217 GS migration was notable with ERMi treatment within 0.75% (w/v) HA hydrogels (Figure 4.12.A; Figure 4.12.B). HK408 GSs had similar levels of invasion with ERMi as controls in ≥0.25% (w/v) HA hydrogels. Interestingly, and inconsistent with previously reported findings in literature,[145,190] the 5 μM inhibitor regimen led to heightened HK408 ($p = 0.0019$) and HK217 ($p < 0.0001$) GS invasiveness compared to untreated GSs when encapsulated in a 0.10% (w/v) HA matrix (Figure 4.11.B; Figure 4.12.A). Phenotypically, both HK408 and HK217 GSs exhibited rounded, single cell invasion along sphere peripheries with ERMi (FIG 10C; FIG 11B). HK408 GSs had instances of multicellular protrusions and HK217 also displayed instances of single cell protrusions resembling the migration of untreated GSs in ≥0.25% (w/v) HA hydrogels. In contrast to HK408 and HK217 GSs, a complete loss of invasion was observed in GS054 GSs in 0.10% (w/v) HA hydrogels following the 5 μM ERMi treatment.

Administration of 10 μM ERMi completely halted HK217 and GS054 GS invasiveness across hydrogel conditions and remained consistent even following the 20 μM ERMi regimen (Figure 4.11.A; Figure 4.12.A). HK408 GSs in ≥0.25% (w/v) HA hydrogels treated with ERMi displayed similar levels of invasion as compared to controls. Yet, HK408 GS invasion increased in 0.10% (w/v) HA hydrogels ($p < 0.0001$), a phenomenon which persisted even with the administration of a 20 μM inhibitor regimen ($p < 0.0001$) (Figure 4.11.B). The migratory phenotypes observed in the 0.10% (w/v) HA condition HK408 GSs treated with 10 μM and 20 μM ERMi were similar to those treated with 5 μM ERMi. In ≥0.25% (w/v) HA conditions, administration of 20 μM ERMi resulted in a stark reduction in HK408 GS migration ($p < 0.0001$ [0.25%-0.75% (w/v)]. While the density of multicellular protrusions was reduced compared to control conditions, single cell invasion persisted and was phenotypically similar to treated GSs in 0.10% (w/v) HA hydrogels (Figure 4.11.C). These invading single cells could be the result of new single cell invasion from the sphere periphery and/or cellular dismemberment of the multicellular protrusions present within control GSs. Moreover, single cells may exhibit matrix-independent migration, such as non-binding or ameboid.

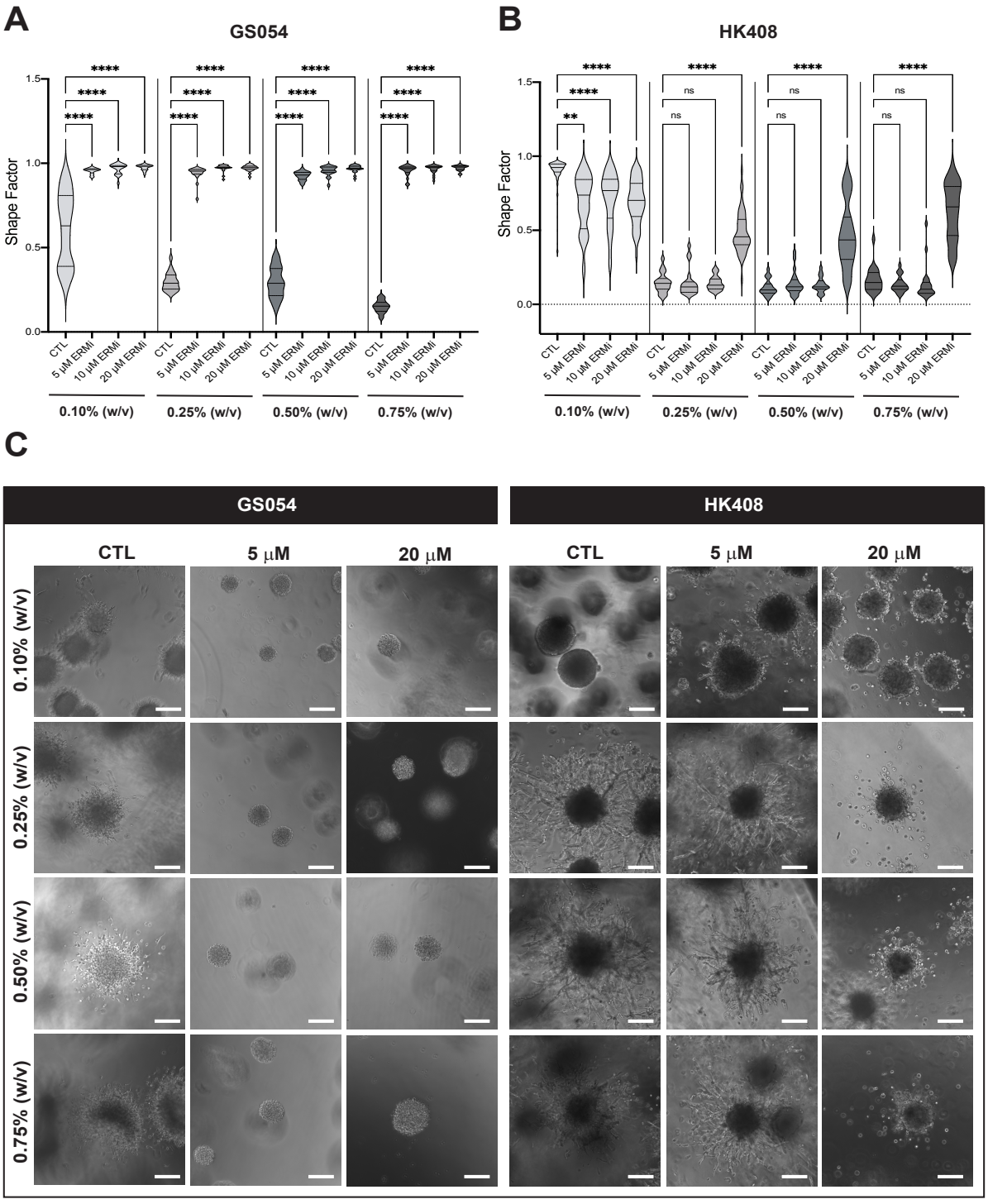

Figure 4.11: ERM inhibition studies on HK408 and GS054 GSs. A) Shape factor distribution of GS054 GSs at endpoint following treatment with 0 – 20 μM of ERMi. B) Shape factor distribution of HK408 GSs at endpoint following treatment with 0 – 20 μM of ERMi. C) Representative images of HK408 and GS054 GSs at endpoint following treatment with 0, 5, and 20 μM ERMi. Scale bar = 100 μm. **, $p < 0.01$; ****, $p < 0.0001$.

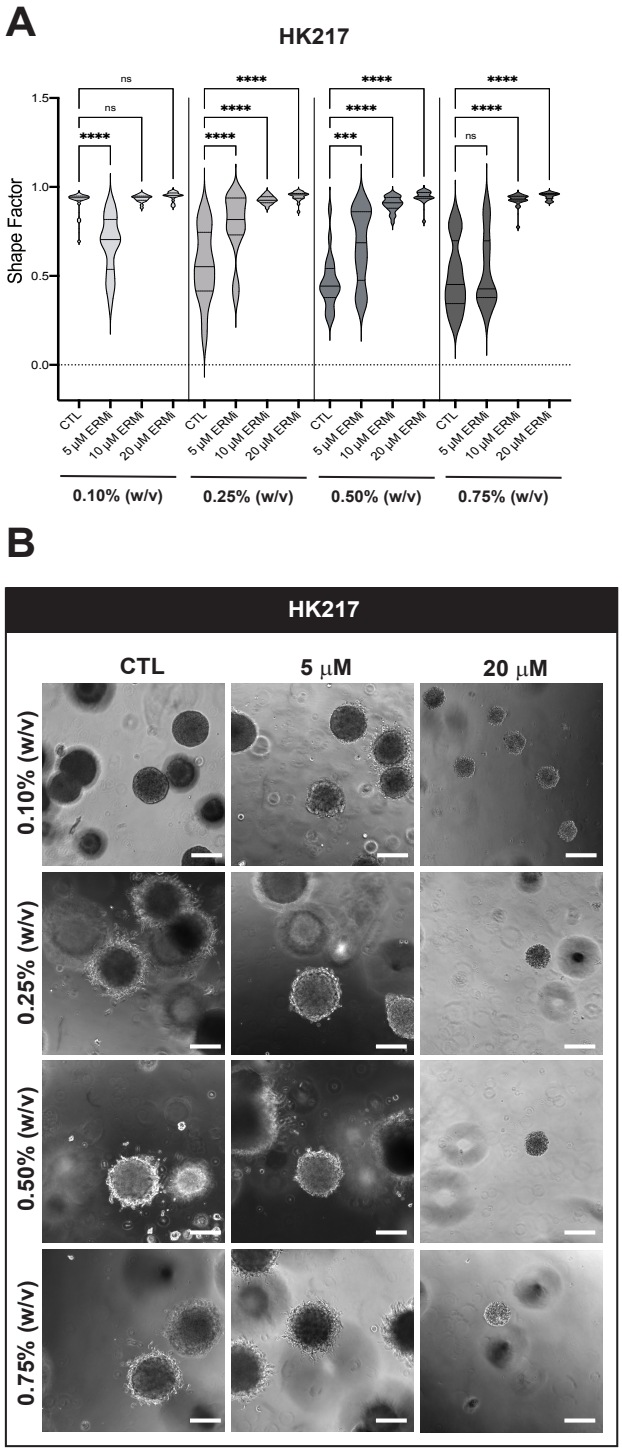

Figure 4.12: ERM inhibition studies on HK217 GSs. A) Shape factor distribution of HK217 GSs at endpoint following treatment with 0 – 20 μM of ERMi. B) Representative images of HK217 and GS054 GSs at endpoint following treatment with 0, 5, and 20 μM ERMi. Scale bar = 100 μm. ***, $p < 0.001$; ****, $p < 0.0001$.

RGD-Integrin and CD44-ERM Engagements Modulate Migration

A similar rise in single cell migration ensued in HK408 GSs when RGD peptides functionalized to the hydrogel scaffold were substituted with cysteine (CYS) (FIG 12). Higher magnification (400x) images of the HK408 GSs provide a clearer view of the sphere periphery populated by colonies of cells (Figure 14.13). In the 0.50% and 0.75% (w/v) HA conditions, clear instances of lamellipodia-like structures, indicating migration, were apparent. Thus, when individually abrogating ERM and integrin signaling within the HK408 patient line, the multicellular protrusions noted in control ≥0.25% (w/v) HA hydrogels were unable to form while instances of single cell invasion became apparent in 0.10% (w/v) HA hydrogels. Importantly, besides HA, the RGD peptides incorporated within the scaffold were critical for the rise of the observed migration phenotypes.

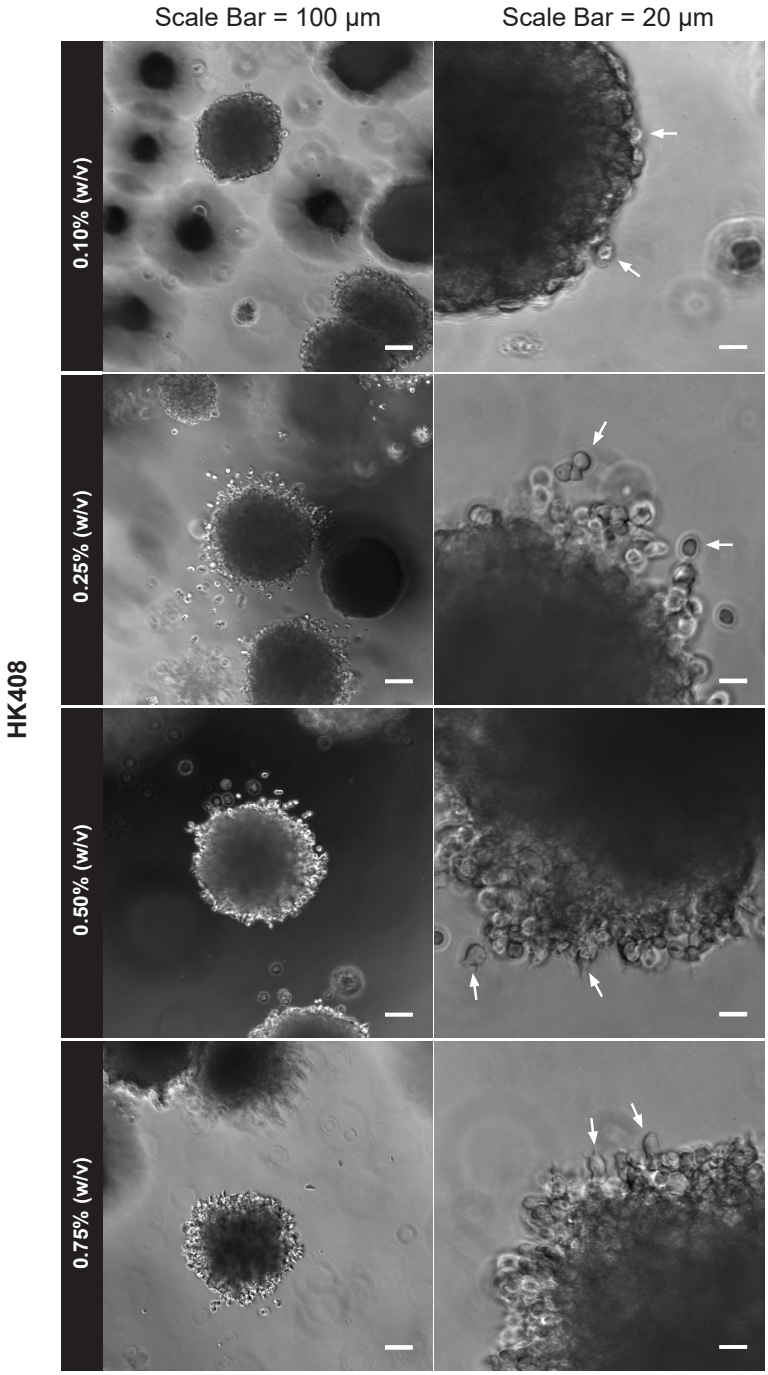

Figure 4.13: Representative images of HK408 GSs following 6 days in culture in HA hydrogels with CYS substituted for RGD peptides. Arrows in images of zoomed insets indicate instances of cell motility at GS peripheries.

HA-RHAMM Inhibition Increases GBM Invasiveness in High HA Environments

Given that RHAMM was not completely absent from the periphery of GSs, we further interrogated the importance of perimembranous RHAMM on GS motility using an HA-mimetic RHAMM blocking peptide (RBP). Esguerra *et al.* (2015) previously demonstrated that this peptide exclusively interacts with the HA binding site of RHAMM and does not interact with CD44. 32 μM of peptide was sufficient for high HA binding.[158] Initially, we administered the 32 μM of blocking peptide immediately following the initiation of migration in HK217 cell lines and assessed invasion every 12 hours. Surprisingly, 36 hours following administration, migration lengths were significantly increased in GSs encapsulated in 0.50% (w/v) and 0.75 (w/v) HA hydrogels ($p < 0.0001$ [0.50% (w/v)]; $p = 0.0282$ [0.75% (w/v)]) (Figure 4.14.A).

Given vast studies identifying RHAMM inhibition results in reduced cell motility, in general, we decided to evaluate the effects of RBP administration to a second patient line. We designed a similar, preliminary study to the aforementioned ERM inhibition studies to evaluate the effects of peptide administration over time. Specifically, we administered 100 μM of RBP exactly 15 hours following encapsulation of HK408, given this was when initial instances of invading cells were notable. We then administered a second 100 μM dose of RBP exactly 48 hours after the initial administration and monitored invasiveness over the course of 3 days. On day 1, the RBP regimen had increased the migration lengths of HK408 GSs cultured in hydrogels with 0.25% (w/v) HA ($p = 0.0126$). On day 3, treated and untreated GSs in 0.25% (w/v) HA hydrogels had similar migration lengths, however, treated GSs in 0.50% (w/v) HA hydrogels had increased migration lengths ($p = 0.0013$) (Figure 4.14.B, Figure 4.14.C). Interestingly, the initial 100 μM administration of RBP was sufficient to increase invasion in GSs in 0.25% (w/v) HA conditions, but a second administration was required to see any effect in the higher 0.50% (w/v) HA

environment. We hypothesize that greater HA-RHAMM interactions are present in higher HA environments. Furthermore, when the HA-RHAMM binding is targeted, cells may activate compensatory mechanisms to return to normal rates of invasion. At day 1, the average migration length of treated GSs in 0.25% (w/v) HA environments even surpasses that of GSs in 0.50% (w/v) HA. It is possible that excessive invasion is unfavorable to cells given it reduces their propensity for proliferation according to the "Go or Grow" hypothesis.

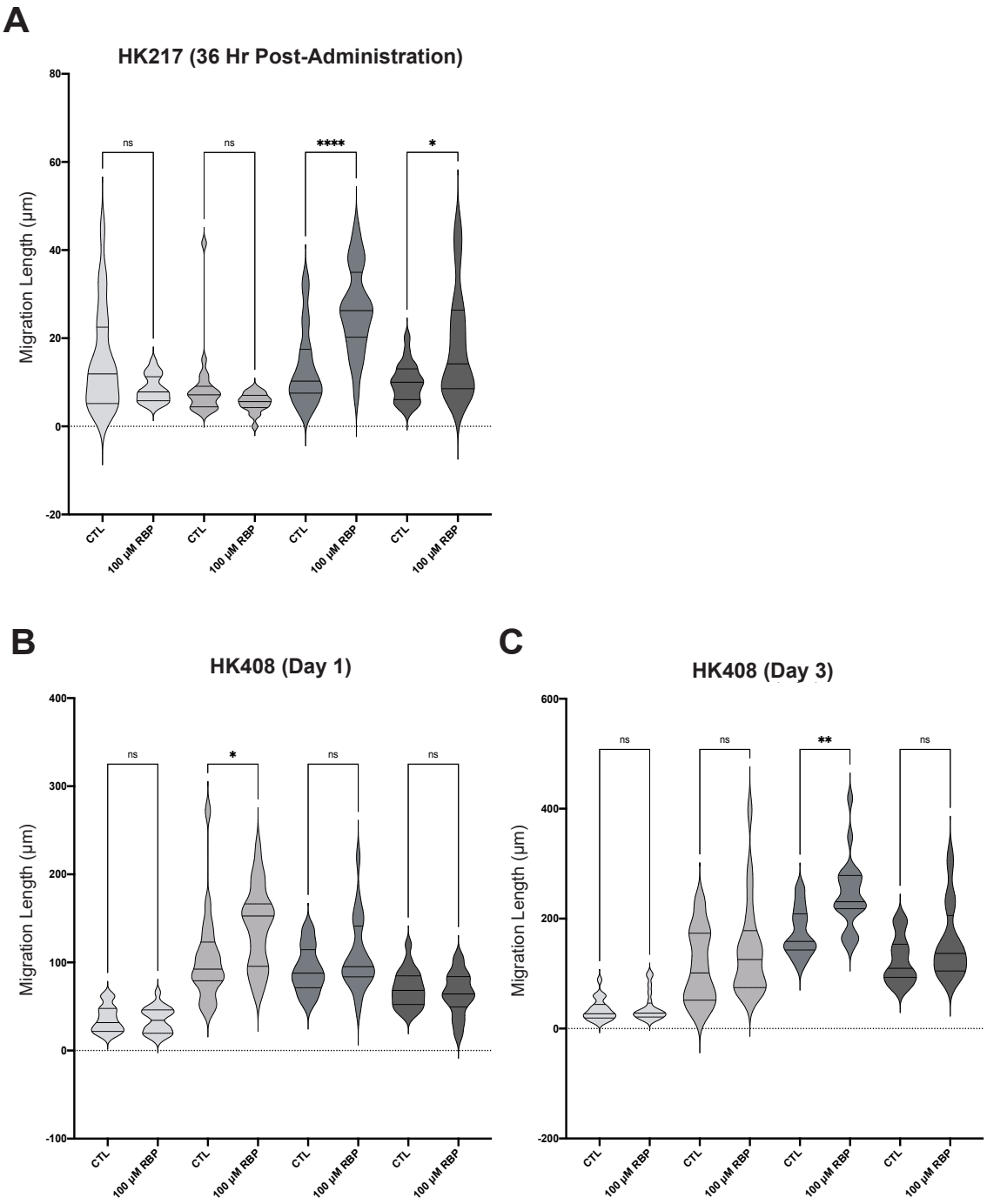

Figure 4.14: RHAMM inhibition studies on HK217 and HK408 GSs. A) Migration length quantification of HK217 GSs 36 hours following administration of RBP. B) Migration length quantification of HK408 GSs at day 1 timepoint (9 hours post administration of RBP). C) Migration length quantification of HK408 GSs at day 3 timepoint (9 hours following 2nd administration of RBP). *, $p < 0.05$; **, $p < 0.01$; ***, $p < 0.001$.

CHAPTER 5: DISCUSSION

The glioblastoma (GBM) tumor microenvironment is highly enriched with hyaluronic acid (HA) relative to that of lower grade CNS cancers, which include meningioma, astrocytoma, and oligodendroglioma. Moreover, the concentration of HA synthases in GBM patient biopsies positively correlates with disease lethality.[124,128] HA deposition is a significant feature of GBM cells extending from nascent tumor, as demonstrated by the presence of HA following *in vivo* xenografting as well as *in vitro* gliomasphere culture. Moreover, the concentrations of HA distributed throughout individual, GBM patient tumors widely vary, which likely contributes to the high intratumoral heterogeneity associated with GBM.[116,191] Yet, few studies have systematically evaluated the effects of local HA concentration on GBM cell invasion. The earliest study, to our knowledge, reporting on HA concentration effects utilized a 2D systems approach in which the investigators impregnated 0 - 1000 mg/mL of HA – of an unidentified molecular weight – in Matrigel constructs onto which U251 cells were seeded.[163] While maximal cell migration occurred in Matrigel with 200 mg/mL HA, the authors provided no potential explanations for the finding. Moreover, akin to many studies of GBM invasion *in vitro,*[32,166,183,192,193] the investigators utilized clonal cell lines which both genotypically and phenotypically differ from patient-derived cells.

In this work, we developed biomimetic hydrogels based on the bio-orthogonal thiol-ene click reactions, which form more stable crosslinks and have faster reaction rates relative to thiol-maleimide or thiol-methacrylate reaction chemistries typically utilized by other groups investigating GBM pathology with hydrogels.[169,176,177,179,181,184] By tuning the relative concentrations of thiolated HA by substituting thiolated polyethylene glycol (PEG) and

crosslinking with norbornene-functionalized PEG, we produced hydrogels with 0.10%, 0.25%, 0.50%, and 0.75% (w/v) HA concentrations that retained comparable poroelastic properties. Stiffness of all hydrogels was fixed to match the range of reported storage moduli for healthy brain tissue (100 – 1000 Pa).[194–197] While most studies have focused on ranges of higher HA concentrations (e.g. 1% - 5% (w/v)), we established GBM patient cells display sufficient variation in their degrees of sensitivity to local HA concentration changes within the finer 0.10% - 0.75% (w/v) range, more representative of physiological HA concentrations found in mammalian tissues.[186,187]

Morphological characterization could be used to inform machine learning paradigms for performing image based GBM classification, as being conducted by current researchers.[198,199] In accordance with past findings, higher concentrations of HA were generally associated with greater amounts of GS invasiveness across patient lines. However, in hydrogels with greater than 0.25% (w/v) HA, high variation in the degrees of motility were apparent between patient lines. HK177 and HK408 GSs exhibited a biphasic response to HA concentration within the 0.10% - 0.75% (w/v) range. However, the use of shape factor and migration lengths metrics to quantify migration allowed us to determine whether a biphasic relationship existed between HA concentration and sphere protrusion density (shape factor) or maximal protrusion lengths per sphere (migration length), specifically, for each patient line. The overall sphere protrusion density for HK177 GSs peaked in 0.25% (w/v) HA conditions, while the maximal protrusion length per sphere for HK408 GSs peaked in 0.50% (w/v) HA hydrogels. The HK217 patient line demonstrated similar invasiveness in all hydrogels with at least 0.25% (w/v) HA, while GS054 cells were most invasive in hydrogels with 0.75% (w/v) HA. Given a biphasic relationship was not observed for the HK217 and GS054 patient lines, we hypothesize the HA concentrations required for maximal migration

are greater than 0.75% (w/v) HA. Moreover, our findings complement those of the only other group to evaluate GBM cell migration within a HA concentration range similar to our study. Specifically, Pedron *et al.* (2013) developed hydrogels with equal concentrations of poly-ethylene glycol (PEG) diacrylate and varied concentrations of methacrylate-functionalized, 1630 kDa HA(0.10%, 0.30%, 0.50%, 0.7%, 1%, and 1.5% (w/v)).[183] A biphasic relationship between the gene expressions of FN, MMP-9, VEGF, and HIF1a - all proteins associated with GBM malignancy- and hydrogel HA concentration over the course of 7 days was present within the 0.10% - 1.5% (w/v) HA range. Three days following encapsulation, significant upregulations in the gene expression profiles were apparent for cells encapsulated in 0.30% compared to 0.10% (w/v) HA hydrogels.[183] As a continuation of their initial findings, Pedron *et al.* (2017) would demonstrate matrix metalloprotease (MMP)-2 and MMP-9 gene expression had varying levels of sensitivity to changes in HA concentration between the 0 – 2.0 wt% range. For example, GBM10 demonstrated peak expression in the 0.30 – 0.50 wt% HA range, while GBM6 showed no changes in gene expression in the full gamut.[185] However, it should be noted the hydrogels used in the studies did not have uniform elasticity moduli or diffusivity across HA conditions. Here, our findings build upon the studies by using hydrogels of similar mechanical properties for interrogating the morphologies of invading gliomaspheres, providing a direct link between local HA concentrations and GS invasiveness.

Moreover, our findings accompany work by Klank *et al.* (2017) in a study establishing a biphasic relationship between cluster of differentiation 44 (CD44) expression and GBM invasiveness *in vitro* and *in vivo*. Furthermore, GBM mice with CD44 knockout or vector-induced CD44 overexpression experienced greater survival compared to wildtype controls.[141] Based on their findings, the investigators reasoned wildtype, or intermediate, levels of CD44 are optimal for

maximal GBM invasion. They further suggested CD44, like integrin receptors, could operate as a molecular clutch critical for GBM mechanotransduction, an idea previously theorized by Kim and Kumar (2014) who identified changes in GBM cell motility due to stiffness occur through the HA-CD44 axis.[165] However, the 2014 study was unable to elucidate the molecular basis of CD44-mediated mechanosensation. While CD44 has been well-studied as a mechanosensory receptor in chondrocytes and fibroblasts,[200–202] it has not been addressed in GBM.

We decided to further explore potential differences in CD44-mediated mechanosensation through ezrin, an adaptor protein in the ezrin-radixin-moesin (ERM) complex that links the intracellular domain of CD44 to the actin cytoskeleton.[203] Like HA, ezrin is present in higher concentrations in GBM relative to lower grade gliomas.[152] Yet, the significance of the ERM complex in GBM migration and mechanosensitivity has not been systematically investigated except for during two *in vitro* studies.[153,154] More importantly, there are no studies regarding the relationship of ERM and GBM cell migration using 3D culture methods and non-transformed patient cell lines. Our results demonstrate that the propensity for GBM cells to invade depends on the degree of CD44-ERM-actin engagement, not overall levels of CD44 expressed, providing a direct answer to how CD44-mediated mechanotransduction can occur in GBM as pondered by Klank *et al.* (2017) and Kim and Kumar (2014).[141,165] First, GS054 GSs in 0.10%-0.75% (w/v) HA environments overall had lower densities of CD44 expression per cell, and thus CD44-HA binding events, compared to HK408 GSs across HA conditions. Yet, GS054 GSs in environments with 0.10% (w/v) HA were more migratory than HK408 GSs in the same HA condition at experimental endpoints. Correspondingly, HK408 GSs in low, 0.10% (w/v) HA concentrations exhibited low CD44-ezrin colocalization, and hence CD44-ERM engagement, while GS054 GSs under the same conditions demonstrated high levels of engagement comparable to both patient line GSs in

hydrogels with greater than 0.25% (w/v) HA. Thus, greater CD44 engagement of filamentous actin through the ERM domain increases the propensity of GBM cells to invade in low HA environments even when relatively less HA-CD44 binding events occur. Yet, HK408 GSs in 0.25% and 0.50% (w/v) HA conditions exhibited greater migration lengths than GS054 GSs in the same conditions. Moreover, GS054 GSs exhibited significantly greater migration lengths as well as crescent-like collective migration in 0.75% (w/v) HA conditions relative to 0.25% and 0.50% (w/v) HA environments. Thus, within a single cell line, greater HA densities also contributed to increased invasion and greater overall collective migration, which was the primary mode of migration observed in HK408 GSs in 0.25%-0.75% (w/v) HA hydrogels. Thus, we further hypothesize that even though the ratio of HA-CD44 binding may not determine the propensity for cellular invasion, it may determine the extent of cellular migration into the matrix in higher HA environments such that greater HA-CD44 binding events results in greater ERM-Actin engagements. Furthermore, the mesenchymal GBM patient line had far less CD44 expression compared to the proneural line. This discrepancy with past findings that CD44 is typically more expressed by mesenchymal patient lines could be due to the patient's stage of disease progression, history of administered treatments, or chance occurrence. In future studies, we will utilize the high throughput system developed by Liang *et al.* (in publication) to study a larger number of patient lines of varying GBM classifications. Such studies will better inform how the ratios of HA and CD44 as well as CD44-mediated cytoskeletal engagement drive the overall migration and invasive propensity of GBM cells on a per-patient basis.

To further evaluate the role of ERM in GBM motility and test out hypotheses, we pharmacologically inhibited ERM using a small molecule inhibitor (ERMi) at dosage concentrations of 5 - 20 μM. Interestingly, in conditions with high CD44-ERM engagement,

invasion ultimately decreased with sufficient ERMi administration; however, in the condition with low CD44-ERM engagement, ERMi increased cell migration. Specifically, increased invasion was noted in 0.10% HA hydrogels for HK408 GSs having undergone 5 - 20 μM treatments. Interestingly, 5 μM ERMi treatment also increased the invasiveness of HK217 GSs in 0.10% (w/v) HA hydrogel, suggesting spheroids in the low HA condition may exhibit similarly low levels of CD44-ERM engagement. Moreover, the 5 μM treatment of HK217 GSs in higher HA environments only reduced invasion in 0.25% and 0.50% (w/v) HA conditions, which suggests that the strengths of cytoskeleton engagements through ERM increase with greater HA. We hypothesize that excessive ERM-actin engagements in 0.75% (w/v) HA hydrogels may contribute, in part, to the biphasic responses noted in the HK408 and HK177 patient lines. Ultimately, ERMi treatment provided in excess (10 μM) to HK217 completely shut down invasion across conditions, demonstrating that inhibition of the HA-CD44-ERM-Actin axis completely substantially slows migration regardless of effects at lower concentrations. We further confirmed that GS054 not only has less CD44 relative to HK408, but also displays far lower CD44-ERM-Actin engagements overall given only a 5 μM dose of ERMi was necessary to shut down invasion, while 20 μM was necessary for stopping HK408 invasion. The greater overall CD44-ERM-actin binding events for HK408 GSs in higher HA environments compared to GS054 GSs also could explain their higher migration lengths into matrix. Moreover, the effective doses of GS054 (5 μM) and HK217 (10 μM) spheroids, which had lower migration lengths compared to HK408, further substantiate that greater CD44-ERM-actin binding events in a patient line promote greater invasiveness. Still, we hypothesize excessive cytoskeletal engagement may further reduce the propensity for cell migration. Overall, inhibition of ERM is presented as a potential therapeutic for targeting CD44-mediated invasion in GBM. However, effective doses at halting invasion vary according to the

strengths of cytoskeletal engagement displayed by individual patient lines, not necessarily the relative ratios of environmental HA and cellular CD44.

Still, targeting the CD44-ERM-actin axis alone may not suffice and should be evaluated on a per-patient basis, as aforementioned. Interestingly, even following the 20 μM treatment, single cell migration still occurred in HK408 GSs in ≥0.25% (w/v) HA matrices, while such a phenotype was absent from GS054 and HK217 with reduced invasiveness. A similar single cell invasion ensued in HK408 GSs when encapsulated in matrices with cysteine (CYS) substituted for RGD peptides and, thus, lacking integrin engagement. Mechanotransduction through RGD-Integrin ensues in the absence of CD44-ERM-actin engagements and vice versa, which could, in part, explain the poor efficacy of Cilengitide in treating GBM and suggests co-targeting of integrins and CD44 is more apropos for translational therapeutics. Changing the ratios of RGD-Integrin and CD44-ERM-actin axis engagements in higher HA environments (≥0.25% (w/v) HA) results in rounded, single cell migration with lower affinity adhesions to ECM. Yet, reducing either RGD- or CD44-ERM-mediated mechanotransduction for HK408 GSs in low HA conditions also promotes greater single cell invasion into the surrounding matrix. Thus, counterintuitively, both increased and decreased force transmission through integrins and CD44 can increase GBM cell motility, although the elongated, mesenchymal-like morphologies are only present when both integrin and CD44 engagements are sufficiently high. Given more invasion was noted in previously non-migratory GSs in 0.10% (w/v) following inhibition of ERM and removal of RGD peptides, we hypothesize modest reductions in clutch activity result in shifts in actin contractility dynamics within GBM cells, propelling cellular motion. In conclusion, our work echoes sentiments expressed by Klank *et al*. (2017) that CD44 is as integral as integrins in driving GBM invasion.[141]

Given more invasion was noted in previously non-migratory GSs in 0.10% (w/v) following inhibition of ERM, we hypothesize modest reductions in clutch activity result in shifts in actin contractility dynamics within GBM cells, propelling cellular motion. However, it remains unknown whether the single cell migration observed for both HK217 and HK408 GSs may be cells transitioning from mesenchymal to ameboid migration states, given such cellular transitions ensue following pharmacological inhibition. Future studies should more importantly investigate load-and-fail and frictional-slippage dynamics, presented by Odde and Chan (2008), in states of high and low ECM-actin engagements, respectively.[83] Our results echo findings by Bangasser *et al.* (2017), in which it was reported that U251 cells, which were not migratory in softer hydrogels, became invasive following modulation of integrin molecular clutches and myosin motors with targeted inhibitors. Simultaneously, U251 cells in stiff conditions became less migratory in presence of inhibitors.[84] However, our findings add a new dimension to GBM mechanobiology by demonstrating such differentials in actin-myosin dynamics may present not only as a function of changes in tissue mechanics but also changes in tissue densities of chemicals GBM cells encounter throughout the ECM. We build upon work by Klank *et al.* (2017) and Kim and Kumar (2014) and propose targeting the ERM domain as sufficient for studying CD44-mediated mechanosensing in GBM rather than targeting the whole CD44 receptor.[141,165] While we identified ERM as a single molecular clutch driving GBM mechanosensing, we hypothesize more high-throughput studies in conjunction with elucidating the proteomic and RNA-level expression profiles of GSs in various hydrogel conditions will provide more nuanced explanations for the patient-dependent changes in GBM invasion noted in across HA concentrations, especially following inhibition with ERMi. In said future studies, additional cell adhesion proteins should be evaluated for their contributions to GBM mechanotransduction occurring through CD44 and integrins. Given the high intratumoral

and intertumoral heterogeneity observed in GBM, we hypothesize GBM cell types between patients and from single patients exhibit varying levels of molecular activity (e.g. ERK/MAPK signaling, protease activation, epigenetic regulations) which, in turn, modulate mechanosensing through CD44 and integrins and give rise to the varying modes of invasion observed in our hydrogels.

We further investigated the effects of blocking HA binding to extracellular receptor for hyaluronan-mediated motility (RHAMM). Counterintuitively, RHAMM blocking lead to increased invasion for HK217 in 0.50% (w/v) and 0.75% (w/v) HA hydrogels as well as HK408 GSs encapsulated in 0.25% (w/v) & 0.50% (w/v) HA hydrogels. Interestingly, only a transient increase was noted in HK408 GSs encapsulated in 0.25% (w/v) HA environments, suggesting cells may deploy measures countering HA-RHAMM interaction disruption to return to homeostatic levels of migration as seen in control. The return to normal migration modes may be explained, in part, due to the "Go or Grow" hypothesis such that excess cell migration may result in lower levels of cell proliferation which could be unfavorable for tumor survival. The effects of RHAMM blocking on HK217 became visible as soon as 36 hours post-administration. Our findings are in contradiction to past studies demonstrating that reduced HA-RHAMM interactions in GBM cells results in decreased invasiveness.[116,155] However, unlike past studies, we utilize a 3D system to interrogate the nature of extracellular HA-RHAMM binding events. Relatively greater HA-RHAMM associations in 3D environments compared to 2D environments may result in tighter matrix binding, contributing to reduced motility. Thus, blocked HA-RHAMM associations could result in increased cell migration. Our results are not completely novel given a recent study by Tolg *et al.* (2020) reports RHAMM knockdown in mice results in reduced fibroblast motility.[204] Moreover, based on findings by Tolg *et al.* (2020), reduced RHAMM activity could result in

reduced MMP-9 expression, thereby decreasing mesenchymal mode of migration. Future studies should study varying concentrations of extracellular RHAMM inhibition and its effects on GBM cell invasion. Moreover, future investigators should target both intracellular and extracellular RHAMM given its variable effects on migration and proliferation given its localization within cells.

CHAPTER 6: CONCLUSION & FUTURE DIRECTIONS

We establish GBM cell mechanotransduction can occur through the HA-CD44-ERM-actin axis. While higher HA-CD44 binding events can promote greater invasion distances of GBM cells into tissues, the propensity for GBM cells to invade tissues depends on levels of ERM-mediated CD44 anchoring to the actin cytoskeleton. Compared to HK408 GSs, GS054 GSs had lower densities of membranous CD44 and, correspondingly, lesser migration lengths into matrix when high rates of invasion ensued. Even though less CD44-HA binding events occurred in GS054 GSs relative to HK408s, greater CD44-ERM engagements resulted in higher GS invasiveness in low, 0.10% (w/v) HA conditions. Moreover, the elicitation of invasion depends on balanced filamentous actin engagement through not only HA-CD44-ERM but also RGD-integrin axes. Strengthened actin engagement in HK408 GSs within 0.25% (w/v) HA environments increased invasion relative to the rather stationary 0.10% (w/v) HA condition with lesser CD44-ERM engagements. Interestingly, further weakening of CD44-ERM-actin engagements for HK408 GSs in 0.10% (w/v) HA through pharmacological inhibition of ERM also resulted in greater invasion, although varied, single cell phenotype. The same single cell phenotype was observed when RGD peptides were removed from the hydrogel, suggesting both mechanotransduction through RGD-integrin and HA-CD44 are required for maximized cell invasion into parenchyma. Altogether, we propose further characterization is necessary regarding the nature of HA-driven migration through the CD44-ERM axis on a patient-specific basis to map the molecular level interactions causing the observed heterogeneity in CD44-ERM-Actin axis inhibition response. This further substantiates the need to study other molecular clutch proteins, like Ankyrin, as well as myosin motors using our experimental model in a high throughput fashion.

High-Throughput Screening Platform

A first generation, high-throughput system based on our hydrogel model was recently described in Liang *et al.* (in publication) and could provide substantial benefits as a theranostic tools. Using such a system, future studies could entail screening molecular clutch inhibitors on patient cells in varying concentrations of HA, varying stiffnesses, and varying types and concentrations of peptides promoting aggressive phenotypes. In combination with protein multiplexing assays, the system developed by Liang *et al.* (in publication) could improve means of rapid screening and patient GBM classification based on pathway activations or phosphokinase activity. In a preliminary study, performed Luminex multiplex assay on lysates collected from HK408 GSs cultured in 0.10%-0.75% (w/v) HA hydrogels and media as well as GS054 GSs cultured in media. We specifically assessed abundances of phosphokinase proteins associated with the ERK-MAPK and AKT-mTOR pathways. Linear discriminant analysis followed by leave-one-out cross validation was performed on fluorescence values per analyte to assess potential variations between samples. While no differences were notable in HK408 GSs in any conditions, stark contrasts could be noted between GS054 and HK408 GSs, suggesting heavy patient heterogeneity in ERK-MAPK and AKT-mTOR activity (Figure 6.1). Such knowledge of relative phosphokinase activity between patient lines could inform decisions on therapeutics targeting the ERK-MAPK and AKT-mTOR axes as well as their associated regimens on a per-patient basis. In future experiments, we will expand our Luminex assay analytes to consider the activities of a wider range of proteins pertinent to GBM invasion or proliferation.

As Liang *et al.* (in publication) demonstrated, cellular transfection with a fluorescent reporter provided the means of automated proliferation analysis downstream. Automated means of shape factor and migration length analysis can supplement such a high throughput system by

providing patient cell- or patient GS-specific morphometrics. Beyond current means of patient GBM classification using genetic, molecular, or histopathological characterization of resected tissues, morphological and similar phenotypic expressions of patient-resected cells in 3D hydrogel cultures of varying mechanochemical properties can provide another means of GBM classification. 3D morphometric modeling has been explored as a diagnostic tool for GBM patients but has not been adopted as a clinical standard to date.

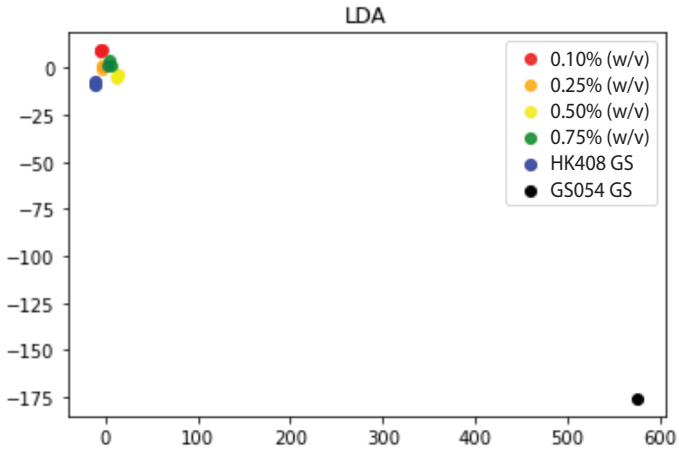

Figure 6.1: Linear discriminant analysis (LDA) performed on median fluorescence intensity values collected from Luminex multiplex assay of phosphoproteins.

Interface Hydrogels

As a continuation of our studies, we are developing interfacing hydrogels to better interrogate the sensitivity of patient cells to changes in local concentrations of HA. Specifically, rather than using single hydrogels of defined HA concentration, the interfacing hydrogels can provide a gradient of concentrations over a range (i.e., 0.10% - 0.75% (w/v)). Such a model would provide a means of characterizing phenotypes, like invasion, treating HA concentration as a continuous rather than discrete variable, as in our studies. For example, while we defined HK177 as having a maximal invasion at 0.25% (w/v), we cannot determine whether this concentration is

the true optimum for maximal migration without considering the range of HA concentrations between 0.10% (w/v) and 0.50% (w/v) HA. Using interface hydrogels, we can evaluate how changes in gradient slopes or chemical densities may modulate cell invasion velocity as has been previously demonstrated on non-GBM cells.[205,206] Furthermore, cytochemical analysis and NextGen sequencing methods can be utilized to study how gradual changes in ECM concentrations result in changes in intracellular states (e.g. protein activity, protein-protein interactions). Given our findings of the biphasic relationship between HA concentration and HK177 invasiveness, we hypothesize encapsulating HK177 cells in fusion gel of concentrations 0.10% - 2.00% (w/v) HA could better model the rates of gain and loss of invasion from the concentration of maximum invasion.

Figure 14 provides the means of engineering an interfaced hydrogel based on our thiol-ene photo click chemistry (Figure 6.2.A). First, an 80 μL hydrogels solution of defined HA concentration would be gelated and then be immediately hole-punched to extract a 30 μL volume of hydrogel. Next, a 30 μL volume of hydrogel solution of another HA concentration would be applied along with a photomask to prevent UV emission to the originally gelated hydrogel. Secondary exposure results in fusion of both hydrogels. Initial studies characterizing such interface hydrogels have been performed by Sohrabi *et al.* (in publication) but focused on hydrogels of varying mechanics rather than HA concentrations. As an initial trial, we developed interface hydrogels using FITC- and DsRed- labeling of 0.10% (w/v) HA and 0.50% (w/v) HA hydrogels, respectively (Figure 6.2.B).

Future models must build upon the current by designing modes of cell extraction at specific radial distances from the hydrogel center. This would allow further characterization of the

extracted cells along with differential expression analysis. Spatial transcriptomics can be a valuable tool in combination with interface hydrogel technology.

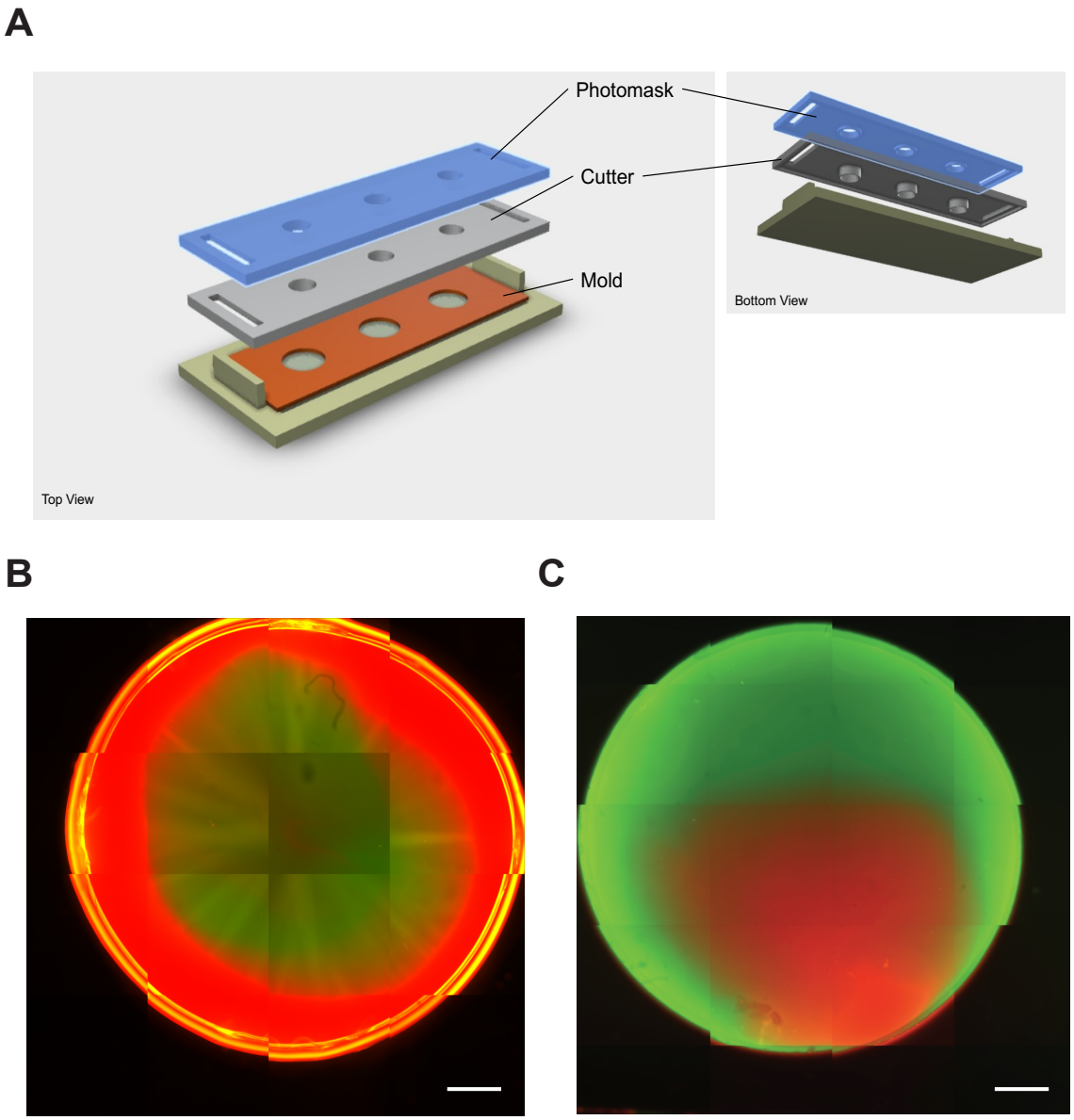

Figure 6.2: Interface gel development. A) 3D model render of interface hydrogel maker indicating the photomask for secondary UV exposure, cutter to remove 30 mm^3 inner volume, and mold to hold 80 mm^3 total hydrogel volume. B) Image of interface gel with 3 mM thiols (red) and 1.5 mM thiols (green). Scale bar = 10 µm. C) Image of interface gel with 1.5 mM thiols (green) and 3 mM thiols (red). Scale bar = 10 µm.

Characterization of Patient GBM Heterogeneity with Hydrogels

As elaborated in Chapter 1, high intratumoral and intertumoral heterogeneity are key features of GBM. Building upon DNA microarray technologies utilized in the early 2000's, single-cell RNA sequencing allows for clustering of GBM cells within or between GBM patient samples based on their RNA expression profiles. Current efforts seek to expand upon the conventional molecular classifications designated to GBM subtypes by the WHO, such as proneural and mesenchymal. For example, given the theory that GBM arises from neural stem/progenitor cells (NS/PCs), investigators have rationalized that GBM subtypes could be associated with specific lineages of NS/PCs. Specifically, Neftel *et al.* (2019) identified GBM subtypes from 20 adult and 8 pediatrics GBM samples as being neural progenitor-like, oligodendrocyte-like, astrocyte-like, and mesenchymal-like based on genetic expression patterns of CDK4, PDGFRA, EGFR, and NF1.[207] Bhaduri *et al.* (2020) expanded on the classifications provided by Neftel *et al.* (2019), including more specific early-stage cellular states, such as radial glial cells, central ganglionic eminence interneurons, and protoplasmic astrocytes. Interestingly, the radial glial-like GBM cells could exhibit mitotic spindle translocation, typical of normal radial glial cells, when cultured *in vitro.* Moreover, these radial glial-like cells gave rise to proliferative daughter cells.[24] Specifically, one group showed isodehydrogenase wildtype (IDHwt) glial stem cells (GSCs) display plasticity and can differentiate into cell states mimicking astrocytic, neuronal, and oligodendrocytic cell lineages associated with neural development in healthy CNS.[208] The identification, isolation, and clonal expansion of clustered GBM cell types could inform the heterogeneous phenotypic presentations within individual patient samples. In combination with our high-throughput model described in Chapter 6, phenotypes can be evaluated over a range of mechanochemically distinct microenvironments.

As discussed in Chapter 1., the *in vitro* culture models and methods GBM can influence observed cell behaviors and phenotypes in studies. To study how culture methods influence GBM cell types, we performed a preliminary single-cell RNA sequencing on patient line GS025 cells cultured as 2D monolayer (GS25), GS (GS25NS), and single cells encapsulated in 0.50% (w/v) HA hydrogels (GS25Gel). RNA extraction and cDNA library construction was performed using the Chromium 10X Genomics microfluidic chip, while HiSeq3000 was used for sequencing. Seurat v4 was used for downstream quality control, clustering, and differential expression analysis. Cells with less than 200 genes, greater than 7,500 unique RNAs, and greater than 15% mitochondrial genes were removed. Dimensionality reduction and shared nearest neighbor clustering was then performed on the integrated dataset. Cluster annotation was performed following a modified version of the protocol presented by Bhaduri *et al.* (2020). Uniform manifold approximation (UMAP) was utilized for dimensionality reduction and visualization of clusters (Figure 6.3.A)

While many of the same cell types are across conditions, there is clear variation in the relative counts of oligodendrocyte-like GBM cells between the *in vitro* models. Oligodendrocyte-like cells are highly enriched within the hydrogels, whereas dividing OPCs and OPCs are generally more represented in 2D monolayer and GS cultures. Next, we evaluated the RNA expression profiles for exosome marker CD63, HA receptors CD44, RHAMM, and integrin subunit αV (ITGAV). CD63 expression was highest in GS culture, indicating cell-cell contacts may augment extracellular vesicle development, while local HA-cell interactions play a lesser role for the patient line (Figure 6.3.B) More notably, oligodendrocyte-like and dividing neuron-like GBM cells have higher expression of integrin αV and HA receptors when in hydrogels (Figure 6.3.C-E) Such preliminary findings can be expanded to more multiple experimental models, such as PDOX, and

multiple patient lines to provide insight into potential changes in cell phenotypes when studied with various experimental models.

GBM classification based on transcriptional states alone is insufficient given that levels of RNA transcription and translation into protein are not correlative. Thus, we seek to perform differential expression analysis of single cell RNA sequencing data in combination with multiplexed protein assays, as aforementioned, to provide meaningful insights into the transcriptional and translational states of GBM patient cells. All in all, our efforts would both improve GBM classification and inform patient-specific therapeutic development and/or administration.

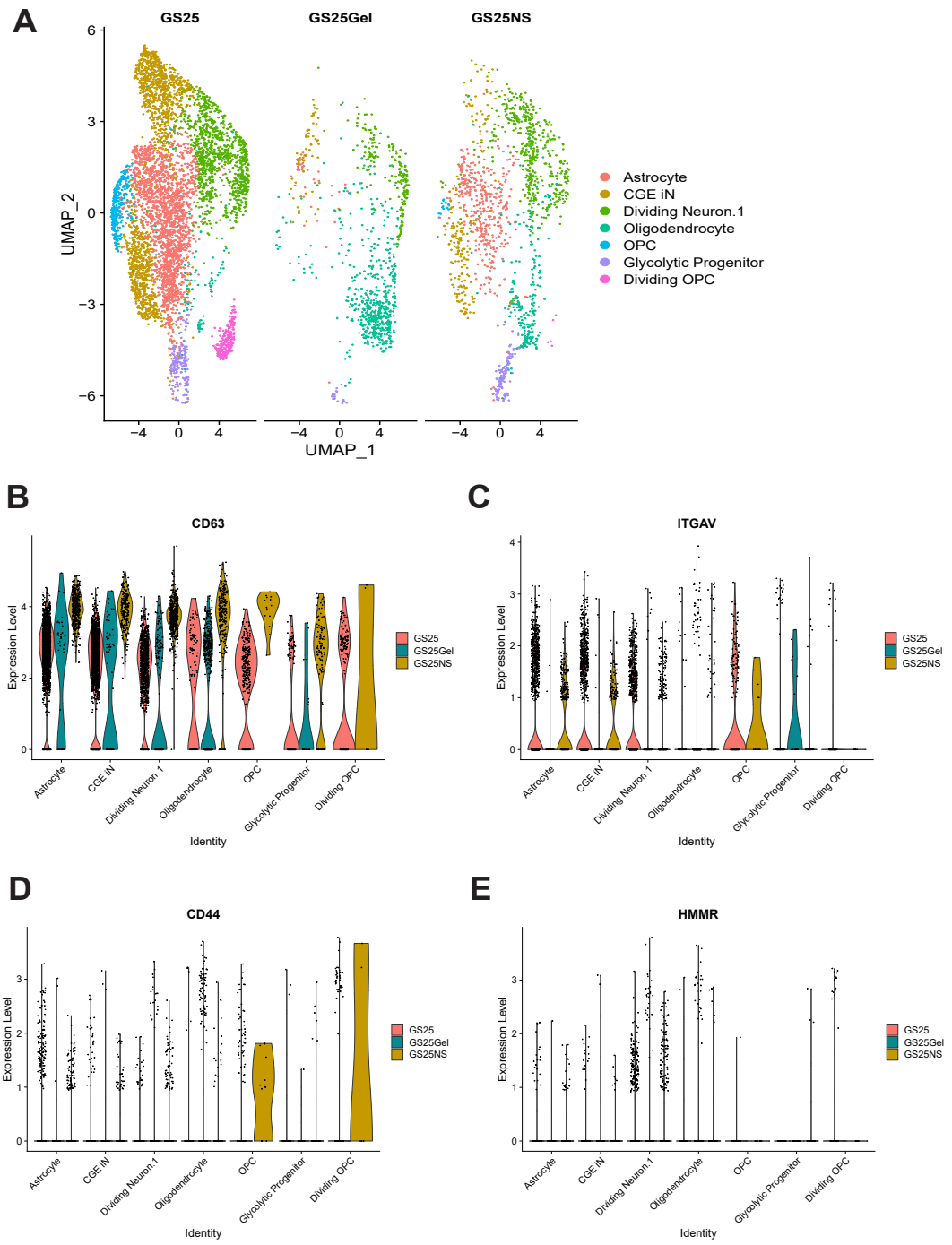

Figure 6.3: Single cell RNA sequencing of GS25 patient line. A) UMAP plot of clusters for each GS25 patient cell condition. GS25 is 2D monolayer culture; GS25Gel is 3D hydrogel culture n 0.50% (w/v) HA hydrogel; GS25NS is 3D gliomasphere culture. B-E) Violin plots of CD63, ITGAV, CD44, and HMMR genes per cluster per condition.

CHAPTER 7: BIBILIOGRAPHY

1. Tan, A. C. *et al.* Management of glioblastoma: State of the art and future directions. *CA. Cancer J. Clin.* **70**, 299–312 (2020).
2. Ostrom, Q. T. *et al.* CBTRUS Statistical Report: Primary Brain and Other Central Nervous System Tumors Diagnosed in the United States in 2011-2015. *Neuro. Oncol.* **20**, iv1–iv86 (2018).
3. Faraz, S., Pannullo, S., Rosenblum, M., Smith, A. & Wernicke, A. G. Long-term survival in a patient with glioblastoma on antipsychotic therapy for schizophrenia: a case report and literature review. *Ther. Adv. Med. Oncol.* **8**, 421 (2016).
4. Omuro, A. & DeAngelis, L. M. Glioblastoma and other malignant gliomas: a clinical review. *JAMA* **310**, 1842–1850 (2013).
5. Keime-Guibert, F. *et al.* Radiotherapy for Glioblastoma in the Elderly. *N. Engl. J. Med.* **356**, 1527–1535 (2007).
6. Stupp, R. *et al.* Radiotherapy plus concomitant and adjuvant temozolomide for glioblastoma. *N. Engl. J. Med.* **352**, 987–996 (2005).
7. TAMIMI, A. F. & JUWEID, M. Epidemiology and Outcome of Glioblastoma. *Glioblastoma* 143–153 (2017) doi:10.15586/CODON.GLIOBLASTOMA.2017.CH8.
8. Fisher, J. L., Schwartzbaum, J. A., Wrensch, M. & Wiemels, J. L. Epidemiology of brain tumors. *Neurol. Clin.* **25**, 867–890 (2007).
9. Ostrom, Q. T. *et al.* CBTRUS Statistical Report: Primary Brain and Central Nervous System Tumors Diagnosed in the United States in 2008-2012. *Neuro. Oncol.* **17 Suppl 4**, iv1–iv62 (2015).
10. Alexander, B. M. & Cloughesy, T. F. Adult glioblastoma. *J. Clin. Oncol.* **35**, 2402–2409

(2017).

11. Ostrom, Q. T., Cote, D. J., Ascha, M., Kruchko, C. & Barnholtz-Sloan, J. S. Adult Glioma Incidence and Survival by Race or Ethnicity in the United States From 2000 to 2014. *JAMA Oncol.* **4**, 1254 (2018).

12. Liu, E. K., Yu, S., Sulman, E. P. & Kurz, S. C. Racial and socioeconomic disparities differentially affect overall and cause-specific survival in glioblastoma. *J. Neurooncol.* **149**, 55–64 (2020).

13. Gately, L., McLachlan, S., Dowling, A. & Philip, J. Life beyond a diagnosis of glioblastoma: a systematic review of the literature. *J. Cancer Surviv.* **11**, 447–452 (2017).

14. McKinnon, C., Nandhabalan, M., Murray, S. A. & Plaha, P. Glioblastoma: clinical presentation, diagnosis, and management. *BMJ* **374**, (2021).

15. Shukla, G. *et al.* Advanced magnetic resonance imaging in glioblastoma: a review. *Chinese Clin. Oncol.* **6**, (2017).

16. Schneider, T., Mawrin, C., Scherlach, C., Skalej, M. & Firsching, R. Gliomas in Adults. *Dtsch. Arztebl. Int.* **107**, 799 (2010).

17. Perry, A. & Wesseling, P. Histologic classification of gliomas. *Handb. Clin. Neurol.* **134**, 71–95 (2016).

18. Sallinen, S.-L., Salllinen, P. K., Haapasalo, H. K. & Helin, H. J. Identification of Differentially Expressed Genes in Human Gliomas by DNA Microarray and Tissue Chip Techniques. *Cancer Res.* **60**, 6617–6622 (2000).

19. Rickman, D. S. *et al.* Distinctive Molecular Profiles of High-Grade and Low-Grade Gliomas Based on Oligonucleotide Microarray Analysis 1. *CANCER Res.* **61**, 6885–6891 (2001).

20. Phillips, H. S. *et al.* Molecular subclasses of high-grade glioma predict prognosis, delineate a pattern of disease progression, and resemble stages in neurogenesis. *Cancer Cell* **9**, 157–173 (2006).

21. Zhang, P., Xia, Q., Liu, L., Li, S. & Dong, L. Current Opinion on Molecular Characterization for GBM Classification in Guiding Clinical Diagnosis, Prognosis, and Therapy. *Front. Mol. Biosci.* **7**, 241 (2020).

22. McLendon, R. *et al.* Comprehensive genomic characterization defines human glioblastoma genes and core pathways. *Nature* **455**, 1061–1068 (2008).

23. Verhaak, R. G. W. *et al.* Integrated genomic analysis identifies clinically relevant subtypes of glioblastoma characterized by abnormalities in PDGFRA, IDH1, EGFR, and NF1. *Cancer Cell* **17**, 98–110 (2010).

24. Bhaduri, A. *et al.* Outer Radial Glia-like Cancer Stem Cells Contribute to Heterogeneity of Glioblastoma. *Cell Stem Cell* **26**, 48-63.e6 (2020).

25. Garofano, L. *et al.* Pathway-based classification of glioblastoma uncovers a mitochondrial subtype with therapeutic vulnerabilities. *Nat. Cancer 2020 22* **2**, 141–156 (2021).

26. Louis, D. N. *et al.* The 2021 WHO Classification of Tumors of the Central Nervous System: a summary. *Neuro. Oncol.* **23**, 1231–1251 (2021).

27. Louis, D. N. *et al.* The 2016 World Health Organization Classification of Tumors of the Central Nervous System: a summary. *Acta Neuropathol.* doi:10.1007/s00401-016-1545-1.

28. Xiao, Z. Z. *et al.* Carmustine as a Supplementary Therapeutic Option for Glioblastoma: A Systematic Review and Meta-Analysis. *Front. Neurol.* **11**, 1036 (2020).

29. Shergalis, A., Bankhead, A., Luesakul, U., Muangsin, N. & Neamati, N. Current challenges and opportunities in treating glioblastomas. *Pharmacol. Rev.* **70**, 412–445

(2018).

30. Pacheco, C. *et al.* Glioblastoma Vasculature: From its Critical Role in Tumor Survival to Relevant in Vitro Modelling. *Front. Drug Deliv.* **0**, 1 (2022).

31. Muthukrishnan, S. D. *et al.* Radiation-induced reprogramming drives glioma vascular transdifferentiation and tumor recurrence. *bioRxiv* 2021.06.03.447005 (2021) doi:10.1101/2021.06.03.447005.

32. Liu, Y. *et al.* IGFBP2 promotes vasculogenic mimicry formation via regulating CD144 and MMP2 expression in glioma. *Oncogene 2018 3811* **38**, 1815–1831 (2018).

33. Angara, K., Borin, T. F. & Arbab, A. S. Vascular Mimicry: A Novel Neovascularization Mechanism Driving Anti-Angiogenic Therapy (AAT) Resistance in Glioblastoma. *Transl. Oncol.* **10**, 650–660 (2017).

34. Medikonda, R., Dunn, G., Rahman, M., Fecci, P. & Lim, M. A review of glioblastoma immunotherapy. *J. Neurooncol.* **151**, 41–53 (2021).

35. Brown, C. E. *et al.* Optimization of IL13Rα2-Targeted Chimeric Antigen Receptor T Cells for Improved Anti-tumor Efficacy against Glioblastoma. *Mol. Ther.* **26**, 31 (2018).

36. Ahmed, N. *et al.* HER2-Specific Chimeric Antigen Receptor-Modified Virus-Specific T Cells for Progressive Glioblastoma: A Phase 1 Dose-Escalation Trial. *JAMA Oncol.* **3**, 1094–1101 (2017).

37. O'Rourke, D. M. *et al.* A single dose of peripherally infused EGFRvIII-directed CAR T cells mediates antigen loss and induces adaptive resistance in patients with recurrent glioblastoma. *Sci. Transl. Med.* **9**, (2017).

38. Yang, T., Kong, Z. & Ma, W. PD-1/PD-L1 immune checkpoint inhibitors in glioblastoma: clinical studies, challenges and potential. *Hum. Vaccin. Immunother.* **17**, 546 (2021).

39. Frederico, S. C. *et al.* Making a Cold Tumor Hot: The Role of Vaccines in the Treatment of Glioblastoma. *Front. Oncol.* **11**, 1591 (2021).

40. Landry, A. P., Balas, M., Alli, S., Spears, J. & Zador, Z. Distinct regional ontogeny and activation of tumor associated macrophages in human glioblastoma. *Sci. Reports 2020 101* **10**, 1–13 (2020).

41. Buonfiglioli, A. & Hambardzumyan, D. Macrophages and microglia: the cerberus of glioblastoma. *Acta Neuropathol. Commun. 2021 91* **9**, 1–21 (2021).

42. Kennedy, B. C. *et al.* Tumor-Associated Macrophages in Glioma: Friend or Foe? *J. Oncol.* **2013**, 11 (2013).

43. Wang, L. *et al.* Therapeutic peptides: current applications and future directions. *Signal Transduct. Target. Ther. 2022 71* **7**, 1–27 (2022).

44. Guidotti, G., Brambilla, L. & Rossi, D. Cell-Penetrating Peptides: From Basic Research to Clinics. *Trends Pharmacol. Sci.* **38**, 406–424 (2017).

45. Raucher, D. Tumor targeting peptides: novel therapeutic strategies inglioblastoma. *Curr. Opin. Pharmacol.* **47**, 14 (2019).

46. Stupp, R. *et al.* Effect of Tumor-Treating Fields Plus Maintenance Temozolomide vs Maintenance Temozolomide Alone on Survival in Patients With Glioblastoma: A Randomized Clinical Trial. *JAMA* **318**, 2306–2316 (2017).

47. Vollmann-Zwerenz, A., Leidgens, V., Feliciello, G., Klein, C. A. & Hau, P. Tumor Cell Invasion in Glioblastoma. *Int. J. Mol. Sci.* **21**, (2020).

48. Friedl, P. & Wolf, K. Tumour-cell invasion and migration: diversity and escape mechanisms. *Nat. Rev. Cancer* **3**, 362–374 (2003).

49. Chouleur, T., Tremblay, M. L. & Bikfalvi, A. Mechanisms of invasion in glioblastoma.

Curr. Opin. Oncol. **32**, 631–639 (2020).

50. Scherer, H. J. A CRITICAL REVIEW: THE PATHOLOGY OF CEREBRAL GLIOMAS. *J. Neurol. Psychiatry* **3**, 147 (1940).

51. Bastola, S. *et al.* Glioma-initiating cells at tumor edge gain signals from tumor core cells to promote their malignancy. *Nat. Commun. 2020 111* **11**, 1–17 (2020).

52. Larsson, I. *et al.* Modeling glioblastoma heterogeneity as a dynamic network of cell states. *Mol. Syst. Biol.* **17**, (2021).

53. Dirkse, A. *et al.* Stem cell-associated heterogeneity in Glioblastoma results from intrinsic tumor plasticity shaped by the microenvironment. *Nat. Commun.* **10**, (2019).

54. Anderson, A. R. A. A hybrid mathematical model of solid tumour invasion: the importance of cell adhesion. *Math. Med. Biol. A J. IMA* **22**, 163–186 (2005).

55. de Montigny, J. *et al.* An in silico hybrid continuum-/agent-based procedure to modelling cancer development: Interrogating the interplay amongst glioma invasion, vascularity and necrosis. *Methods* **185**, 94–104 (2021).

56. Himes, B. T. *et al.* Immunosuppression in Glioblastoma: Current Understanding and Therapeutic Implications. *Front. Oncol.* **11**, 4194 (2021).

57. Hambardzumyan, D. & Bergers, G. Glioblastoma: Defining Tumor Niches. *Trends in cancer* **1**, 252 (2015).

58. Ye, X. *et al.* Tumor-associated microglia/macrophages enhance the invasion of glioma stem-like cells via TGF-β1 signaling pathway. *J. Immunol.* **189**, 444–453 (2012).

59. Martinez, F. O. & Gordon, S. The M1 and M2 paradigm of macrophage activation: time for reassessment. *F1000Prime Rep.* **6**, (2014).

60. Kingsmore, K. M. *et al.* Interstitial flow differentially increases patient-derived

glioblastoma stem cell invasion via CXCR4, CXCL12, and CD44-mediated mechanisms. *Integr. Biol. (Camb).* **8**, 1246–1260 (2016).

61. Cornelison, R. C., Brennan, C. E., Kingsmore, K. M. & Munson, J. M. Convective forces increase CXCR4-dependent glioblastoma cell invasion in GL261 murine model. *Sci. Reports 2018 81* **8**, 1–11 (2018).

62. J. Richardson, P. CXCR4 and Glioblastoma. *Anticancer. Agents Med. Chem.* **16**, 59–74 (2016).

63. Lam, D. *et al.* Tissue-specific extracellular matrix accelerates the formation of neural networks and communities in a neuron-glia co-culture on a multi-electrode array. *Sci. Reports 2019 91* **9**, 1–15 (2019).

64. Nicholson, C. & Syková, E. Extracellular space structure revealed by diffusion analysis. *Trends Neurosci.* **21**, 207–215 (1998).

65. Wade, A. *et al.* Proteoglycans and their roles in brain cancer. *FEBS J.* **280**, 2399–2417 (2013).

66. Yu, Q. *et al.* Extracellular Matrix Proteins Confer Cell Adhesion-Mediated Drug Resistance Through Integrin αv in Glioblastoma Cells. *Front. Cell Dev. Biol.* **9**, 240 (2021).

67. Ruoslahti, E. RGD and other recognition sequences for integrins. *Annu. Rev. Cell Dev. Biol.* **12**, 697–715 (1996).

68. Gingras, M. claude, Roussel, E., Bruner, J. M., Branch, C. D. & Moser, richard P. Comparison of cell adhesion molecule expression between glioblastoma multiforme and autologous normal brain tissue. *J. Neuroimmunol.* **57**, 143–153 (1995).

69. Ellert-Miklaszewska, A., Poleszak, K., Pasierbinska, M. & Kaminska, B. Integrin

Signaling in Glioma Pathogenesis: From Biology to Therapy. *Int. J. Mol. Sci.* **21**, (2020).

70. Zagzag, D. *et al.* Tenascin-C promotes microvascular cell migration and phosphorylation of focal adhesion kinase. | Semantic Scholar. *Cancer Res.* **62**, 2660–2668 (2002).

71. Miroshnikova, Y. A. *et al.* Tissue mechanics promote IDH1-dependent HIF1α-tenascin C feedback to regulate glioblastoma aggression. *Nat. Cell Biol.* **18**, 1336–1345 (2016).

72. Tilak, M., Holborn, J., New, L. A., Lalonde, J. & Jones, N. Receptor Tyrosine Kinase Signaling and Targeting in Glioblastoma Multiforme. *Int. J. Mol. Sci.* **22**, 1–35 (2021).

73. Liu, Z. *et al.* EGFRvIII/integrin β3 interaction in hypoxic and vitronectinenriching microenvironment promote GBM progression and metastasis. *Oncotarget* **7**, 4680 (2016).

74. Zhang, J. fei *et al.* IL-33/ST2 axis promotes glioblastoma cell invasion by accumulating tenascin-C. *Sci. Reports 2019 91* **9**, 1–10 (2019).

75. Agudelo-Garcia, P. A. *et al.* Glioma Cell Migration on Three-dimensional Nanofiber Scaffolds Is Regulated by Substrate Topography and Abolished by Inhibition of STAT3 Signaling. *Neoplasia* **13**, 831 (2011).

76. Beliveau, A., Thomas, G., Gong, J., Wen, Q. & Jain, A. Aligned Nanotopography Promotes a Migratory State in Glioblastoma Multiforme Tumor Cells. *Sci. Reports 2016 61* **6**, 1–13 (2016).

77. Espina, J. A., Marchant, C. L. & Barriga, E. H. Durotaxis: the mechanical control of directed cell migration. *FEBS J.* **289**, 2736–2754 (2022).

78. Grundy, T. J. *et al.* Differential response of patient-derived primary glioblastoma cells to environmental stiffness. *Sci. Reports 2016 61* **6**, 1–10 (2016).

79. Marhuenda, E. *et al.* Glioma stem cells invasive phenotype at optimal stiffness is driven by MGAT5 dependent mechanosensing. *J. Exp. Clin. Cancer Res.* **40**, (2021).

80. Goodman, S. L., Risse, G. & Von Der Mark, K. The E8 subfragment of laminin promotes locomotion of myoblasts over extracellular matrix. *J. Cell Biol.* **109**, 799–809 (1989).

81. Schmid-schonbein, G. W., Paul Sung, K.-L., Tozeren, H., Skalak, R. & Chien, S. PASSIVE MECHANICAL PROPERTIES OF HUMAN LEUKOCYTES. *Biophys. J.* **36**, 243–256.

82. DiMilla, P. A., Barbee, K. & Lauffenburger, D. A. Mathematical model for the effects of adhesion and mechanics on cell migration speed. *Biophys. J.* **60**, 15–37 (1991).

83. Chan, C. E. & Odde, D. J. Traction dynamics of filopodia on compliant substrates. *Science (80-.).* **322**, 1687–1691 (2008).

84. Bangasser, B. L. *et al.* Shifting the optimal stiffness for cell migration. *Nat. Commun. 2017 81* **8**, 1–10 (2017).

85. Prahl, L. S. *et al.* Microtubule-Based Control of Motor-Clutch System Mechanics in Glioma Cell Migration. *Cell Rep.* **25**, 2591-2604.e8 (2018).

86. Bangasser, B. L., Rosenfeld, S. S. & Odde, D. J. Determinants of Maximal Force Transmission in a Motor-Clutch Model of Cell Traction in a Compliant Microenvironment. *Biophys. J.* **105**, 581 (2013).

87. Friedl, P. & Gilmour, D. Collective cell migration in morphogenesis, regeneration and cancer. *Nat. Rev. Mol. Cell Biol. 2009 107* **10**, 445–457 (2009).

88. Diao, W. *et al.* Behaviors of Glioblastoma Cells in in Vitro Microenvironments. *Sci. Reports 2019 91* **9**, 1–9 (2019).

89. Serres, E. *et al.* Fibronectin expression in glioblastomas promotes cell cohesion, collective invasion of basement membrane in vitro and orthotopic tumor growth in mice. *Oncogene* **33**, 3451–3462 (2014).

90. Nousi, A., Søgaard, M. T., Audoin, M. & Jauffred, L. Single-cell tracking reveals super-spreading brain cancer cells with high persistence. *Biochem. Biophys. Reports* **28**, 101120 (2021).

91. Ramaswamy, P., Nanjaiah, N. D. & Borkotokey, M. Role of MEK-ERK signaling mediated adhesion of glioma cells toextra-cellular matrix: Possible implication on migration andproliferation. *Ann. Neurosci.* **26**, 52 (2019).

92. Ou, A., Ott, M., Fang, D. & Heimberger, A. B. The Role and Therapeutic Targeting of JAK/STAT Signaling in Glioblastoma. *Cancers (Basel).* **13**, 1–25 (2021).

93. Al-Koussa, H., Atat, O. El, Jaafar, L., Tashjian, H. & El-Sibai, M. The Role of Rho GTPases in Motility and Invasion of Glioblastoma Cells. *Anal. Cell. Pathol. (Amst).* **2020**, (2020).

94. Armento, A., Ehlers, J., Schötterl, S. & Naumann, U. Molecular Mechanisms of Glioma Cell Motility. *Glioblastoma* 73–93 (2017) doi:10.15586/CODON.GLIOBLASTOMA.2017.CH5.

95. Glen, C. M., Kemp, M. L. & Voit, E. O. Agent-based modeling of morphogenetic systems: Advantages and challenges. *PLOS Comput. Biol.* **15**, e1006577 (2019).

96. Gallaher, J. A. *et al.* From cells to tissue: How cell scale heterogeneity impacts glioblastoma growth and treatment response. *PLoS Comput. Biol.* **16**, (2020).

97. Frieboes, H. B. *et al.* An integrated computational/experimental model of tumor invasion. *Cancer Res.* **66**, 1597–1604 (2006).

98. Martínez-González, A., Calvo, G. F., Pérez Romasanta, L. A. & Pérez-García, V. M. Hypoxic Cell Waves Around Necrotic Cores in Glioblastoma: A Biomathematical Model and Its Therapeutic Implications. *Bull. Math. Biol.* **74**, 2875 (2012).

99. Sander, L. M. & Deisboeck, T. S. Growth patterns of microscopic brain tumors. *Phys. Rev. E. Stat. Nonlin. Soft Matter Phys.* **66**, 7 (2002).

100. Paňková, K., Rösel, D., Novotný, M. & Brábek, J. The molecular mechanisms of transition between mesenchymal and amoeboid invasiveness in tumor cells. *Cell. Mol. Life Sci.* **67**, 63 (2010).

101. Hatoum, A., Mohammed, R. & Zakieh, O. The unique invasiveness of glioblastoma and possible drug targets on extracellular matrix. *Cancer Manag. Res.* **11**, 1843 (2019).

102. Siney, E. J. *et al.* Metalloproteinases ADAM10 and ADAM17 Mediate Migration and Differentiation in Glioblastoma Sphere-Forming Cells. *Mol. Neurobiol.* **54**, 3893 (2017).

103. Watkins, S. & Sontheimer, H. Hydrodynamic Cellular Volume Changes Enable Glioma Cell Invasion. *J. Neurosci.* **31**, 17250 (2011).

104. Wu, J. shun *et al.* Plasticity of cancer cell invasion: Patterns and mechanisms. *Transl. Oncol.* **14**, 100899 (2021).

105. Huang, Y. *et al.* Three-dimensional hydrogel is suitable for targeted investigation of amoeboid migration of glioma cells. *Mol. Med. Rep.* **17**, 250–256 (2018).

106. Yan, S. *et al.* MMP inhibitor Ilomastat induced amoeboid-like motility via activation of the Rho signaling pathway in glioblastoma cells. *Tumour Biol.* **37**, 16177–16186 (2016).

107. Graziani, V., Rodriguez-Hernandez, I., Maiques, O. & Sanz-Moreno, V. The amoeboid state as part of the epithelial-to-mesenchymal transition programme. *Trends Cell Biol.* **32**, 228–242 (2022).

108. Ribatti, D., Tamma, R. & Annese, T. Epithelial-Mesenchymal Transition in Cancer: A Historical Overview. *Transl. Oncol.* **13**, 100773 (2020).

109. Tao, C. *et al.* Genomics and Prognosis Analysis of Epithelial-Mesenchymal Transition in

Glioma. *Front. Oncol.* **10**, 183 (2020).

110. Iser, I. C., Lenz, G. & Wink, M. R. EMT-like process in glioblastomas and reactive astrocytes. *Neurochem. Int.* **122**, 139–143 (2019).

111. Xu, A. *et al.* Overexpressed P75CUX1 promotes EMT in glioma infiltration by activating β-catenin. *Cell Death Dis. 2021 122* **12**, 1–15 (2021).

112. Fedele, M., Cerchia, L., Pegoraro, S., Sgarra, R. & Manfioletti, G. Proneural-Mesenchymal Transition: Phenotypic Plasticity to Acquire Multitherapy Resistance in Glioblastoma. *Int. J. Mol. Sci.* **20**, (2019).

113. Halliday, J. *et al.* In vivo radiation response of proneural glioma characterized by protective p53 transcriptional program and proneural-mesenchymal shift. *Proc. Natl. Acad. Sci. U. S. A.* **111**, 5248–5253 (2014).

114. Segerman, A. *et al.* Clonal Variation in Drug and Radiation Response among Glioma-Initiating Cells Is Linked to Proneural-Mesenchymal Transition. *Cell Rep.* **17**, 2994–3009 (2016).

115. Renner, G. *et al.* Integrin α5β1 and p53 convergent pathways in the control of anti-apoptotic proteins PEA-15 and survivin in high-grade glioma. *Cell Death Differ.* **23**, 640–653 (2016).

116. Pibuel, M. A., Poodts, D., Díaz, M., Hajos, S. E. & Lompardía, S. L. The scrambled story between hyaluronan and glioblastoma. *J. Biol. Chem.* **296**, (2021).

117. Abatangelo, G., Vindigni, V., Avruscio, G., Pandis, L. & Brun, P. Hyaluronic Acid: Redefining Its Role. *Cells* **9**, 1–19 (2020).

118. Park, J. B., Kwak, H. J. & Lee, S. H. Role of hyaluronan in glioma invasion. *Cell Adh. Migr.* **2**, 202 (2008).

119. Litwiniuk, M., Krejner, A. & Grzela, T. Hyaluronic Acid in Inflammation and Tissue Regeneration. *Wounds a Compend. Clin. Res. Pract.* **28**, 78–88 (2016).

120. Nagy, N. *et al.* Hyaluronan in Autoimmunity and Immune Dysregulation. *Matrix Biol.* **78**–**79**, 292 (2019).

121. Dorfman, A. & Ho, P. L. Synthesis of acid mucopolysaccharides by glial tumor cells in tissue culture. *Proc. Natl. Acad. Sci. U. S. A.* **66**, 495–499 (1970).

122. Glimelius, B., Norling, B., Westermark, B. & Wasteson, A. Composition and distribution of glycosaminoglycans in cultures of human normal and malignant glial cells. *Biochem. J.* **172**, 443–456 (1978).

123. Misra, S., Hascall, V. C., Markwald, R. R. & Ghatak, S. Interactions between hyaluronan and its receptors (CD44, RHAMM) regulate the activities of inflammation and cancer. *Front. Immunol.* **6**, (2015).

124. Yan, T. *et al.* Interfering with hyaluronic acid metabolism suppresses glioma cell proliferation by regulating autophagy. *Cell Death Dis. 2021 125* **12**, 1–15 (2021).

125. Jadin, L. *et al.* Hyaluronan expression in primary and secondary brain tumors. *Ann. Transl. Med.* **3**, 80 (2015).

126. Varga, I. *et al.* Expression of invasion-related extracellular matrix molecules in human glioblastoma versus intracerebral lung adenocarcinoma metastasis. *Cent. Eur. Neurosurg.* **71**, 173–180 (2010).

127. Valkonen, M. *et al.* Elevated expression of hyaluronan synthase 2 associates with decreased survival in diffusely infiltrating astrocytomas. *BMC Cancer* **18**, (2018).

128. Qin, J., Kilkus, J. & Dawson, G. The hyaluronic acid inhibitor 4-methylumbelliferone is an NSMase2 activator-role of Ceramide in MU anti-tumor activity. *Biochim. Biophys.*

Acta **1861**, 78 (2016).

129. Pibuel, M. A. *et al.* 4-Methylumbelliferone as a potent and selective antitumor drug on a glioblastoma model. *Glycobiology* **31**, 29–43 (2021).

130. Yang, L. *et al.* Development a hyaluronic acid ion-pairing liposomal nanoparticle for enhancing anti-glioma efficacy by modulating glioma microenvironment. *Drug Deliv.* **25**, 388–397 (2018).

131. Chen, C. *et al.* Hyaluronic Acid-Conjugated Nanoparticles for the Targeted Delivery of Cabazitaxel to CD44-Overexpressing Glioblastoma Cells. *J. Biomed. Nanotechnol.* **17**, 595–605 (2021).

132. Straehla, J. *et al.* Layer-by-Layer Nanoparticles Designed for Dual Blood-Brain Barrier and Glioma Targeting. *Neuro. Oncol.* **23**, vi168–vi169 (2021).

133. Roszkowska, M. *et al.* CD44: a novel synaptic cell adhesion molecule regulating structural and functional plasticity of dendritic spines. *Mol. Biol. Cell* **27**, 4055–4066 (2016).

134. Dzwonek, J. & Wilczyński, G. M. CD44: molecular interactions, signaling and functions in the nervous system. *Front. Cell. Neurosci.* **9**, (2015).

135. Si, D., Yin, F., Peng, J. & Zhang, G. High Expression of CD44 Predicts a Poor Prognosis in Glioblastomas. *Cancer Manag. Res.* **12**, 769 (2020).

136. Anido, J. *et al.* TGF-β Receptor Inhibitors Target the CD44(high)/Id1(high) Glioma-Initiating Cell Population in Human Glioblastoma. *Cancer Cell* **18**, 655–668 (2010).

137. Pietras, A. *et al.* Osteopontin-CD44 signaling in the glioma perivascular niche enhances cancer stem cell phenotypes and promotes aggressive tumor growth. *Cell Stem Cell* **14**, 357 (2014).

138. Ranuncolo, S. M. *et al.* CD44 expression in human gliomas. *J. Surg. Oncol.* **79**, 30–35 (2002).

139. Wu, G. *et al.* Expression of CD44 and the survival in glioma: A meta-analysis. *Biosci. Rep.* **40**, (2020).

140. Wei, K. *et al.* Evaluation of the prognostic value of CD44 in glioblastoma multiforme. *Anticancer Res.* **30**, 253–259 (2010).

141. Klank, R. L. *et al.* Biphasic Dependence of Glioma Survival and Cell Migration on CD44 Expression Level. *Cell Rep.* **18**, 23 (2017).

142. Senbanjo, L. T. & Chellaiah, M. A. CD44: A multifunctional cell surface adhesion receptor is a regulator of progression and metastasis of cancer cells. *Front. Cell Dev. Biol.* **5**, 18 (2017).

143. Lokeshwar, V. B., Fregien, N. & Bourguignon, L. Y. W. Ankyrin-binding domain of CD44(GP85) is required for the expression of hyaluronic acid-mediated adhesion function. *J. Cell Biol.* **126**, 1099–1109 (1994).

144. Martin, T. A., Harrison, G., Mansel, R. E. & Jiang, W. G. The role of the CD44/ezrin complex in cancer metastasis. *Crit. Rev. Oncol. Hematol.* **46**, 165–186 (2003).

145. Bulut, G. *et al.* Small molecule inhibitors of ezrin inhibit the invasive phenotype of osteosarcoma cells. *Oncogene 2012 313* **31**, 269–281 (2011).

146. Luu, A. K. & Viloria-Petit, A. M. Targeting Mechanotransduction in Osteosarcoma: A Comparative Oncology Perspective. *Int. J. Mol. Sci.* **21**, 1–30 (2020).

147. Ren, L. & Khanna, C. Role of ezrin in osteosarcoma metastasis. *Adv. Exp. Med. Biol.* **804**, 181–201 (2015).

148. Hughes, D. P. M. How the NOTCH pathway contributes to the ability of osteosarcoma

cells to metastasize. *Cancer Treat. Res.* **152**, 479–496 (2009).

149. Parnell, E. & Yarwood, S. J. Interactions between Epac1 and ezrin in the control of endothelial barrier function. *Biochem. Soc. Trans.* **42**, 274–278 (2014).

150. Simó-Servat, O., Hernández, C. & Simó, R. The ERM Complex: A New Player Involved in Diabetes-induced Vascular Leakage. *Curr. Med. Chem.* **27**, 3012–3022 (2018).

151. García-Ponce, A., Citalán-Madrid, A. F., Velázquez-Avila, M., Vargas-Robles, H. & Schnoor, M. The role of actin-binding proteins in the control of endothelial barrier integrity. *Thromb. Haemost.* **113**, 20–36 (2015).

152. Tynninen, O., Carpén, O., Jääskeläinen, J., Paavonen, T. & Paetau, A. Ezrin expression in tissue microarray of primary and recurrent gliomas. *Neuropathol. Appl. Neurobiol.* **30**, 472–477 (2004).

153. Qin, J. J. *et al.* Radixin knockdown by RNA interference suppresses human glioblastoma cell growth in vitro and in vivo. *Asian Pac. J. Cancer Prev.* **15**, 9805–9812 (2014).

154. Zhu, X. *et al.* Moesin is a glioma progression marker that induces proliferation and Wnt/β-catenin pathway activation via interaction with CD44. *Cancer Res.* **73**, 1142–1155 (2013).

155. Akiyama, Y. *et al.* Hyaluronate receptors mediating glioma cell migration and proliferation. *J. Neurooncol.* **53**, 115–127 (2001).

156. Shortt, C., Luyt, L. G., Turley, E. A., Cowman, M. K. & Kirsch, T. A Hyaluronan-binding Peptide (P15-1) Reduces Inflammatory and Catabolic Events in IL-1β-treated Human Articular Chondrocytes. *Sci. Reports 2020 101* **10**, 1–11 (2020).

157. Tolg, C. *et al.* A RHAMM mimetic peptide blocks hyaluronan signaling and reduces inflammation and fibrogenesis in excisional skin wounds. *Am. J. Pathol.* **181**, 1250–1270 (2012).

158. Esguerra, K. V. N. *et al.* Identification, design and synthesis of tubulin-derived peptides as novel hyaluronan mimetic ligands for the receptor for hyaluronan-mediated motility (RHAMM/HMMR). *Integr. Biol. (United Kingdom)* **7**, 1547–1560 (2015).

159. Xiao, W., Sohrabi, A. & Seidlits, S. K. Integrating the glioblastoma microenvironment into engineered experimental models. *Futur. Sci. OA* **3**, (2017).

160. Kapałczyńska, M. *et al.* 2D and 3D cell cultures – a comparison of different types of cancer cell cultures. *Arch. Med. Sci.* **14**, 910 (2018).

161. Cukierman, E. Preparation of Extracellular Matrices Produced by Cultured Fibroblasts. *Curr. Protoc. Cell Biol.* **16**, 10.9.1-10.9.15 (2002).

162. Cukierman, E., Pankov, R., Stevens, D. R. & Yamada, K. M. Taking cell-matrix adhesions to the third dimension. *Science (80-.).* **294**, 1708–1712 (2001).

163. Rao, J. S. *et al.* Role of plasminogen activator and of 92-KDa type IV collagenase in glioblastoma invasion using anin vitro Matrigel model. *J. Neuro-Oncology 1994 182* **18**, 129–138 (1993).

164. Radotra, B. & McCormick, D. Glioma invasion in vitro is mediated by CD44-hyaluronan interactions. *J. Pathol.* **181**, 434–438 (1997).

165. Kim, Y. & Kumar, S. CD44-mediated adhesion to hyaluronic acid contributes to mechanosensing and invasive motility. *Mol. Cancer Res.* **12**, 1416–1429 (2014).

166. Jin, S. G. *et al.* The effect of hyaluronic acid on the invasiveness of malignant glioma cells: Comparison of invasion potential at hyaluronic acid hydrogel and Matrigel. *J. Korean Neurosurg. Soc.* **46**, 472–478 (2009).

167. Florczyk, S. J. *et al.* Porous chitosan-hyaluronic acid scaffolds as a mimic of glioblastoma microenvironment ECM. *Biomaterials* **34**, 10143–10150 (2013).

168. Hermida, M. A. *et al.* Three dimensional in vitro models of cancer: Bioprinting multilineage glioblastoma models. *Adv. Biol. Regul.* **75**, (2020).

169. Xiao, W. *et al.* Brain-mimetic 3D culture platforms allow investigation of cooperative effects of extracellular matrix features on therapeutic resistance in glioblastoma. *Cancer Res.* **78**, 1358–1370 (2018).

170. Fraley, S. I. *et al.* A distinctive role for focal adhesion proteins in three-dimensional cell motility. *Nat. Cell Biol.* **12**, 598–604 (2010).

171. Wolfenson, H., Lavelin, I. & Geiger, B. Dynamic regulation of the structure and functions of integrin adhesions. *Dev. Cell* **24**, 447–458 (2013).

172. de Ridder, L. I., Laerum, O. D., Mørk, S. J. & Bigner, D. D. Invasiveness of human glioma cell lines in vitro: relation to tumorigenicity in athymic mice. *Acta Neuropathol.* **72**, 207–213 (1987).

173. Fang, Y. & Eglen, R. M. Three-Dimensional Cell Cultures in Drug Discovery and Development. *Slas Discov.* **22**, 456 (2017).

174. Aisenbrey, E. A. & Murphy, W. L. Synthetic alternatives to Matrigel. *Nat. Rev. Mater.* **5**, 539 (2020).

175. Ahmed, E. M. Hydrogel: Preparation, characterization, and applications: A review. *J. Adv. Res.* **6**, 105–121 (2015).

176. Pedron, S. & Harley, B. A. C. Impact of the biophysical features of a 3D gelatin microenvironment on glioblastoma malignancy. *J. Biomed. Mater. Res. Part A* **101**, 3404–3415 (2013).

177. Yoo, K. M., Murphy, S. V. & Skarda, A. A Rapid Crosslinkable Maleimide-Modified Hyaluronic Acid and Gelatin Hydrogel Delivery System for Regenerative Applications.

Gels (Basel, Switzerland) **7**, 1–17 (2021).

178. Rao, S. S. *et al.* Glioblastoma behaviors in three-dimensional collagen-hyaluronan composite hydrogels. *ACS Appl. Mater. Interfaces* **5**, 9276–9284 (2013).

179. Ananthanarayanan, B., Kim, Y. & Kumar, S. Elucidating the mechanobiology of malignant brain tumors using a brain matrix-mimetic hyaluronic acid hydrogel platform. *Biomaterials* **32**, 7913–7923 (2011).

180. Wang, C. *et al.* Matrix Stiffness Modulates Patient-Derived Glioblastoma Cell Fates in Three-Dimensional Hydrogels. *Tissue Eng. Part A* **27**, 390–401 (2021).

181. Xiao, W. *et al.* Bioengineered scaffolds for 3D culture demonstrate extracellular matrix-mediated mechanisms of chemotherapy resistance in glioblastoma. *Matrix Biol.* **85**–**86**, 128 (2020).

182. Wolf, K. J. *et al.* A mode of cell adhesion and migration facilitated by CD44-dependent microtentacles. *Proc. Natl. Acad. Sci. U. S. A.* **117**, (2020).

183. Pedron, S., Becka, E. & Harley, B. A. C. Regulation of glioma cell phenotype in 3D matrices by hyaluronic acid. *Biomaterials* **34**, 7408–7417 (2013).

184. Pedron, S. *et al.* Hyaluronic acid-functionalized gelatin hydrogels reveal extracellular matrix signals temper the efficacy of erlotinib against patient-derived glioblastoma specimens. *bioRxiv* 556324 (2019) doi:10.1101/556324.

185. Pedron, S., Hanselman, J. S., Schroeder, M. A., Sarkaria, J. N. & Harley, B. A. C. Extracellular Hyaluronic Acid Influences the Efficacy of EGFR Tyrosine Kinase Inhibitors in a Biomaterial Model of Glioblastoma. *Adv. Healthc. Mater.* **6**, 1700529 (2017).

186. Cowman, M. K., Lee, H. G., Schwertfeger, K. L., McCarthy, J. B. & Turley, E. A. The

Content and Size of Hyaluronan in Biological Fluids and Tissues. *Front. Immunol.* **6**, (2015).

187. Kogan, G., Šoltés, L., Stern, R. & Gemeiner, P. Hyaluronic acid: A natural biopolymer with a broad range of biomedical and industrial applications. *Biotechnol. Lett.* **29**, 17–25 (2007).

188. Amsden, B. Solute Diffusion within Hydrogels. Mechanisms and Models. *Macromolecules* **31**, 8382–8395 (1998).

189. Rizzardi, A. E. *et al.* Quantitative comparison of immunohistochemical staining measured by digital image analysis versus pathologist visual scoring. *Diagn. Pathol.* **7**, (2012).

190. Proudfit, A. *et al.* Pharmacologic Inhibition of Ezrin-Radixin-Moesin Phosphorylation is a Novel Therapeutic Strategy in Rhabdomyosarcoma. *Sarcoma* **2020**, (2020).

191. Giordana, M. T. *et al.* Glycosaminoglycans in human cerebral tumors. Part II. Histochemical findings and correlations. *Acta Neuropathol.* **57**, 299–305 (1982).

192. Nakod, P. S., Kim, Y. & Rao, S. S. Three-dimensional biomimetic hyaluronic acid hydrogels to investigate glioblastoma stem cell behaviors. *Biotechnol. Bioeng.* **117**, 511–522 (2020).

193. Lyon, J. G., Carroll, S. L., Mokarram, N. & Bellamkonda, R. V. Electrotaxis of Glioblastoma and Medulloblastoma Spheroidal Aggregates. *Sci. Rep.* **9**, 1–19 (2019).

194. Tabet, A. *et al.* Mechanical Characterization of Human Brain Tissue and Soft Dynamic Gels Exhibiting Electromechanical Neuro-Mimicry. *Adv. Healthc. Mater.* **8**, 1900068 (2019).

195. Budday, S., Ovaert, T. C., Holzapfel, G. A., Steinmann, P. & Kuhl, E. Fifty Shades of Brain: A Review on the Mechanical Testing and Modeling of Brain Tissue. *Arch. Comput.*

Methods Eng. **27**, 1187–1230 (2019).

196. Budday, S. *et al.* Rheological characterization of human brain tissue. *Acta Biomater.* **60**, 315–329 (2017).

197. Budday, S. *et al.* Mechanical characterization of human brain tissue. *Acta Biomater.* **48**, 319–340 (2017).

198. Zhang, Z. *et al.* Morphology-based Prediction of Cancer Cell Migration Using an Artificial Neural Network and a Random Decision Forest. *Integr. Biol. (Camb).* **10**, 758 (2018).

199. Mencattini, A. *et al.* Discovering the hidden messages within cell trajectories using a deep learning approach for in vitro evaluation of cancer drug treatments. *Sci. Reports 2020 101* **10**, 1–11 (2020).

200. Sobue, Y. *et al.* Inhibition of CD44 intracellular domain production suppresses bovine articular chondrocyte de-differentiation induced by excessive mechanical stress loading. *Sci. Rep.* **9**, (2019).

201. Knudson, W. & Loeser, R. F. CD44 and integrin matrix receptors participate in cartilage homeostasis.

202. Razinia, Z. *et al.* Stiffness-dependent motility and proliferation uncoupled by deletion of CD44. *Sci. Reports 2017 71* **7**, 1–10 (2017).

203. Martin, T. A., Harrison, G., Mansel, R. E. & Jiang, W. G. The role of the CD44/ezrin complex in cancer metastasis. *Crit. Rev. Oncol. Hematol.* **46**, 165–186 (2003).

204. Tolg, C. *et al.* Cell-specific expression of the transcriptional regulator RHAMM provides a timing mechanism that controls appropriate wound re-epithelialization. *J. Biol. Chem.* **295**, 5427–5448 (2020).

205. Smith, J. T., Elkin, J. T. & Reichert, W. M. Directed cell migration on fibronectin gradients: effect of gradient slope. *Exp. Cell Res.* **312**, 2424–2432 (2006).

206. Guarnieri, D. *et al.* Covalently immobilized RGD gradient on PEG hydrogel scaffold influences cell migration parameters. *Acta Biomater.* **6**, 2532–2539 (2010).

207. Neftel, C. *et al.* An Integrative Model of Cellular States, Plasticity, and Genetics for Glioblastoma. *Cell* **178**, 835-849.e21 (2019).

208. Couturier, C. P. *et al.* Single-cell RNA-seq reveals that glioblastoma recapitulates a normal neurodevelopmental hierarchy. *Nat. Commun. 2020 111* **11**, 1–19 (2020).